2018

Elucidating the role of serine protease kallikrein 6 in oligodendrocyte maturation & myelination

BOSTON UNIVERSITY

SCHOOL OF MEDICINE

Dissertation

ELUCIDATING THE ROLE OF SERINE PROTEASE KALLIKREIN 6 IN OLIGODENDROCYTE MATURATION & MYELINATION

by

SHARON M. O'NEILL

B.Sc., Haverford College, 2007
M.A., Brown University, 2010

Submitted in partial fulfillment of the

requirements for the degree of

Doctor of Philosophy

2018

Approved by

First Reader _____

Tarik Haydar, Ph.D.
Professor of Anatomy & Neurobiology

Second Reader _____

Tarek Samad, Ph.D.
Special Appointment
Head of Neurodegeneration, Pfizer

Third Reader _____

Mark Moss, Ph.D.
Professor and Chair of Anatomy & Neurobiology

ACKNOWLEDGMENTS

The National Multiple Sclerosis Society, Rocky Mountain Multiple Sclerosis Center, Multiple sclerosis patients, and patient families for access to invaluable multiple sclerosis brain tissue. This work was supported in part by a grant from the National Multiple Sclerosis Society.

The members of my research and/or dissertation committees:
Tarik Haydar, Jennifer Luebke, Maria Maya Medalla, Mark Moss, Kathleen Rockland, & Tarek Samad.

The following for additional support and/or assistance with experimental work:
Sabra Al-Harthy, Shoh Asano, Luke Appleton, Rita Balice-Gordon, Jason Barricklow, Magalie Boucher, Christopher Butler, Julie Cianfrogna, Teresa Cunio, Marie Debrue, James Duerr, Cathleen Gonzales, Edward Guilmette, Katherine Hales, Ghazal Hariri, Renee Huynh, Thomas Kawabe, Thomas Lanz, Jennifer Larson, David Logan, Kewa Mou, Brian T. O'Neill, Nancy O'Neill, Mary Orczykowski, Sangwoo Ryu, Christopher Taylor, Brendan Tierney, Jincheng Pang, Ingrid Pardo, Karen Percieval, Justin Piro, Georgette Suidan, Jamison Tuttle, Dmitri Volfson, Alexandra Wink, Kathleen Wood, Hualin Xi, A. Matthew Zaino, Le Zhang.

ELUCIDATING THE ROLE OF SERINE PROTEASE KALLIKREIN 6 IN OLIGODENDROCYTE MATURATION & MYELINATION

SHARON M. O'NEILL

Boston University School of Medicine, 2018

Major Professor: Tarik Haydar, Ph.D., Professor of Anatomy & Neurobiology

ABSTRACT

Multiple sclerosis (MS) is a chronic central nervous system disease featuring exacerbations of inflammation and demyelination that cause progressively debilitating clinical effects over time. Current treatments for multiple sclerosis are limited in their ability to impact overall disease progression. Research aimed at generation of novel potential therapeutics for MS is needed. Recently, kallikrein 6 (KLK6), a member of the kallikrein (KLK) family of secreted serine proteases, was found to be elevated in the cerebrospinal fluid and brain of MS patients. The fifteen known tissue-based KLKs cleave proteins through a similar mechanism, but have different binding pocket specificity, diverse localization in human tissues, and multiple biological functions. KLKs have been linked to normal human physiology (e.g. KLK4, enamel formation) and disease (e.g. KLK3, prostate cancer). KLK6 is one of the highest expressed serine proteases in the healthy human brain and is expressed predominately in mature

oligodendrocytes in both human and mouse brain. The role of KLK6 in oligodendrocyte maturation, myelination, and disease is not fully understood.

To evaluate the role of KLK6 in oligodendrocyte maturation, I used a pluripotent *in vitro* primary cell system to assess the impact of exogenous KLK6 and modulators of the KLK6 pathway on oligodendrocyte maturation. I demonstrate that signaling through KLK6 decreases the number of mature oligodendrocytes in culture, whereas blockade of KLK6 signaling increases the number of mature oligodendrocytes in culture in the presence of triiodothyronine higher than either agent alone. This work suggests that KLK6 modulation impacts oligodendrocyte maturation. To understand the potential impact of KLK6 pathway inhibition on remyelination, I used the toxin cuprizone to induce demyelination in mice. I found that animals treated with a KLK6 inhibitor had increased myelin staining in the corpus callosum compared to vehicle-treated. This work suggests that KLK6 modulates oligodendrocyte maturation and myelination and may be relevant for improving myelin-related therapeutic outcomes, particularly in multiple sclerosis.

TABLE OF CONTENTS

LIST OF TABLES

LIST OF FIGURES

LIST OF ABBREVIATIONS

ACN ..... Acetonitrile

AMC 7-Amino-4-methylcoumarin

ANOVA ..... Analysis of variance

bFGF ..... Basic fibroblast growth factor

BID ..... Twice daily

Boc ..... t-Butyloxycarbonyl

C ..... Celsius

C/K ..... Cuprizone/KLK6 inhibitor treatment group

C/N ..... Cuprizone/Naive treatment group

C/P ..... Cuprizone/PAR1 inhibitor treatment group

C/V ..... Cuprizone/Vehicle treatment group

Ca2+ ..... Calcium ions

CAS ..... Chemical abstracts service

cDNA ..... Complementary DNA

CE ..... Collision energy

CHO ..... Chinese hamster ovary

CNS ..... Central Nervous System

CSF ..... Cerebrospinal fluid

CSLT ..... Chronic, severe, long-term multiple sclerosis

CSPG4 ..... Chondroitin sulfate proteoglycan 4

CT ..... Cycle threshold

Cuprizone ..... Bis(cyclohexanone)oxaldihydrazone

D ..... Day

DAPI ..... 4',6-Diamidino-2-Phenylindole, Dihydrochloride

DMSO ..... Dimethylsulfoxide

DNA ..... Deoxyribonucleic acid

DP ..... Declustering potential

EAE ..... Experimental autoimmune encephalomyelitis

EGF ..... Epidermal growth factor

EM ..... Electron microscopy

ESI ..... Electrospray ionization

FAM ..... Fluorescein amidite

FDA ..... Food and Drug Administration

FLIPR ..... Fluorescent Imaging Plate Reader

g ..... Gram

GAPDH ..... Glyceraldehyde 3-phosphate dehydrogenase

GFAP ..... Glial fibrillary acid protein

HLA ..... Human leukocyte antigen

HSS ..... High strength silica

Iba1 ..... Ionized calcium-binding adapter molecule 1

IC50 ..... Half maximal inhibitory concentration

ICV ..... Intracerebroventricular

IgG ..... Immunoglobulin

JC polyomavirus ..... John Cunningham polyomavirus

kg ..... Kilogram

KLKs ..... Kallikreins

KLK6 ..... Kallikrein 6

KLK6i ..... KLK6 inhibitor

LINGO-1 ..... Leucine-rich repeat and immunoglobulin domain containing Nogo receptor interacting protein1

LC-MS/MS ..... Liquid chromatography tandem mass spectrometry

LFB ..... Luxol Fast Blue

LPC ..... Lysophosphatidylcholine

MBP ..... Myelin basic protein

mg ..... Milligram

MHC ..... Major histocompatibility complex

Min ..... Minutes

mL ..... Milliliter

mm ..... Millimeter

MOG ..... Myelin oligodendrocyte glycoprotein

MR ..... Magnetic Resonance

MRI ..... Magnetic Resonance Imaging

MRM ..... Multiple reaction monitoring

mRNA ..... Messenger RNA

MS ..... Multiple sclerosis

MWCO.....Molecular weight cutoff

N..... Number of subjects

N/N .....Normal chow/Naïve treatment

NADPH.....Nicotinamide adenine dinucleotide phosphate

ng ..... Nanogram

NG2..... Neural/Glial proteoglycan antigen 2

nM .....Nanomolar

NRF2 ..... Nuclear factor (erythroid-derived 2)-like 2

NTC .....Non-template control

OL.....Oligodendrocyte

OPC.....Oligodendrocyte precursor cell

P .....Postnatal Day

PAR1 ..... Protease-activated receptor 1

PAR1AP .....Protease-activated receptor 1 Activating Peptide

PAR1i ..... PAR1 inhibitor

PDGF .....Platelet-derived growth factor

PEG 400.....Polyethylene glycol 400

PLP ..... Proteolipid protein

PMI ..... Post-mortem interval

PML ..... Progressive multifocal leukoencephalopathy

PPMS ..... Primary-progressive multiple sclerosis

PRMS ..... Progressive-relapsing multiple sclerosis

PSA-NCAM ..... Polysialylated-neural cell adhesion molecule

qRT-PCR ..... Quantitative reverse-transcription polymerase chain reaction

RFU ..... Relative fluorescence units

RNA ..... Ribonucleic acid

ROI ..... Region of interest

RRMS ..... Relapsing-remitting multiple sclerosis

RT ..... Room temperature

S ..... Seconds

SBECD ..... Sulfobutylether-beta-cyclodextrin

SC ..... Subcutaneous delivery

SPMS ..... Secondary progressive multiple sclerosis

T ..... Tesla

T3 .....Triiodothyronine

TMEV .....Theiler’s murine encephalomyelitis virus

tpm ..... Transcripts per million

µL .....Microliter

µm ..... Micrometer

µM ..... Micromolar

UPLC ..... Ultra performance liquid chromatography

UPLC-MS/MS ..... Ultra performance LC-MS/MS

VEP ..... Visual-evoked potential

VIC ..... Proprietary fluorescent compound

CHAPTER ONE

Introduction

Multiple Sclerosis

Multiple sclerosis (MS) is a chronic, auto-immune disorder of the central nervous system that can lead to lack of coordinated muscle movements, fatigue, decreased cognition, impaired vision, paralysis, and depression (Ben-Zacharia, 2011). MS is typically diagnosed between the ages of 20-40 years old and affects double the number of women compared to men; the overall prevalence of MS is estimated to be over 2.3 million people (Ransohoff *et al.*, 2015). The etiology of MS is currently unknown and thus the disease is likely to be due to multiple factors, such as genetics and environment.

Genetic polymorphisms in human leukocyte antigen (HLA) genes that regulate major histocompatibility complex (MHC) proteins which in turn modulate immune responses have been shown to be either protective or act as risk factors for MS (Moutsianas *et al.*, 2015). One environmental risk factor to developing MS is thought to be lack of exposure to sunlight and/or low vitamin D levels (Pierrot-Deseilligny and Souberbielle, 2017). Prevalence of MS has been inversely associated with the angular distance from latitudes such as those near the equator that experience almost continuous sun exposure/ultraviolet light radiation (Sloka *et al.*, 2011). Further, single nucleotide polymorphisms associated with vitamin D absorption have been implicated in MS genome-wide association

studies (International Multiple Sclerosis Genetics *et al.*, 2011). It is hypothesized that the association between vitamin D levels and multiple sclerosis may be that vitamin D is helpful in control of excessive T-cell mediated responses (Cantorna and Waddell, 2014).

While the mechanisms behind what triggers MS are still unknown, excess inflammation is a significant contributor to pathology in MS. Peripheral T lymphocytes and macrophages infiltrate into the central nervous system and direct damage of the myelin sheath. Myelin sheaths are present on neurons in a variety of areas throughout the central nervous system, but they are especially noticeable grossly when they travel in large groupings such as tracts or funiculi- areas commonly collectively called “white matter” within the brain or spinal cord. Focal areas of damage to the myelin sheath in such areas where it is normally abundant are referred to as lesions or plaques. This damage prevents rapid conduction of neuronal action potentials and leaves underlying neuronal axons more vulnerable to degeneration (Dendrou *et al.*, 2015).

Other neurodegenerative disorders such as Alzheimer’s disease and Parkinson’s disease have a characteristically-defined anatomical localization of pathology (AD: neurofibrillary tangle associated; PD: Lewy body associated) as disease severity increases (Braak *et al.*, 2003; Braak *et al.*, 2006). Multiple sclerosis does not have a defined anatomical localization of plaque progression as severity of disease increases. However, the most frequent area of incidence

of plaques in MS patient gray matter is in cortical sulci (invaginations of cortical tissue, below the pia mater) (Haider *et al.*, 2016). The most frequent area of incidence of plaques in white matter of MS patients is in periventricular locations, or in white matter areas that border the ventricular system of the brain that circulates cerebrospinal fluid (Haider *et al.*, 2016). Plaques can also be present in gray and white matter of spinal cord in MS, but plaques in the brain are generally more common at earlier stages of disease (Kearney *et al.*, 2015a; Kearney *et al.*, 2015b). Less than 10% of MS patients are estimated to have spinal cord plaques only (Nociti *et al.*, 2005). However, magnetic resonance imaging (MRI) to confirm diagnosis and progression in MS clinical trials typically focuses on brain lesions instead of spinal cord due to ease of imaging relative to current technological methods and structure size (Kearney *et al.*, 2015a; Muccilli *et al.*, 2018).

White matter plaques are visible by both MRI methods and histological techniques. Gray matter or cortical plaques are more visible by histological techniques than by MRI, although a recent study reported moderate success with cortical plaque detection using 7 Tesla magnetic resonance scanners (versus 1.5 T scanner) (Kilsdonk *et al.*, 2016). Compared to white matter plaques, gray matter plaques are more correlated to clinical symptom severity in patients, and this is thought to be because these areas may progress to neuronal atrophy and degeneration more rapidly (Calabrese *et al.*, 2011; Kilsdonk *et al.*, 2016; Bergsland *et al.*, 2018).

There are four clinical subtypes of MS: 1) relapsing-remitting (RRMS), 2) secondary progressive (SPMS), 3) primary-progressive (PPMS), and 4) progressive-relapsing (PRMS). The clinical subtypes are largely defined by their manifestation of behavioral symptoms, although presentation of disease-related symptoms is still quite heterogeneous within each subtype. RRMS is the most common clinical subtype of MS. RRMS alternates between periods of symptoms (relapses) followed by some degree of remission. It has been shown that although symptoms may improve in remission, damaged myelin is still present (Stadelmann and Bruck, 2008). There is an approximate 80% conversion rate from RRMS into SPMS, which results in an overall deteriorating condition that includes neuronal damage in addition to myelin damage (Dendrou *et al.*, 2015). Although the slope of increasing disability can differ, PPMS is defined by an almost linear progression of disease worsening without remission. PRMS is the least common form of MS and is characterized by a gradual worsening of overall condition with periods of exacerbated symptoms but no remissions. The progressive forms of MS demonstrate less remyelination and more demyelination than RRMS (Stadelmann and Bruck, 2008).

There is still ongoing discussion among experts of whether these clinical subtypes reflect disease heterogeneity due to other factors or if MS is a disease with discrete sequential stages of pathology. While it is generally accepted that

relapsing patients can become progressive; it is not clear if all progressive MS cases started as relapsing-remitting MS cases (Kuchling *et al.*, 2014). Diagnosis of MS relies heavily on clinical assessment, medical history, and an important criteria that the symptoms are not explained by any other known cause (Katz Sand, 2015; Thompson *et al.*, 2017). There are no definite diagnostic biomarkers of MS or its subtypes, although measurement of white matter using T2 MRI (with or without gadolinium-enhanced contrast imaging) is usually done to confirm incidence of multiple lesions in different regions of the CNS (Katz Sand, 2015; Siva, 2018). Further, the presence of immunoglobulins (IgGs) in cerebrospinal fluid; particularly oligoclonal bands in CSF that are not in serum can be used to confirm a diagnosis combined with medical history and imaging but they are not exclusive to MS (Winger and Zamvil, 2016; Thompson *et al.*, 2017). Historically it has been thought that CSF-specific IgGs were predominately to myelin proteins in MS patients, but recent evidence has suggested they can also be to intracellular proteins more indicative of general cellular debris resulting from cell death (Winger and Zamvil, 2016).

Several therapeutics are currently approved to decrease inflammation in MS, but none are able to restore myelin once it has been damaged (Ransohoff *et al.*, 2015). At this time, there are more therapeutics available for one specific clinical subtype of MS (relapsing-remitting, RRMS) than the other clinical subtypes. The main therapeutic benefit of these treatments is a reduction in

symptoms and length of type in “relapse” phase of RRMS. RRMS is often the presenting form or earliest phase of MS which may enable therapeutic intervention to be more successful by introducing it before endogenous repair mechanisms are no longer effective and neuronal death occurs (Dargahi *et al.*, 2017).

The first pharmacological therapy approved in the United States by the Food and Drug Administration (FDA) was interferon beta-1b injectable Betaseron (Bayer) in 1993 (Ransohoff *et al.*, 2015; Auricchio *et al.*, 2017). Several other interferon beta-based treatments followed. The exact mechanism by which interferon beta is able to decrease MRI white matter lesions is an area of ongoing investigation, but generally, interferons are cytokines which regulate anti-inflammatory and pro-inflammatory signaling (Kieseier, 2011; Ransohoff *et al.*, 2015; Haji Abdolvahab *et al.*, 2016; Auricchio *et al.*, 2017). Interferon beta treatments are still used today, due to their moderate efficacy and reasonable safety profile, however they are not effective for all patients and there is limited ability to predetermine those who would best benefit beforehand (Ottoboni *et al.*, 2012; Ransohoff *et al.*, 2015).

Several effective therapeutics in MS that were more recently developed are also anti-inflammatory. These include Natalizumab (Tysabri, 2004, Elan/Biogen) and Fingolimod (Gilenya, 2010, Novartis, first oral MS treatment), and Dimethyl fumarate (Tecfidera, 2013, Biogen). Natalizumab and Fingolimod

both decrease T cell infiltration into the CNS by targeting integrin-alpha4 or the sphingosine-1-phosphate receptor, respectively (Ransohoff *et al.*, 2015). Dimethyl fumarate reduces inflammation and oxidative stress by activating nuclear factor (erythroid-derived 2)-like-2 (NRF2) to stabilize NADPH:quinolone oxidoreductase1, as well as potentially through additional indirect pathways which are still being clarified (Linker and Gold, 2013; Brennan *et al.*, 2016; Ghadiri *et al.*, 2017). All of these new drugs have potentially serious side effects which include risk of progressive multifocal leukoencephalopathy (PML; Natalizumab, Dimethyl fumarate) as well as herpes zoster or cardiac complications (Fingolimod) (Ransohoff *et al.*, 2015; Auricchio *et al.*, 2017). Immunosuppression causes dormant JC polyomavirus present in a number of adults to convert to PML, which can be fatal (Williamson and Berger, 2017). The most recent treatment to receive FDA approval for MS is also the first ever approval for the PPMS subtype of MS. Ocrelizumab (Ocrevus, 2017, Roche/Genentech) is approved for both PPMS and RRMS due to arms of the clinical trial being run for both MS subtypes concurrently (Jakimovski *et al.*, 2017; Stahnke and Holt, 2017). Ocrelizumab is an anti-inflammatory that works by depleting B cells and thus may reduce increased IgG as well in patients (Winger and Zamvil, 2016; Stahnke and Holt, 2017). Efficacy was shown in terms of reduced clinical disability progression at 12 weeks compared to placebo in PPMS (Stahnke and Holt, 2017). Side effects are still being evaluated, but there was an

increase in infections (the one PML case was confounded due to the patient being on natalizumab just prior to study) and breast cancer in the treatment group compared to placebo (Stahnke and Holt, 2017).

Ongoing areas of research in treatment for MS include multipotent hematopoietic stem cell transplantation (Dargahi *et al.*, 2017; Muraro *et al.*, 2017), other immunomodulation techniques (Dargahi *et al.*, 2017), and, the focus of this dissertation, understanding mechanisms of myelin generation and repair (Domingues *et al.*, 2016; Akkermann *et al.*, 2017; Cole *et al.*, 2017).

Oligodendrocyte maturation and myelination

Oligodendrocyte (OL) processes insulate neuronal axons with myelin in the central nervous system which triggers sodium channel consolidation at nodes of Ranvier (where myelin is not present) and increases conduction velocity of action potentials (Bradl and Lassmann, 2009). In addition, the myelination of neuronal axons by OL processes creates a physical barrier of protection to the ensheathed neurons and also provides trophic support for axonal integrity (Crawford *et al.*, 2013; Schultz *et al.*, 2017).

OLs in the mammalian forebrain derive embryonically first from neural stem cells in the medial ganglionic eminence. Later, a second cohort is derived from the lateral and caudal ganglionic eminences. After parturition, a third cohort is derived from the cortex (Baumann and Pham-Dinh, 2001). It has been shown

that if one group does not occur, another can take its place without disturbance in the developing brain (Jakovcevski and Zecevic, 2005a, b; Kessaris *et al.*, 2006).

The maturation of OLs from neural precursor cells has been characterized well in terms of morphology and molecular identifiers (Nishiyama *et al.*, 2009). Oligodendrocyte precursor cells (OPCs), which precede OLs in cell lineage, are different from OLs in terms of function as well as structure. OPCs are capable of proliferation and migration, even in adult mammals (Purger *et al.*, 2016). Migration of OPCs is dependent on signals such as extracellular matrix proteins, plate-derived growth factor, and semaphorins (Bradl and Lassmann, 2009).

Once in location, OPCs processes make contact with axons through cell-adhesion molecules, then ensheath the axons as they differentiate to myelinating OLs (Purger *et al.*, 2016). Oligodendrocytes undergo normal turnover in the brain. It has been reported that the average rate of oligodendrocyte maturation in the corpus callosum of humans is about one out of 300 cells per year (~0.32%) after age 5 (Yeung *et al.*, 2014). The average number of oligodendrocytes in the normal adult human corpus callosum is estimated to be between 4.0×10^9 and 5.0×10^9 (Yeung *et al.*, 2014).

OLs differ from the myelinating cells of the peripheral nervous system in several ways, most notably in their myelin protein composition and number of axons that a single cell can myelinate (Nave and Werner, 2014; Feltri *et al.*, 2016; Herbert and Monk, 2017). Schwann cells, the myelinating cells of the

peripheral nervous system, only wrap myelin around one axon (Feltri *et al.*, 2016). A single oligodendrocyte can wrap myelin around as many as forty axons (Miron *et al.*, 2011). Schwann cells also have a layer of cytoplasm surrounding the myelinated layer of axon, while the most external facing component of a myelinating oligodendrocyte is the major dense line of its membrane (Peters, 1960).

The myelinated OL-axon complex is structurally intricate. Myelin proteins, such as myelin basic protein (MBP), help tighten layers of wrapped myelin around an axon at the internode, forming compact myelin in order to increase capacitance (Lee *et al.*, 2014; Simons and Nave, 2015; Zuchero *et al.*, 2015). Next to the internode is the juxtaparanode which is also under compact myelin but is notable as the part of an axon where potassium channels that establish resting potential are congregated. The paranode lies between the potassium channel cluster and the unmyelinated node of Ranvier sodium channel cluster segment to allow for efficient depolarization and repolarization. The paranode primarily contains structural proteins (e.g. contactin and contactin-associated protein) that connect the OL plasma membrane to the axon laterally in an area without compact myelin (Poliak and Peles, 2003; Buttermore *et al.*, 2013).

Despite the importance of the myelin proteins in proper myelin function, myelin is predominately composed of lipids. The major types of lipids that compose myelin are: cholesterol, phospholipids (plasmalogens,

phosphatidylethanolamine, phosphatidylcholine), and glycosphingolipids (galactocerebrosides / gatactosylceramides, fast migrating cerebrosides, and gangliosides) (Podbielska *et al.*, 2013). Synthesis of lipid-rich myelin by oligodendrocytes is dependent on astrocytes and to a lesser degree, dietary lipids, as demonstrated by a recent study where genetic deletion of a coactivator required for lipid biosynthesis was targeted in either oligodendrocytes and/or astrocytes (Camargo *et al.*, 2017). Typically, cholesterol required by the CNS is made within the CNS due to the blood-brain barrier (Kiray *et al.*, 2016).

The process of myelination in the brain is not limited to development. Adult mammalian brains are capable of “re-myelination” of damaged areas of myelin (Peters and Sethares, 2003). When the myelin sheath surrounding an axon becomes damaged, OPCs migrate and proliferate at the site of injury in response to secreted factors and/or neuronal electrical activity where they differentiate into mature oligodendrocytes that will engage in remyelination in that area (Barres and Raff, 1993; Demerens *et al.*, 1996; Crawford *et al.*, 2013). Remyelination is more easily observed on larger axons. Remyelinated axons, or axons with newly-wrapped myelin, are discernable due to the fewer layers of myelin around these axons compared to those in which myelin was laid down during development (Franklin and Ffrench-Constant, 2017). Limited longitudinal studies exist that characterize remyelination but there is some evidence to suggest that myelin will

generate more layers with time and look indistinguishable from myelin from development origin (Powers *et al.*, 2013; Bercury and Macklin, 2015).

The initiation and regulation of myelination is impacted both by neurons and OLs directly involved in the process as well as from indirect signaling pathways from a variety of sources. For example, axons that are not permissive to myelination secrete or express inhibitory proteins (e.g. LINGO-1, PSA-NCAM, Jagged/Notch, Wnt) to prevent maturation of OPCs to OLs temporally or spatially (Emery, 2010; Franklin and Ffrench-Constant, 2017). Axon diameter has also been correlated with OL myelination propensity (Lee *et al.*, 2012). It has also been shown that “fully” mature OLs are less likely to myelinate axons than recently differentiated OLs (Watkins *et al.*, 2008). Similarly, mature oligodendrocytes, myelin, or myelin debris can have a negative feedback relationship by inhibiting additional OPCs in the local environment from maturing to OLs (Kotter *et al.*, 2006; Plemel *et al.*, 2013). Calcium-signaling has been shown to be a mechanism with diverse upstream initiation pathways that modulates myelin in different ways: temporally shorter, lower amplitude calcium bursts stabilize myelin formation while higher amplitude, longer calcium bursts cause myelin retraction (Baraban *et al.*, 2018).

Environmental stimuli are capable of altering the volume of myelinated neuronal fibers. For example, social isolation can decrease the volume of white matter (Liu *et al.*, 2012; Makinodan *et al.*, 2012) while plasticity of learning a new

task can elevate myelination in brain regions associated with conducting that task (Scholz *et al.*, 2009; Sampaio-Baptista *et al.*, 2013).

The normal process of aging also has an impact on myelin structure and volume. At the electron microscopy level, aging can cause areas of dense cytoplasm in oligodendrocytes, which is thought to lead to degeneration, due to splitting of the major dense line (Peters, 2002). It also can create “bubbles” of fluid that disturb the intraperiod lines which causes distension of myelin surrounding an axon and is also expected to lead to degeneration (Peters, 2002). Also occurring with age is “redundant” myelin that myelinates above what is typical for the axon diameter. This can also lead to a phenomenon where the excessive myelination around the axon splits into two compact bundles of myelin separated by a gap (Peters, 2002).

Increased ventricular space, which has been correlated with decreased white matter volume, is also associated with aging (Guttmann *et al.*, 1998; Coutu *et al.*, 2016). Evidence from recent studies suggests that decreased vascular perfusion of the brain could be a factor leading to increased white matter pathology in aging. Using cerebral blood flow, cerebrovascular reactivity measurements, white matter structural measures (by diffusion tensor imaging-mean diffusivity or fractional anisotropy, and fluid attenuated inversion recovery using magnetic resonance imaging) it has been shown that hypoperfusion of the brain precedes white matter hyperintensities indicative of pathology;

periventricular areas especially demonstrated hypoperfusion (Promjunyakul *et al.*, 2016; Sam *et al.*, 2016). In disease state, these normal biological events could compound the severity of pathology. For example, periventricular regions are also a frequent area of demyelinated plaques in MS (Haider *et al.*, 2016). In addition, cardiovascular risk factors such as smoking and hypertension have been shown to increase demyelinated plaque area in MS (Kappus *et al.*, 2016).

Serine Proteases

Human proteases are largely classified into families based on mechanism in which they cleave proteins. Several depend on involvement of a particular amino acid and thus are named after said amino acid: aspartic proteases, cysteine proteases, threonine proteases, and serine proteases. Another group is classified based on requirement of a metal ion to cleave proteins: metalloproteases.

Serine proteases are one the largest families of human proteases, making up about twenty-five percent of all known proteases (Di Cera, 2009; Prassas *et al.*, 2015). Serine proteases are involved in a diverse array of biological processes that span from regulation of immunological complement cascades (Bajic *et al.*, 2015), apoptosis (Trapani, 2001), increasing the epithelial barrier in the intestine (Ronaghan *et al.*, 2016), and aiding in iron absorption (Ramsay *et al.*, 2009). The most well-known serine proteases are perhaps thrombin, trypsin

and chymotrypsin. In wound healing, prothrombin is cleaved to become the active enzyme thrombin. Thrombin cleaves fibrinogen to fibrin which allows for the formation of an insoluble clot to stop bleeding (Weisel and Litvinov, 2017). Trypsin and chymotrypsin are digestive serine proteases that are made in zymogen form in the pancreas (trypsinogen and chymotrypsinogen) that are activated in the small intestine to break down food so nutrients can be absorbed (Whitcomb and Lowe, 2007). Trypsin is also commonly used in a research laboratory setting to detach adherent cells in cell culture and chop up proteins for proteomic analysis (Brown *et al.*, 2007; Vandermarliere *et al.*, 2013).

Serine proteases cleave proteins through a well-defined biochemical reaction using a highly conserved “catalytic triad” which is the active site of the enzymes. The canonical catalytic triad is composed of three highly conserved amino acids: serine, aspartic acid, and histidine. The major proteolytic component of the catalytic triad is the hydroxyl group of the serine that cleaves the substrate amino acid at the carbonyl group through a nucleophilic attack mechanism. The aspartic acid and histidine form a hydrogen bond which stabilizes the reaction by creating a stronger nucleophile by making the histidine more basic (Di Cera, 2009). Serine proteases can be further divided into subcategories: chymotrypsins, elastases, kallikreins, matriptases, thrombins, trypsins, and tryptases. These subcategories are largely driven by the binding pocket size and specificity and types of typical substrates. Serine protease

activity is regulated post-transcriptionally. They are secreted as zymogens (inactive precursors which require cleavage to become active), and their activity also depends on pH, metal ions, serpins (serine protease inhibitors), and whether they can self-activate or self-terminate activity through their own cleavage (Prassas *et al.*, 2015).

Introduction & Approach to Dissertation

Recent work has demonstrated that a serine protease, Kallikrein 6 (KLK6; also known as protease M, neurosin, zyme, or myelencephalon-specific protease), is expressed specifically in OPCs/OLs in both rodent and human cells of the brain (Zhang *et al.*, 2014; Bennett *et al.*, 2016; Zhang *et al.*, 2016). In addition, KLK6 levels have been shown to be elevated in MS patient brain (Scarisbrick *et al.*, 2002), cerebrospinal fluid (Hebb *et al.*, 2010), and serum (Scarisbrick *et al.*, 2008) compared to control. The role of KLK6 in normal oligodendrocyte biology and in pathological conditions such as MS is unknown.

In order to elucidate the role of the serine protease KLK6 in these contexts, the aims of this research were threefold. First, I sought to characterize levels of KLK6 over oligodendrocyte maturation. To do this, I evaluated expression levels of KLK6 in OL maturation using rodent primary neurosphere-derived cells and gene expression methods. Second, I sought to determine the consequences of KLK6 modulation on oligodendrocyte maturation and

myelination. To determine the consequences of KLK6 pathway activation and inhibition on maturation of OLs and myelination in the brain, I applied exogenous KLK6 pathway modulators to primary oligodendrocytes *in vivo* or in a cuprizone mouse model of corpus callosum demyelination. Third, I sought to develop further understanding of KLK6 expression in the human CNS and in MS patients. To do this, gene expression of KLK6 was evaluated in a large adult human tissue RNA sequencing dataset. Further, expression of KLK6 in multiple sclerosis patient post-mortem brain was characterized using immunohistochemistry.

Identifying and clarifying the pathways that regulate the maturation of oligodendrocytes (OLs) and myelination is important for developing therapeutics that promote remyelination in the context of multiple sclerosis (MS) and other demyelinating diseases.

CHAPTER TWO

Kallikrein 6 in Oligodendrocyte Maturation

a) Introduction

i. Overview of Diverse Biological Functions of the Kallikrein Family of Serine Proteases

The kallikrein (KLK) family of serine proteases has fifteen known secreted tissue kallikrein members. Several members of the KLK family have unique biological functions, while others are yet unknown. KLK1 is involved in normal physiological functions of lung (airway mucus secretion) and kidney (normal tubule transporter activity). KLK2 (human glandular), and KLK3 (prostate-specific antigen) are expressed in prostate tissue and are a normal component of seminal fluid and their levels can serve as a biomarker of prostate cancer. KLK4 (prostase or enamel-matrix protease 1) is involved in normal dental enamel formation. KLK5 (stratum corneum tryptic enzyme), KLK7 (stratum corneum enzyme or chymotryptic enzyme), and KLK10 (normal epithelial-cell-specific 1 protein) are involved in skin desquamation and skin disorders like rosacea. Less is known about the biological functions of KLK6 (also known as protease M, neurosin, zyme, or myelencephalon-specific protease), KLK8 (neuropsin or ovasin), KLK9, KLK11 (hippostatin), KLK12, KLK13, KLK14, and KLK15 (prostinogen). (Prassas *et al.*, 2015)

ii. Kallikrein 6 Structure and Function

Recently, a large effort was undertaken to profile primary cells of the mouse and human brain in their basal state by RNAseq using specific antibody immunopanning (Zhang *et al.*, 2014; Bennett *et al.*, 2016; Zhang *et al.*, 2016). Neurons, astrocytes, microglia, oligodendrocyte precursor cells, and oligodendrocytes were examined. KLK6 mRNA expression was determined to be specific to OPCs/OLs in the brain of both species (Zhang *et al.*, 2014; Bennett *et al.*, 2016; Zhang *et al.*, 2016).

The human gene KLK6 (Entrez: 5653; Ensembl: ENSG00000167755) is at chromosomal location 19q13.3, is 10,483 base pairs long, and contains seven exons (Yousef and Diamandis, 2001). The human protein KLK6 (UniProt: Q92876, hK6) is 244 amino acids long, including a 16 amino acid N-terminal signaling component and a five amino acid pro-peptide that must be cleaved to activate the enzyme (Yousef *et al.*, 1999).

KLK6 knockout animals are slower to develop oligodendrocytes but adults have a similar number compared to wildtype (Murakami *et al.*, 2013), suggesting a role for KLK6 in OL development. These animals also have thinner epidermal cells and reduced keratinocyte proliferation than wildtype (Kishibe *et al.*, 2016). The precise role of KLK6 in normal oligodendrocyte development, maturation, and function is unknown.

Compared to the other members of the KLK family, the binding pocket of KLK6 has been shown to favor binding of proteins with basic amino acids (Prassas *et al.*, 2015). Myelin basic protein, a protein rich in basic amino acids and a key protein present in OLs and CNS myelination, has been shown to be a substrate of KLK6 (Blaber *et al.*, 2002; Magklara *et al.*, 2003; Sharma *et al.*, 2008; Silva *et al.*, 2017). This provides evidence that KLK6 may have a role in mechanisms related to myelination of neuronal axons by OLs.

In patients with multiple sclerosis, an auto-immune neurodegenerative disease that exhibits loss of CNS myelination and OLs, KLK6 levels are elevated in brain (Scarisbrick *et al.*, 2002), cerebrospinal fluid (Hebb *et al.*, 2010), and serum (Scarisbrick *et al.*, 2008) compared to control samples. The role of KLK6 in pathological conditions with abnormal oligodendrocytes and/or myelination, such as multiple sclerosis, is unknown.

Like other serine proteases, KLK6 is secreted in zymogen form and needs to be cleaved to become active. It can both activate and deactivate its own enzymatic activity through auto-cleavage events, although this action may be more favorably achieved through a different protease. (Blaber *et al.*, 2007; Prassas *et al.*, 2015)

Exogenously added KLK6 *in vitro* has been shown to reduce branching of primary rodent OLs, but to have largely no impact on OPCs (Burda *et al.*, 2013).

As previously mentioned, MBP is a direct substrate of KLK6 which is present in OLs but not OPCs.

Other substrates of KLK6 can cause signaling cascades triggering indirect downstream consequences of KLK6 activity. A few KLK family members, including KLK6, have been shown to regulate proteinase-activated receptor (PAR) activation (Oikonomopoulou *et al.*, 2006a; Oikonomopoulou *et al.*, 2006b; Burda *et al.*, 2013). There are four known PARs [proteins: PAR1-4; corresponding to genes F2R, F2RL1-3, respectively] (Noorbakhsh *et al.*, 2003). PAR1 is a tethered ligand G-protein coupled receptor, where cleavage of a tethered signaling peptide is required for its own activation (Cottrell *et al.*, 2002; Trejo, 2003). Using primary OLs from PAR1 knockout mice, it has been shown that a KLK6-induced reduction in OL branching can be partially rescued (Burda *et al.*, 2013). Further, administration of PAR1 agonists alone can block nerve signal conduction in the peripheral nervous system (Shavit *et al.*, 2008). Thus, exacerbation of KLK6 activity may both directly impact OL and myelination in the CNS by targeting key proteins such as MBP, and also through indirect mechanisms such as activation of protease-activated receptor signaling.

The characterization of KLK6 expression has been studied on mature OLs and immature OPCs separately, but not dynamically throughout the process of maturation. Chapter two of this work focuses on elucidating the role of KLK6 in OL maturation. Levels of KLK6 expression are characterized throughout

maturation in rodent primary OPCs derived from neurospheres in response to growth factors and previously described agents of maturation. The consequences of KLK6 pathway activation and inhibition on maturation of OLs are then investigated using these same neurosphere-derived cells.

b) Methods

i. Neurosphere-derived OPCs

Neurospheres were isolated and passaged using methodology generally as previously described (Pedraza *et al.*, 2014). Briefly, embryonic day 15 mouse cortex (C57BL6 #664, Jackson Laboratories) was harvested from timed-pregnant animals. All procedures performed on these animals were in accordance with regulations and established guidelines and were reviewed and approved by the Institutional Animal Care and Use Committee. Neurospheres were cultivated in DMEM/F12 (Gibco 11330032) with Penicillin-Streptomycin (Gibco 15140122), B27 without vitamin A (Gibco 12587010), and 10 ng/mL EGF (Peprotech AF-100-15). To passage, the mouse NeuroCult Chemical Dissociation Kit (StemCell Technologies 5707) was utilized. To cultivate OPCs after passaging, 10 ng/mL bFGF (Peprotech AF-100-18b) and 10 ng/mL PDGF (Peprotech AF-100-13A) were added to media base and cells were grown on poly-d-lysine-coated 6-well or 96-well plates (N=3 wells per treatment group). To mature OPCs to OLs, the

addition of either 3 µM T3 (3,3',5-triiodo-L-thyronine; Sigma-Aldrich T2752) or 3 µM benztropine [Benztropine mesylate; Sigma-Aldrich SML0847; (Deshmukh *et al.*, 2013)] was added to media at plating.

ii. qRT-PCR

To isolate mRNA from cells, RNA isolation kit (Qiagen 74104) was utilized after QIAzol (Qiagen 79306)-chloroform (EMD Millipore CX10577) extraction from 6-well plated cell substrate. A genomic DNA degradation step was included (Qiagen 79254). Samples were assessed for concentration and purity using a Nanodrop instrument and reverse-transcribed to cDNA using SuperScript VILO mastermix (Invitrogen 11755-050). TaqMan assay probes (Life Technologies, see **Table 1**) were run with TaqMan Gene Expression Master Mix (Life Technologies 4370074) using CFX (Bio-Rad) for qRT-PCR. The 2-[Delta][Delta] CT method was utilized to quantify and compare relative gene expression across treatment groups (Livak and Schmittgen, 2001). Statistical analysis (two-way ANOVA or one-way ANOVAs with Dunnett or Sidak post-hoc comparison) was conducted using GraphPad Prism 7.

iii. Immunocytochemistry

To study distinct cell populations across stages of oligodendrocyte maturation, cell samples for immunocytochemistry were fixed with 4% paraformaldehyde and washed with phosphate-buffered saline. Before staining, samples were generally permeated with 0.5% tritonX-100 and blocked with 10% animal normal serum correlating to the host species of intended secondary antibodies. Primary antibodies (see **Table 2**) were incubated at 4 degrees Celsius overnight. The next day, secondary antibodies (AlexaFluor, Life Technologies or Jackson ImmunoResearch) were added, and DAPI (Life Technologies) was used as a counterstain. Plates were imaged using an InCell 5000 (GE) or Cell Discoverer 7 (Zeiss). The total number of MBP positive cells per well and total MBP process length was counted manually for each well or custom-generated algorithm developed using CellProfiler (Kamentsky *et al.*, 2011). The total number of NG2 positive cells per well was obtained using a custom-generated algorithm developed also using CellProfiler.

iv. Test Materials for KLK6, PAR1 Modulation

To modulate kallikrein 6 the following enzyme and inhibitor were used: a) recombinant full-length human KLK6 protein made in HEK293 cells (Abcam ab155642); b) KLK6 inhibitor [MW 548.68, IC_{50} 1.5 µM; table 1, item 5 shown in (Liang *et al.*, 2012a)] synthesized from a previously published virtual screening

effort which identified small molecules with amidinothiophene P1 group structures capable of KLK6 inhibition (Liang *et al.*, 2012a; Liang *et al.*, 2012b; Liang and Bowen, 2016). This is the first known application of the KLK6 inhibitor in biological assays beyond initial demonstration of KLK6 enzyme inhibition.

To modulate protease activated 1 receptor the following activating peptide and small molecule inhibitor were used: a) PAR1-activating peptide, PAR1 AP, (Peptides International PAR-3665-PI), with the sequence H-Thr-Phe-Leu-Leu-Arg-NH2; b) PAR1 selective inhibitor Q94 hydrochloride (Tocris 4755, IC_{50}: ~10-100 nM). Both PAR1 modulators have previously been used to study PAR1 modulation (Asteriti *et al.*, 2012; Burda *et al.*, 2013), although the specific inhibitor has had limited use in assays similar to those employed in the current study.

v. Fluorescence-based dynamic calcium imaging by FLIPR

To assess PAR1AP activity, cells for calcium-based imaging were cultivated as described above, and plated into poly-d-lysine coated 96-well microclear plates (Greiner Bio-One, 655946). Four days prior to imaging, cells were treated with 3 µM T3 (Sigma-Aldrich T2752). Calcium indicator dye kit Fluo-4 NW (Molecular Devices F36206) was used according to manual specifications on the day of the experiment. Just before analysis, a FLIPR Tetra system (Molecular Devices) was used to apply 150 ng/µL PAR1AP (Peptides

International) or 300 nM KLK6 enzyme (Abcam) directly to the test wells in a pre-warmed 37 degrees Celsius environment. Fluorescent readings were recorded every second for the first five minutes (300 seconds) following treatment application. After this time period, timing between fluorescent readings was increased to be captured every minute for the following 25 minutes. Data was captured using ScreenWorks 4.0.0.30 (Molecular Devices) then analyzed as average relative fluorescent units over the time duration specified.

vi. Serine Protease Activity Assay

A systems fluorogenic peptide substrate, Boc-QAR-AMC (R&D Systems, ES014), was utilized in combination with SpectraMax M5^{e} (Molecular Devices) to assess ability of KLK6 enzyme to cleave basic amino acid arginine-AMC bond which creates detectable fluorescence upon cleavage with excitation/emission at 380/460 nm. A kinetic experiment collected readings every minute for 30 minutes using SoftMaxPro Software version 5.4 (Molecular Devices).

vii. RNA Sequencing

RNA from cell experiment treatment groups was isolated using a RNeasy Plus Universal Mini Kit (Qiagen 73404) after QIAzol (Qiagen 79306)-chloroform (EMD Millipore CX10577) extraction. Concentration and purity of RNA were

accessed using a NanoDrop fluorospectrometer (ThermoFisher Scientific). Stranded cDNA libraries were prepared using a TruSeq HT kit (Illumina), and sequenced on a NextSeq 500 (Illumina) at a read depth of 10-20 million reads per sample. FASTQ (reads generated with quality scores for each read) files were aligned to mouse (mm10) genomes using spliced transcripts alignment to reference method (STAR), and differentially expressed genes were determined in R (R Core Team, https://www.R-project.org) using DeSeq2 (Love *et al.*, 2014), and examining statistical significance of genes with a greater than two-fold change and p value of less than 0.05. Analysis of common pathways of altered genes was done using Ingenuity Pathway Analysis (QIAGEN, version 42012434, latest patch June 2017). Pathways were assessed compared to enrichment score [-log(p value], and thus p values at or lower than $p < 0.050$ translate to a enrichment score at or above 1.3.

c) Results

The process of OPC to OL maturation was examined using embryonically-derived mouse neural stem cells cultured as neurospheres and treated with growth factors, then T3, or muscarinic receptor antagonist benztropine (**Figure 1, A-C**). Immunocytochemical cells counts and relative gene expression assessment by qRT-PCR demonstrate that T3 and benztropine treatment promoted maturation of OPCs to OLs, as defined by an increase in the

expression of mature oligodendrocyte markers MBP or MOG (**Figure 1, D,F,G,J,K**). Compared to vehicle (DMSO) treatment, T3 or benztropine resulted in an increase in endogenous KLK6 gene expression, in addition to an increase in genes indicative of oligodendrocyte maturation like MBP and MOG (**Figure 1, F-H, J-L**). In contrast, gene expression of CSPG4 (NG2) present on oligodendrocyte precursors did not statistically significantly change with T3 or benztropine treatment (**Figure 1 E, I**). In samples that were collected every 24 hours for a maximum of 5 days after plating with T3, peak KLK6 expression was similar to the time of peak MBP expression (day 3; **Figure1 F, H**). MOG was also highly expressed at this time compared to vehicle, but peaked at a later time point (day 4; **Figure 1G**). By two-way ANOVA analysis, a statistically significant interaction was seen with KLK6 expression and with MOG expression over 5 days maturation with both time and T3 treatment ($p < 0.001$). The same analysis for MBP expression was statistically significant interaction with treatment ($p < 0.0001$), but only a trend with regard to time ($p = 0.10$), likely due to variability. By two-way ANOVA analysis, only a statistically significant difference with time was seen with CSPG4/NG2 over the course of maturation ($p < 0.0001$; **Figure 1E**). This latter effect likely reflects factors in culture such as continuation of exposure to growth factors and culture density. A separate experiment was done to statically examine just the timepoint of maturation between 3-4 days with T3 or benztropine treatment compared to DMSO (**Figure 1, I-L**). The same

patterns emerged: no change in CSPG4/NG2 between treatment at this timepoint (**Figure 1I**), indicating that treatment-dependent changes on OPCs are unlikely to be present. Benztropine and T3 both statistically significantly increased MBP expression by five-fold compared to vehicle (DMSO), indicating increases in a gene associated with mature oligodendrocytes (**Figure 1J**). Similar or greater effect size increases were seen with MOG and KLK6 expression with benztropine or T3 maturation of OPCs at this timepoint as well (**Figure 1K-L**). Taken together, these data suggest that KLK6 is more highly expressed at the same time when mature oligodendrocytes genes are expressed.

To examine the consequences of high KLK6 expression, exogenous enzymatically active KLK6 (**Figure 2A**) or PAR1AP **(Figure 2B-C**) was utilized to mimic upregulation of KLK6 in OPCs over the course of their maturation to OLs. The number of OLs, defined as MBP-positive cells per well, was decreased with either KLK6 or PAR1AP treatment (**Figure 2D**). The MBP-positive cell mean process length was also reduced with PAR1AP treatment, but this effect was not seen with KLK6 **(Figure 2E)**. Thus, the data suggest that KLK6 has a negative effect on mature oligodendrocytes.

To examine the role of KLK6 inhibition on OPC to OL maturation, a KLK6 inhibitor was used. First, it was determined that pre-incubation with a KLK6 inhibitor could block KLK6 enzyme cleavage activity in a cell-free assay (**Figure 2F**). As a control, pre-incubation of a PAR1 inhibitor did not block KLK6 activity in

the same assay. Next, the KLK6 inhibitor was applied to OPCs with or without the presence of T3. KLK6 inhibition increased the number of cells positive for mature oligodendrocyte marker MBP (**Figure 2G, O,** green) and OPC marker NG2 (**Figure 2I, O,** red). However, the largest effect size, a 50% increase, was seen in MBP positive cell count when comparing T3 to T3/KLK6i combination treatment (**Figure 2 G, P,** green). Compared to T3 treatment alone, T3/KLK6i treatment also increases the median MBP-positive cell process length in a statistically significant fashion (**Figure 2H**). Overall, these data suggest that KLK6 inhibition can promote an increase in oligodendrocytes, and potentially more so in the presence of other maturation factors. To understand the differences between the T3 and T3/KLK6i combination treatments, RNA from a similar experimental design was analyzed using RNAseq and Ingenuity Pathway Analysis. **Table 3** demonstrates the top 5 canonical pathways elevated across treatment contrasts where T3/KLK6i has a larger enrichment score compared to T3 alone. All five of these pathways reflect changes in genes relevant to cholesterol biosynthesis.

To examine whether PAR1 inhibition could mediate similar effects as KLK6i inhibition, application a PAR1 inhibitor was applied to OPCs in a similar experiment. PAR1 inhibition did not increase gene expression of MBP or NG2 relative to T3 alone treatment or when combined with T3 treatment (**Figure 2J, L,**

S-T). Additionally, PAR1 inhibition did not impact process length of MBP positive cells in culture (**Figure 2K**).

d) Discussion

In chapter two of this work the endogenous levels of KLK6 are examined in response to maturation of primary murine neural stem cell-derived oligodendrocytes. Over the course of maturation of oligodendrocytes from neural stem cells I found that peak KLK6 expression levels during maturation *in vitro* are associated with early myelinating oligodendrocytes that express MBP. Expression of KLK6 decreases in more mature oligodendrocytes as determined by MOG messenger RNA levels. Taken together, these data suggest that in an *in vitro* system of primary rodent oligodendrocyte maturation, KLK6 is most highly associated with myelinating oligodendrocytes instead of oligodendrocyte precursor cells or more mature oligodendrocytes. This dynamic examination of KLK6 expression throughout maturation of oligodendrocytes complements previously published static data which has demonstrated KLK6 expression in newly-differentiated to myelinating rodent primary oligodendrocytes obtained via RNA sequencing analysis by immunopanning technique and single-cell level isolation methods (Zhang *et al.*, 2014; Zeisel *et al.*, 2015).

The use of neural stem-cell derived primary rodent oligodendrocytes as a model allows for a more high-throughput investigation in of maturation than in

isolated primary cells because neural stem cells are a continuously regenerative source of starting material. This approach also allows for the exploration of oligodendrocyte dynamics *in vitro* while in a heterogeneous environment that includes other cells types such as oligodendrocyte precursor cells and astrocytes. Unlike the cellular environment *in vivo,* this paradigm does not include the contributions of neurons, an important component in oligodendrocyte maturation and myelination. Another caveat of this model of oligodendrocyte maturation is that the process of maturation is artificially induced. The neural stem cells are driven towards oligodendrocyte precursors with growth factors present endogenously during maturation, and matured to oligodendrocytes with exogenous differentiation factors (like thyroid hormone T3 and muscarinic antagonist benztropine). Immunopanning is an example of a technique in which cells can be isolated at their current state of maturation versus artificial induction, although this process results in fewer cells and involves manipulation that may damage cells. The similarities of the overall results of KLK6 expression inquiry using these different techniques suggests that the result is reproducible and the *in vitro* maturation model system comparably models *in vivo* maturation. Further, the high expression level of KLK6 has now been shown by *in vivo* maturation and two different exogenous maturation factors: T3 and muscarinic antagonist benztropine. It remains to be further explored whether different maturation environments or agents produce different levels of KLK6 or whether KLK6 is

driven by oligodendrocyte maturation state. The result of the timecourse experiments with T3 treatment suggests that KLK6 expression may be driven by oligodendrocyte maturation state. Although the data within this work could be interpreted as benztropine induces a higher level of KLK6 expression than T3, another explanation is that different concentrations of each agent result in maturation differences driven by potency or mechanism at the same time point analyzed.

The next question is what are the functional consequences of elevated KLK6 expression? It is known that KLK6 levels are increased in normal newly-differentiating and mature oligodendrocytes (Zhang *et al.*, 2014; Zeisel *et al.*, 2015; Zhang *et al.*, 2016). In addition, KLK6 has been shown to be increased in multiple sclerosis patients compared to control (Scarisbrick *et al.*, 2002; Scarisbrick *et al.*, 2008; Hebb *et al.*, 2010). However, multiple sclerosis patients generally have less myelination and less mature oligodendrocytes (Lucchinetti *et al.*, 1999). Does KLK6 promote or refine maturation by oligodendrocytes or does it negatively regulate maturation? KLK6 knockout animals have been found to be largely normal (Murakami *et al.*, 2013). However, early in development (P7) they showed a slight delay in maturation that was resolved by P14 (Murakami *et al.*, 2013). They also showed that after white matter injury, KLK6 knockout animals had less white matter damage as indicated by increased MBP expression (Murakami *et al.*, 2013). These results suggest that the absence or abundance of

KLK6 may negatively regulate maturation of oligodendrocytes and myelination. MBP, a protein found on mature oligodendrocytes, has been shown to be a substrate of KLK6 (Blaber *et al.*, 2002), which provides rationale for why an abundance of KLK6 could be result in a decrease of myelination, as in seen in MS patients. Exogenous KLK6 has also been shown to decrease branching in mature rodent oligodendrocytes, with no impact on oligodendrocyte number (Burda *et al.*, 2013).

After validating the activity of a commercially available human full length recombinant KLK6 enzyme to cleave basic amino acids, I applied the enzyme to neural stem cell-derived OPCs in the presence of maturation factor T3. I found that the exogenous application of KLK6 decreased the number of MBP-positive oligodendrocytes over a 4 day maturation period. In contrast to previous literature, exogenous application of KLK6 did not decrease the amount of branching of MBP-positive cells during the same period. The results suggest that application of exogenous KLK6 negatively regulates oligodendrocyte maturation. However, a decrease in number of oligodendrocytes and decreased branching of oligodendrocytes could point to either a lack of oligodendrocyte maturation or an increase in cellular pathology and death. Burda et al. demonstrated that exogenous application of KLK6 to primary oligodendrocytes increased exogenously-introduced ATP excitotoxicity while also decreasing structural complexity of the cells and resulting in a decrease of oligodendrocytes (Burda *et*

al., 2013). I evaluated whether levels of lactate dehydrogenase (LDH) increased in cell media due to cell death after KLK6 application, and did not see a difference between treatment and control (data not shown). However, this result could be due to the dilution and heterogeneous nature of the maturation culture model. Current data from the combined studies suggests that although KLK6 can exacerbate cell death, it doesn't directly promote it on its own. Thus, KLK6 is likely negatively impacting maturation of OPCs to oligodendrocytes.

Differences in phenotypes observed with exogenous KLK6 application between this work and the literature (such as changes in cell number vs. branching complexity) could be attributed to different assay parameters. For example, I examined MBP as an oligodendrocyte marker in neural stem cell-derived OPC cultures while Burda et al. examined sulfatide (O4) in mixed glia derived OPC cultures. Distribution of staining is unlikely to be the same due to the nature of MBP as a protein and sulfatide as a sulfated form of lipid galactocerebroside (Coetzee *et al.*, 1996). It is likely that using a lipid marker would result in more robust resolution of myelin structure and oligodendrocyte branching, especially as it is one of the earlier markers of oligodendrocyte maturation, is expressed before MBP, and can impact MBP function in packing myelin (Dyer *et al.*, 1997). Thus, fewer cells may be staining with MBP versus O4, and the cells may represent different time points in maturation. Additionally, different treatment and analysis paradigms were utilized, with my paradigm being

slightly stronger in concentration and longer in duration. This might result in visualization of a more pronounced (cell loss) phenotype compared to the decreased branching phenotype observed with a shorter incubation by Burda et al. Further, the KLK6 enzymes across the studies were from different species: human versus mouse. Alignment of protein for human (NP_002765) and mouse (NP_001158170) KLK6 demonstrates only 68% homology across species via NCBI BLAST (http://blast.ncbi.nlm.nih.gov/Blast.cgi), which could be associated with functional consequences across species.

In order to determine if the negative effect of KLK6 on oligodendrocyte maturation could be blocked, a small molecule KLK6 inhibitor was identified in the literature and synthesized (Liang *et al.*, 2012a). In a cell-free assay, the KLK6 inhibitor was confirmed to block KLK6 enzyme activity from cleaving basic amino acids. Next, the KLK6 inhibitor was applied to neural stem cell-derived OPCs at twice the concentration of the IC_{50} (1.5 µM; 3 µM) with and without exogenous maturation agent T3. I found that the KLK6 inhibitor increased the number of MBP-positive oligodendrocytes in culture and the number of NG2-positive OPCs in culture. There was a trend for an increase in MBP-positive cell branch length with KLK6 inhibitor treatment, but it did not achieve statistical significance at $p = 0.055$. When combined with T3, the KLK6 inhibitor increased the number of MBP-positive oligodendrocytes compared to either treatment alone. Additionally, the combination treatment increased the total branching length of MBP-positive

cell processes per cell compared to T3 treatment alone, indicating the cells to have greater complexity. The number of NG2-positive OPCs did not differ between the T3 alone and combined treatment conditions, indicating that KLK6 inhibitor treatment could not maximize maturation at this stage compared to T3 alone. This is the first demonstration of a KLK6 small molecule inhibitor to enhance maturation of oligodendrocytes *in vitro*. Previously, KLK6-neutralizing antibodies have been shown to enhance myelination in the spinal cord during early stages of a viral model of demyelination (Scarisbrick *et al.*, 2012b). It is expected that an increase in branching and number of oligodendrocytes would translate to an increase in myelination, but this remains to be evaluated in *in vitro* model systems such as dorsal root ganglion neuron/OPC co-cultures or *in vivo*.

To determine the mechanism by which the combination of KLK6 inhibitor and T3 treatment synergistically increased MBP expression compared to either treatment alone, RNA sequencing was conducted on a separate cohort of cells run in a similar way as the experiment where analysis was done at the protein level. Then, Ingenuity Pathway Analysis was used to examine expression changes in common canonical biological pathways of genes across treatment contrasts. The five top pathways with highest enrichment score for the combination treatment are all involved in cholesterol synthesis. Additionally, the enrichment scores across comparisons reflect the same pattern seen with the protein cohort: lowest enrichment with KLK6 inhibitor alone, higher enrichment

with T3 alone, and highest enrichment with the combination of the two. Given this finding, future research might include lipidomics analysis to see whether differential lipid structures are being produced in response to combination treatment.

Cholesterol synthesis in the brain, unlike elsewhere in the body, is derived largely from astrocytes instead of from diet due to the blood-brain barrier (Kiray *et al.*, 2016). Thus, by extension it is hypothesized that KLK6 inhibition enhances maturation of oligodendrocytes by promoting astrocyte synthesis of cholesterol. Although the neural stem cell model system being used favors development of OPCs and oligodendrocytes, astrocytes and oligodendrocytes are derived from a shared developmental precursor (Li *et al.*, 2016), and GFAP-positive astrocytes are present within the cultures (data not shown).

It has previously been reported that KLK6 signaling is at least partially mediated through the protease-activated receptor 1 (PAR1), which then activates the ERK pathway and ultimately results in modulation of calcium ions (Burda *et al.*, 2013). I validated activity of a PAR1-activating peptide (PAR1AP) to induce calcium release in neural stem-cell derived OPCs/oligodendrocytes using a calcium-sensitive dye and FLIPR. Under the parameters tested, PAR1AP induced a calcium response with the first five minutes, but a KLK6 enzyme, whose ability to cleave proteins also validated, did not elicit a calcium response

within 30 minutes. This suggests that a mechanism link between KLK6 and PAR1 that elicits calcium modulation is not direct. However, it could also be that the concentration KLK6 enzyme used was not sufficient or comparable to the amount of PAR1AP used, as PAR1AP is a direct agonist of the pathway. When I applied the PAR1AP to neural stem cell-derived OPCs in the presence of T3, I found the number of MBP-positive cells and the length of MBP-positive branching per cell to be decreased. This corroborates the literature finding that PAR1AP reduces branching of oligodendrocytes as visualized using sulfatide (O4) (Burda *et al.*, 2013). It is also a similar finding to what was achieved with the KLK6 enzyme in this work: both reduced oligodendrocyte maturation in neural stem cell-derived OPCs despite the presence of T3. If the PAR1AP is more direct stimulation of a downstream pathway, this could also explain a more pronounced phenotype in that decreased MBP branching was a result with PAR1AP but not with KLK6 treatment.

To evaluate if PAR1 inhibition can enhance oligodendrocyte maturation, a commercially available small molecule PAR1 inhibitor was obtained. It was evaluated against KLK6 enzyme in a cell-free activity assay to determine if the PAR1 inhibitor could block KLK6 cleavage and it was found that it could not. The PAR1 inhibitor (IC_{50} 10-100 nm) was applied at two concentrations: 100 nm and 500 nm. Neither concentration alone or in combination with maturation agent T3 elicited a change in number of MBP-positive oligodendrocytes, NG2-positive

OPCs, or in MBP process length compared to vehicle treatment. Thus, while PAR1AP induced deficits in oligodendrocyte maturation *in vitro*, inhibition with this PAR1 inhibitor did not enhance maturation. Because this compound has been shown to modulate PAR1-specific calcium signaling (Asteriti *et al.*, 2012), and because it was dosed well above the IC_{50}, alternate explanations include that the pathway cannot be modulated in the reverse direction, or that the model system of oligodendrocyte maturation that is being used leaves out an important component required for inhibitor modulation and perhaps it would be efficacious in a more holistic environment (such as *in vivo*). However, a different PAR1 inhibitor (SCH79797) has been recently found to promote maturation of OPCs *in vitro* (Yoon *et al.*, 2015). The two compounds are structurally distinct, although they have similar IC_{50}s, and are both reported to be PAR1-selective compared to other PAR receptors (2-4). The reason why this particular PAR1 inhibitor was chosen for this work was ultimately so we could test the compound in *in vivo* myelination assays, as its chemical structure suggested it was the most likely to be brain penetrant compared to other commercially available PAR1 inhibitors (J. Tuttle, B. O'Neill, personal communication). To better compare and contrast properties of these PAR1 inhibitors, it would be ideal to test them at the same time in the OPC maturation assay, and to further profile these compounds for specific binding and selectivity differences. Because use of PAR1 knockout mouse oligodendrocytes reduce pathology induced by KLK6 enzyme in culture

compared to wildtype (Burda *et al.*, 2013), further development towards a single small molecule that is both brain-penetrant and selectively inhibits PAR1 may be a useful secondary approach to inhibiting KLK6.

In summary, the work within this chapter demonstrates KLK6 to be a negative regulator of oligodendrocyte maturation *in vitro*, and identifies a KLK6 inhibitor that promotes oligodendrocyte maturation. The effects of the KLK6 inhibitor are synergistic in the presence of another maturation agent (T3) than either agent alone, and this is likely due to enhancement of astrocyte cholesterol synthesis pathway. Next steps include testing whether KLK6 inhibition can also promote myelination in addition to oligodendrocyte maturation.

Additionally, KLK6 downstream impact on oligodendrocyte pathway has been previously shown to be partially mediated through PAR1. A PAR1AP demonstrated that exogenous agonism of PAR1 resulted in decreased oligodendrocyte maturation. A PAR1 inhibitor was unsuccessful at enhancing oligodendrocyte maturation in the *in vitro* model. Although it is expected that the results of test compounds in the oligodendrocyte maturation *in vitro* assay will inform likelihood of success in an *in vivo* myelination model, this is a prediction until it is tested.

Full Name	Gene Name	Catalog Code	Dye
Chondroitin sulfate proteoglycan 4 (Neural/Glial proteoglycan antigen 2)	CSPG4	Mm00507257_m1	FAM
Glyceraldehyde 3-phosphate dehydrogenase	GAPDH	4352339E	VIC
Kallikrein 6	KLK6	Mm00478322_m1	FAM
Myelin basic protein	MBP	Mm01266402_m1	FAM
Myelin oligodendrocyte glycoprotein	MOG	Mm00447824_m1	FAM
Plate-derived growth factor receptor alpha	PDGFRa	Mm00440701_m1	FAM

Table 1. qRT-PCR TaqMan Primer Assays

Full Name	Short Name	Vendor	Catalog Code	Host Species	Tissue Tested Species
Myelin Basic Protein	MBP	AbD Serotec	MCA409S	Rat	Mouse, Human
Neural/Glial proteoglycan antigen 2	NG2	Millipore	AB5320	Rabbit	Mouse, Human

Table 2. Chapter 2 Antibody Information

Canonical Pathway	KLK6i vs DMSO	T3 vs DMSO	KLK6i T3 vs T3	KLK6i T3 vs KLK6i
Superpathway of Cholesterol Biosynthesis	0.5010	**5.2434**	**15.5056**	1.0993
Cholesterol Biosynthesis I	0.7923	**4.5960**	**11.9348**	1.0527
Cholesterol Biosynthesis II	0.7923	**4.5960**	**11.93487**	1.0527
Cholesterol Biosynthesis III	0.7923	**4.5960**	**11.9348**	1.0527
Zymosterol Biosynthesis	1.108	**3.2463**	**5.3883**	1.0782

Table 3. Top 5 canonical pathways of OPC altered gene expression with KLK6/T3 treatment versus T3 alone

Table 3 values demonstrate enrichment scores within canonical pathways from Ingenuity Pathway Analysis. Enrichment score is representative of a negative log of the associated p value based on RNAseq data. Thus, a p value of p = 0.050 is equal to a score of 1.3, and as the p value becomes smaller in magnitude than p = 0.050, the enrichment score becomes larger in magnitude than 1.3. The top 5 canonical pathways are shown that demonstrate RNA changes with KLK6/T3 treatment compared to the treatments alone on stem cell-derived OPCs in culture.

Figure 1. Peak of KLK6 Expression in Oligodendrocyte Maturation is Similar to MBP Peak of Expression.

To examine maturation of oligodendrocytes *in vitro*, embryonically-derived mouse neural stem cells were passaged as neurospheres (**A**; brightfield, 200 µm scale bar). Growth factors were used to commit cell lineage to oligodendrocyte precursor cells (**B**; red, NG2, 50 µm scale bar), whereupon they were plated and used for maturation experiments. Thyroid hormone T3 and muscarinic antagonist benztropine have been previously shown in the literature to mature oligodendrocyte precursor cells to oligodendrocytes. **C:** An example of a mature oligodendrocyte (green, MBP, 50 µm scale bar) in culture by T3 or benztropine. **D:** Quantification of number of MBP-positive cell T3-mediated maturation versus vehicle control, stained by immunocytochemical methods (n = 3-12 ninety-six wells per treatment). **E-L**: OPCs were treated with T3, benztropine, or vehicle and incubated for up to five days with samples taken for mRNA expression analysis by qRT-PCR (n = 3 six-wells per timepoint/treatment). All expression data is normalized by GAPDH control. **E-H**: A five-day timecourse illustrates KLK6 mRNA expression to be increased in T3-treated OPCs at day 3 compared to vehicle treatment. This is notably similar to oligodendrocyte data shown with MBP expression. Peak MOG expression, expressed later than MBP in maturation, is right-shifted compared to both KLK6 and MBP expression. NG2 (CSPG4) expression is unaffected by T3 maturation of OPCs but increases over

time, likely due to factors such as cell density and continued presence of growth factors. **I-L**: Static timepoint four days after benztropine or T3 administration to OPCs shows statistically significant increases in KLK6, MBP, and MOG (but not NG2/CSPG4) expression compared to vehicle treatment. Statistical analyses were done using two-way ANOVA or one-way ANOVA with Dunnett post-hoc comparison. All graphs within the figure represent the data as mean plus or minus the standard error of the mean.

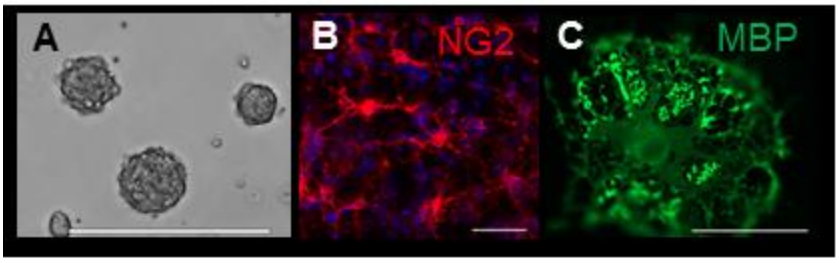

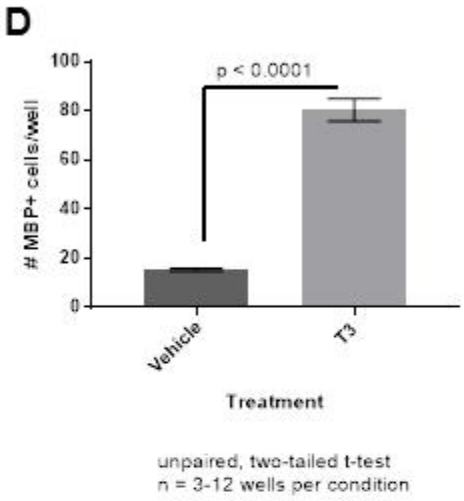

unpaired, two-tailed t-test
n = 3-12 wells per condition

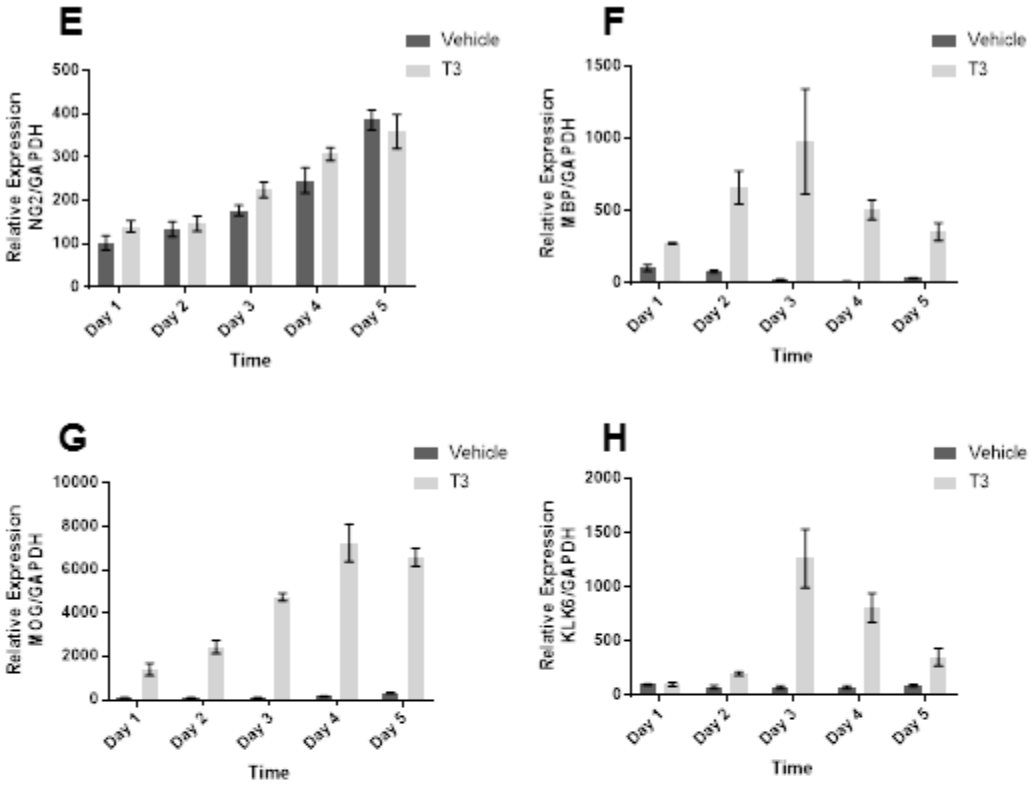
E
Vehicle
T3
Relative Expression
NG2/GAPDH
500
400
300
200
100
0
Day 1
Day 2
Day 3
Day 4
Day 5
Time
F
Vehicle
T3
Relative Expression
MBP/GAPDH
1500
1000
500
0
Day 1
Day 2
Day 3
Day 4
Day 5
Time
G
Vehicle
T3
Relative Expression
MOG/GAPDH
10000
8000
6000
4000
2000
0
Day 1
Day 2
Day 3
Day 4
Day 5
Time
H
Vehicle
T3
Relative Expression
KLK6/GAPDH
2000
1500
1000
500
0
Day 1
Day 2
Day 3
Day 4
Day 5
Time

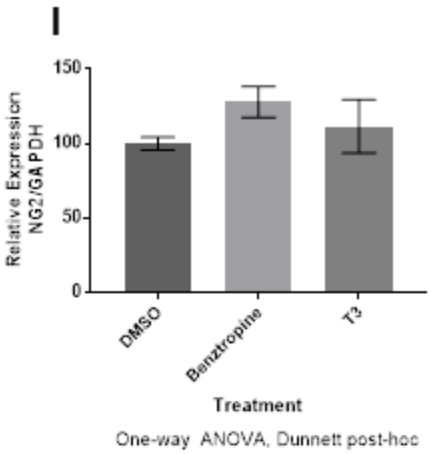
I
Relative Expression
NG2/GAPDH
150
100
50
0
DMSO
Benztropine
T3
Treatment
One-way ANOVA, Dunnett post-hoc

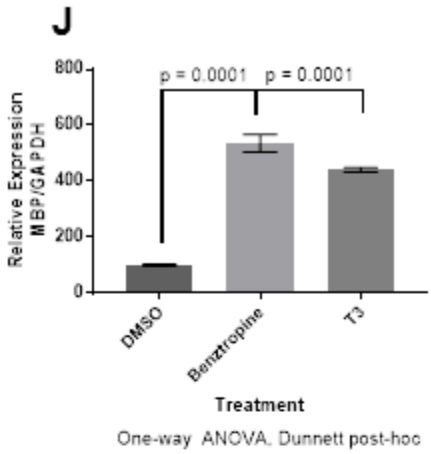
J
Relative Expression
MBP/GAPDH
p = 0.0001
p = 0.0001
800
600
400
200
0
DMSO
Benztropine
T3
Treatment
One-way ANOVA, Dunnett post-hoc

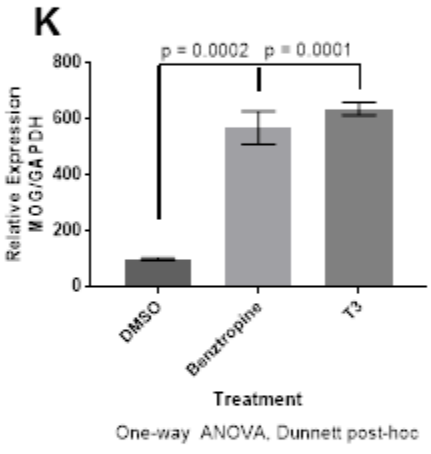
K
Relative Expression
MOG/GAPDH
p = 0.0002
p = 0.0001
800
600
400
200
0
DMSO
Benztropine
T3
Treatment
One-way ANOVA, Dunnett post-hoc

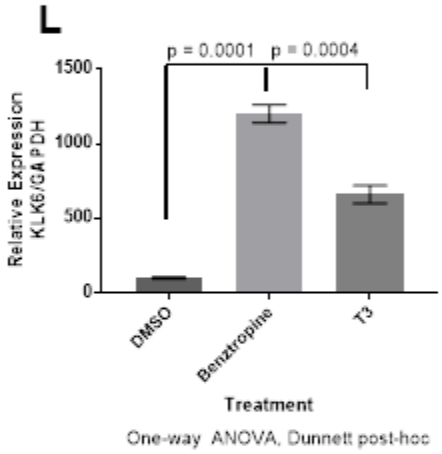
L
Relative Expression
KLK6/GAPDH
p = 0.0001
p = 0.0004
1500
1000
500
0
DMSO
Benztropine
T3
Treatment
One-way ANOVA, Dunnett post-hoc

Figure 2. Exogenous Activation of KLK6 Pathway Decreases OL-Related Markers; Inhibition of KLK6 Increases OL-Related Markers

A: Recombinant full-length human KLK6 protein is determined to be enzymatically active using Boc-QAR-AMC serine protease cleavage assay. **B-C:** T3 (3 µM) was applied to OPCs for 3-4 days whereupon Fluo-4 calcium dye was added and then fluorescence was monitored in response to enzymatically-active KLK6 (300 nM) or PAR1 Activating-Peptide (PAR1AP; 150 ng/µL) using a FLIPR Tetra (every second for the first 5 minutes, every minute for the following 25 minutes). PAR1AP but not KLK6 enzyme induces a calcium response in OPCs / OLs. **D-E**: Enzymatically-active KLK6 (300 nM) or PAR1AP (150 ng/µL) was applied to OPCs and incubated in the presence of T3 for 3-4 days, whereupon samples were collected for immunocytochemical analysis. **D**: The number of MBP+ cells/well is decreased with either PAR1AP or active KLK6 treatment. **E**: The mean length of processes on MBP+ cells was reduced with PAR1AP treatment, but not KLK6 treatment. **F**: Pre-incubation of an inhibitor of KLK6 blocks activity of KLK6 in a cell-free assay. As expected, pre-incubation of a PAR1 inhibitor does not block KLK6 activity. N = 2 ninety-six wells per treatment condition. Statistical analyses were done using a one-way ANOVA with a Dunnett post-hoc comparison. **G-T:** OPCs were plated and incubated with vehicle (DMSO), T3 (3 µM), KLK6 inhibitor (3 µM), PAR1 inhibitor (100 or 500 nM), or T3/test compound combination for 3-4 days & then stained for MBP &

NG2. KLK6 inhibition increased the number of MBP+ (green) and NG2+ (red) cells. However, a larger increase was seen in combination with T3 treatment (MBP+ cells & length of MBP+ processes). PAR1 inhibition did not have an impact on number of NG2+ cells or number of cells and length of processes in MBP+ cells. N = 6 ninety-six wells per treatment condition. Statistical analyses were done using a one-way ANOVA with a Sidak post-hoc comparison. Scale bar = 100 µm. All graphs within the figure represent the data as mean plus or minus the standard error of the mean.

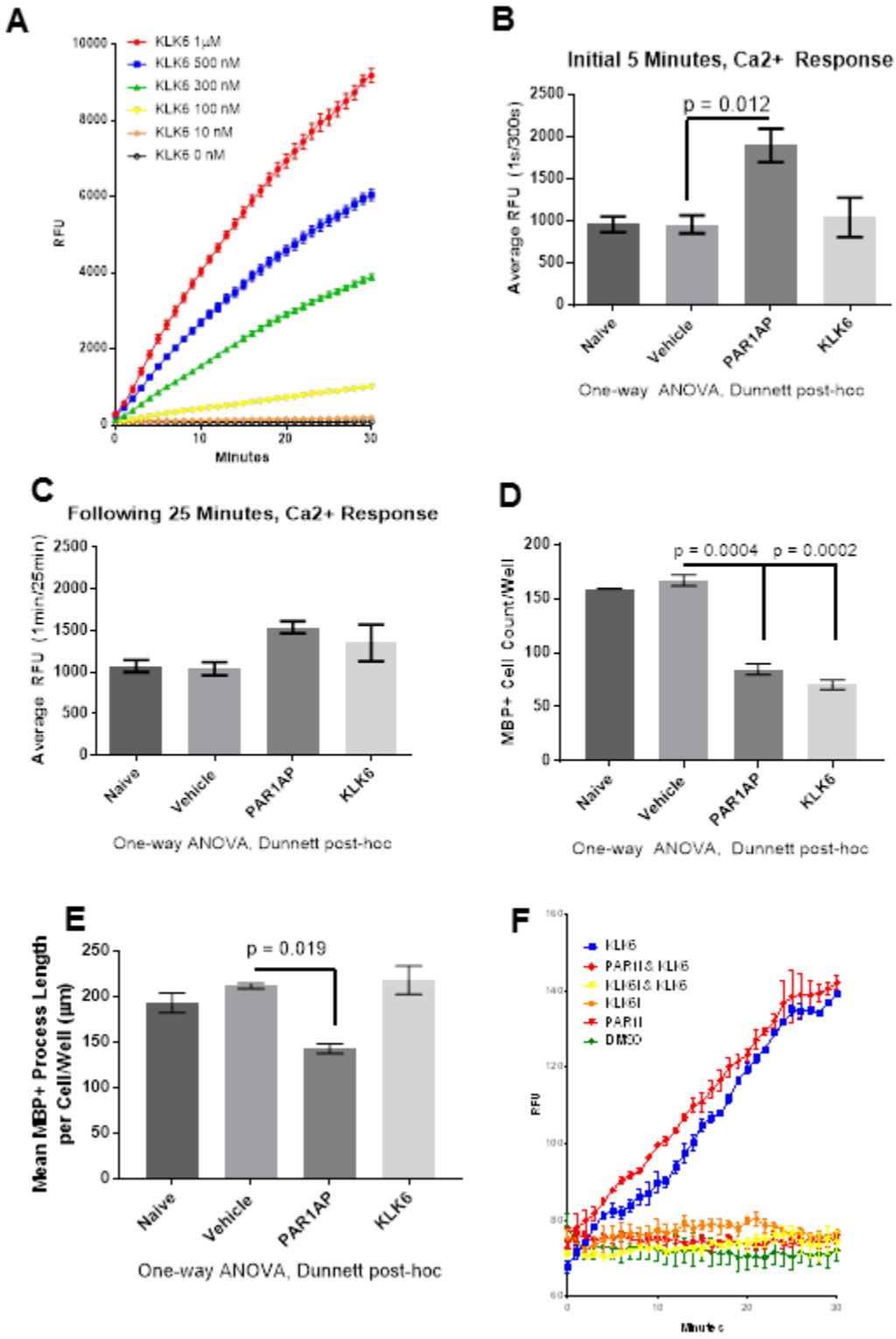
A
KLK6 1μM
KLK6 500 nM
KLK6 300 nM
KLK6 100 nM
KLK6 10 nM
KLK6 0 nM
RFU
Minutes
B
Initial 5 Minutes, Ca2+ Response
p = 0.012
Average RFU (1s/300s)
Naive
Vehicle
PAR1AP
KLK6
One-way ANOVA, Dunnett post-hoc
C
Following 25 Minutes, Ca2+ Response
Average RFU (1min/25min)
Naive
Vehicle
PAR1AP
KLK6
One-way ANOVA, Dunnett post-hoc
D
p = 0.0004
p = 0.0002
MBP+ Cell Count/Well
Naive
Vehicle
PAR1AP
KLK6
One-way ANOVA, Dunnett post-hoc
E
p = 0.019
Mean MBP+ Process Length per Cell/Well (μm)
Naive
Vehicle
PAR1AP
KLK6
One-way ANOVA, Dunnett post-hoc
F
KLK6
PAR1I & KLK6
KLK6I & KLK6
KLK6I
PAR1I
DMSO
RFU
Minutes

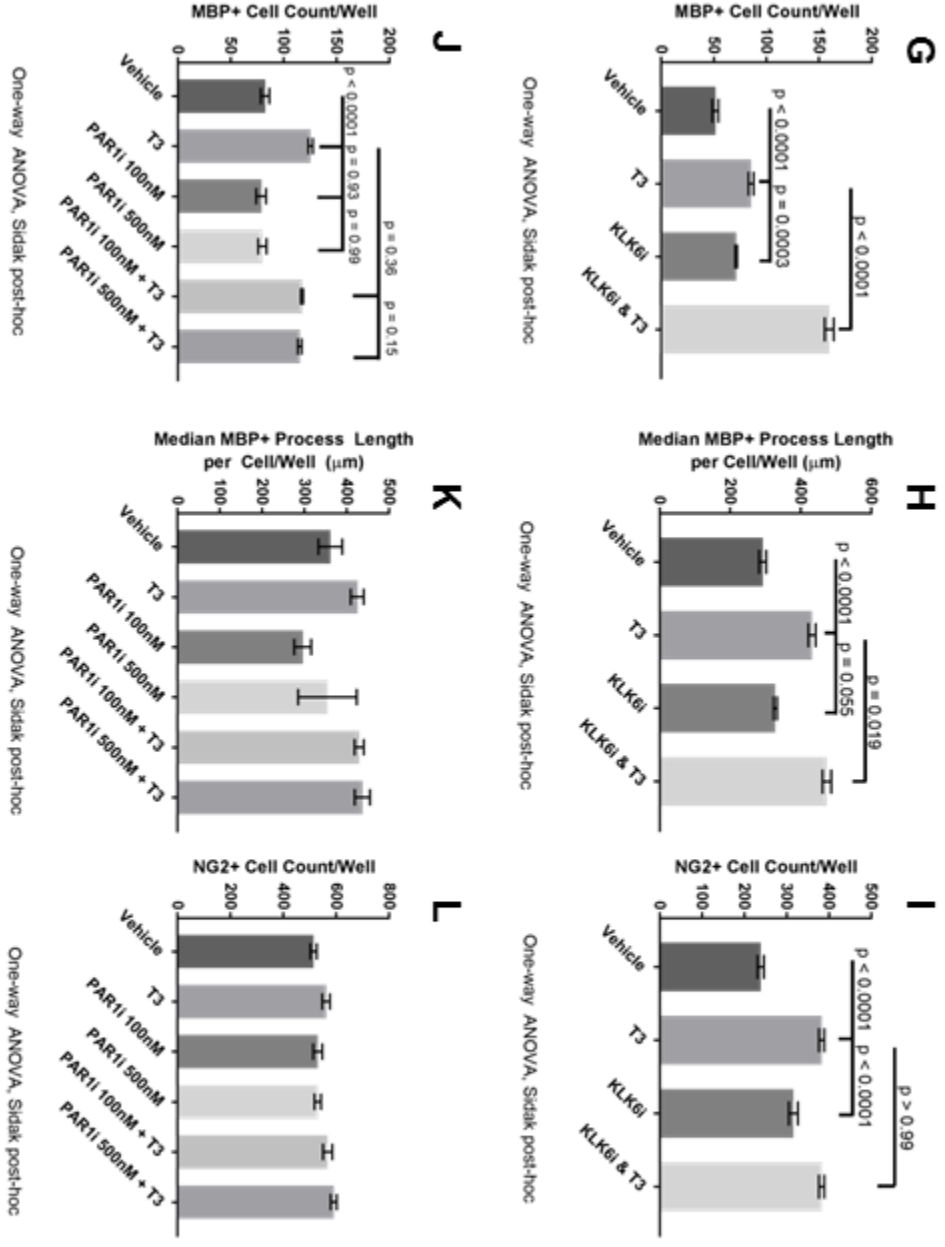
G
MBP+ Cell Count/Well
Vehicle
T3
KLK6i
KLK6i & T3
p < 0.0001
p < 0.0001
p = 0.0003
One-way ANOVA, Sidak post-hoc
H
Median MBP+ Process Length per Cell/Well (μm)
p < 0.0001
p = 0.055
p = 0.019
One-way ANOVA, Sidak post-hoc
I
NG2+ Cell Count/Well
p < 0.0001
p < 0.0001
p > 0.99
One-way ANOVA, Sidak post-hoc
J
MBP+ Cell Count/Well
PAR1i 100nM
PAR1i 500nM
PAR1i 100nM + T3
PAR1i 500nM + T3
p < 0.0001
p = 0.93
p = 0.99
p = 0.36
p = 0.15
One-way ANOVA, Sidak post-hoc
K
Median MBP+ Process Length per Cell/Well (μm)
One-way ANOVA, Sidak post-hoc
L
NG2+ Cell Count/Well
One-way ANOVA, Sidak post-hoc

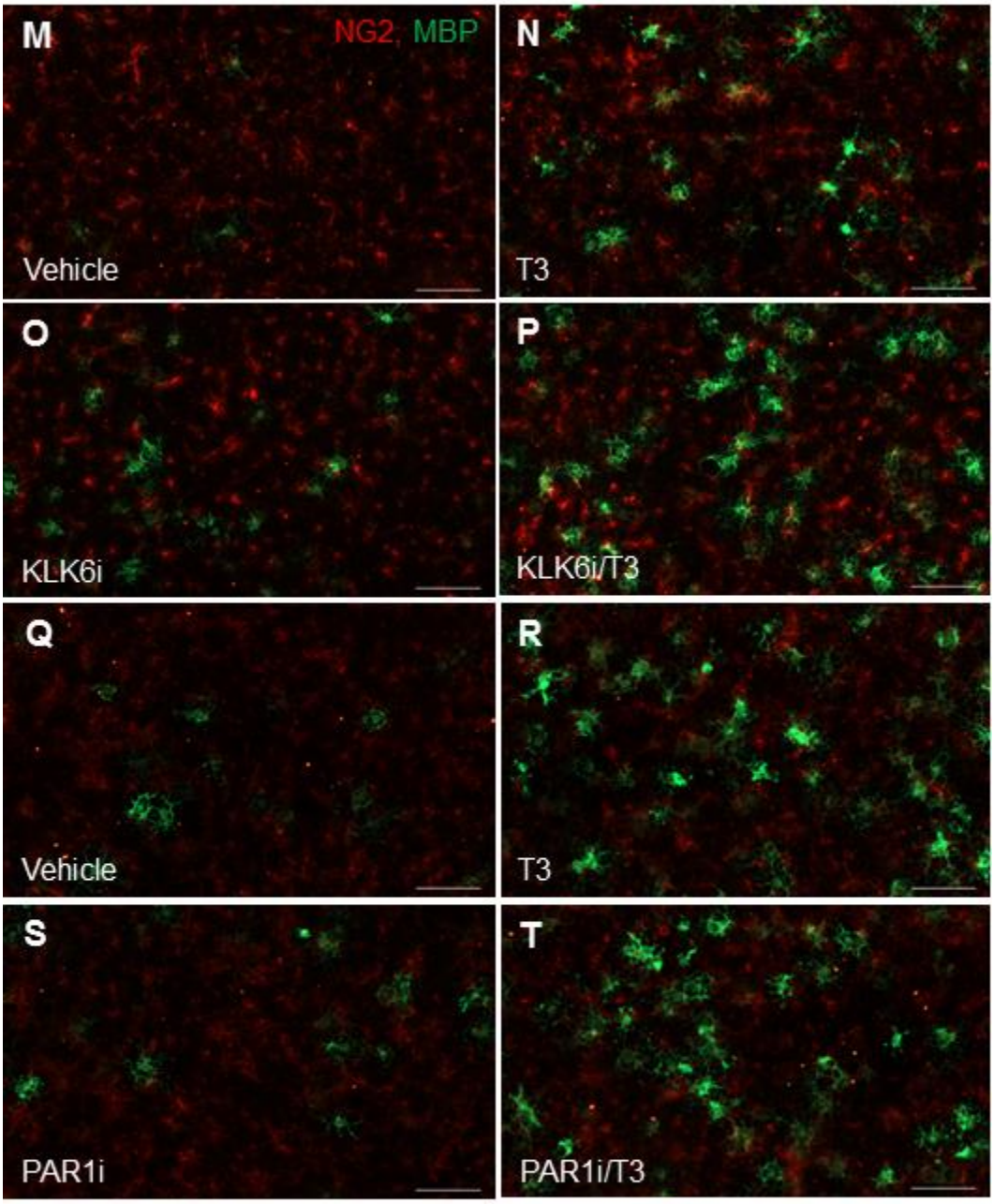
M
NG2, MBP
Vehicle
N
T3
O
KLK6i
P
KLK6i/T3
Q
Vehicle
R
T3
S
PAR1i
T
PAR1i/T3

CHAPTER THREE

Kallikrein 6 in Oligodendrocyte Myelination

a) Introduction

i. Animal Models of Oligodendrocyte Demyelination & Remyelination

Several *in vivo* assays model aspects of demyelination in rodents and are used with the hope of understanding and reversing pathology in a mammalian species similar enough to apply findings to human patients, such as those with chronically demyelinating disorder multiple sclerosis (MS). Neuroinflammation is a significant contributor to MS pathology (Dendrou *et al.*, 2015). Models such as experimental autoimmune encephalomyelitis (EAE) and Theiler's murine encephalomyelitis virus (TMEV) are used to study remyelination in the context where demyelination is a direct consequence of induced inflammation in the CNS (Ransohoff, 2012).

The EAE model is one of the most extensively used to study demyelination and potential therapies for MS. Similar to MS, the EAE model induces demyelination of white matter tracts through inflammation-driven processes that involve T lymphocytes. There are multiple paradigms in which the EAE model can be established; paradigms to create the EAE model generally include the peripheral injection of inflammation-inducing agents (e.g. complete/incomplete Freud's adjuvant, *mycobacterium tuberculosis*, pertussis

toxin) in conjunction with a myelin protein peptide (e.g. MOG_{35-55}, MBP_{84-104}, $PLP_{178-191}$) (McCarthy *et al.*, 2012). In this way, an immune response is directed at a component of myelin. Demyelination and inflammation depends on the major histocompatibility complex type of the mouse strain and antigen provided. For example, in C57BL6 mice MOG_{35-55} primarily demyelinates white matter of the spinal cord and not the brain; in SJL/J mice $PLP_{139-151}$ leads to demyelination in both the brain and spinal cord (Constantinescu *et al.*, 2011). In addition to demyelination and T cell infiltration visible by immunohistochemistry, the EAE model induces behaviorally observed motor deficits. Depending on the parameters of induction, paralysis can take two to four weeks to plateau; paralysis is scored by grades 0-5 where grade 0 is no paralysis, grade 2 is both hind limb and tail weakness, grade 4 is full hind limb paralysis, and grade 5 is complete limb paralysis (McCarthy *et al.*, 2012; Rangachari and Kuchroo, 2013).

The TMEV model of progressive demyelination (also termed TMEV-induced demyelinating disease) is another animal model which induces myelin loss via an inflammatory process. TMEV is a picornavirus that is normally found in without pathogenic symptoms in the mouse gut (DePaula-Silva *et al.*, 2017). The TMEV model is very dependent on mouse strain used: introduction of the virus in SJL/J mice evokes MS-like symptoms while C57BL6/J mice instead experience seizures hypothesized to be due to stronger innate immune system and different major histocompatibility complex subtype (Denic *et al.*, 2011;

DePaula-Silva *et al.*, 2017). It is injected into the brain directly (McCarthy *et al.*, 2012). Acutely after injection TMEV infects mainly neurons, but about a month later the virus is found in oligodendrocytes, microglia, and astrocytes (DePaula-Silva *et al.*, 2017). It is during this latter phase that demyelination begins in the spinal cord and paralytic motor deficits similar to those described above for the EAE model develop, although generally at a slower pace, with full hind limb paralysis expected around 6 months after injection (Denic *et al.*, 2011; McCarthy *et al.*, 2012). Similar to progressive forms of MS, the demyelination is progressive in nature and leads to neuronal death (Denic *et al.*, 2011). The TMEV model itself is interesting because it creates a model in which viral load could result in MS-like symptoms. Of note, while there is not a causative link of viral induction to MS, the Epstein-Barr virus (a double-stranded DNA herpesvirus) has been associated with MS or MS-like development in human and rodent (Pender and Burrows, 2014; Lomakin *et al.*, 2017). The mechanism of TMEV model of demyelination is suggested to induce demyelination by regulatory T cell epitope spreading (McMahon *et al.*, 2005; Richards *et al.*, 2011).

To study remyelination without the complexity of triggering inflammation to attack myelin, as EAE and TMEV models described above enact, toxin-driven models such as lysophosphatidylcholine or cuprizone are used. Currently FDA-approved therapeutics for MS target only neuroinflammatory aspects of the

disease (Ransohoff *et al.*, 2015; Stahnke and Holt, 2017). A combination therapy that uses both an anti-inflammatory and a remyelination agent may be important to effectively treat MS as inflammation is a substantial pathology-inducing agent but also remyelination propensity decreases with age and promoting myelin repair can further protect axonal degeneration (Franklin and Ffrench-Constant, 2017). While toxin-based models lack an immune-central component to the initiation of disease which could be interpreted as less appropriate for modeling MS in animals, they allow for dissection of remyelination aside from inflammatory injury.

Lysophosphatidylcholine (LPC; also known as lysolecithin) models of demyelination are derived from phospholipase A_2 digestion of phosphatidylcholines, a lipid component of myelin (Pavelko *et al.*, 1998). LPC recruits macrophages, microglia, T cells, and monocytes to digest myelin and myelin debris (Ousman and David, 2000; Ghasemlou *et al.*, 2007). LPC creates focal lesions when injected into white matter- often directed into funiculi of spinal cord (Keough *et al.*, 2015). Myelin debris from these processes is usually cleared by 7 days post-injection depending on parameters of model (Jeffery and Blakemore, 1995). LPC will deteriorate white matter regardless of CNS location, age, or gender of subject. Although it is delivered locally *in vivo*, as opposed to systemically, one to two microliters of a 1% solution in saline can affect an area as wide as 3-8 mm (Blakemore and Franklin, 2008; Keough *et al.*, 2015). LPC

can also demyelinate *ex vivo* in organotypic CNS slice culture systems (Meffre *et al.*, 2015). Remyelination of axons in this model is spontaneous; in an aforementioned sized demyelinated area it takes a little over 20 days to completely remyelinate all axons and involves astrocyte recruitment to the area (Jeffery and Blakemore, 1995).

The cuprizone model of demyelination uses bis-cyclohexanone-oxaldihyrazone (also known as cuprizone), administered systemically, generally by incorporation into animal chow. Cuprizone is a chemical compound that binds or chelates copper (Benetti *et al.*, 2010). At low doses it is exclusively toxic to mature oligodendrocytes (Matsushima and Morell, 2001). However, cuprizone does not demyelinate all CNS white matter to the same extent. This model is preferentially used to study the brain, due to lack of spinal cord demyelination with treatment (Herder *et al.*, 2011). The corpus callosum is the white matter region in the brain most studied in this model. White matter pathology has also been noted in the hippocampal commissure (fornix and fimbria), as well as the cerebellar peduncles (Blakemore and Franklin, 2008). Smaller effects have been noted in gray matter regions such as the cerebral cortex (Petiet *et al.*, 2016).

The exact mechanism by which cuprizone is toxic to mature OLs is unknown. However, it is hypothesized to be due to the disproportionately high cellular respiration levels of mature OLs (heavy metals are necessary cofactors in this process) compared to other cell types (Thorburne and Juurlink, 1996;

Matsushima and Morell, 2001; Gudi *et al.*, 2014). Evidence for this postulate includes that cuprizone treatment has been shown to inhibit the mitochondrial enzymes carbonic monoamine oxidase and cytochrome c oxidase, as well as to enlarge mitochondria in the brain and liver of rodents (Gudi *et al.*, 2014).

Differences in demyelination in this model can be caused by mouse strain, age, and gender, in addition to concentration and duration of dosing paradigm (Blakemore and Franklin, 2008; Kipp *et al.*, 2009; Taylor *et al.*, 2009; Skripuletz *et al.*, 2011). In the corpus callosum these parameters can also exacerbate a rostrocaudal axis gradient in demyelination (Blakemore and Franklin, 2008; Steelman *et al.*, 2012; Tagge *et al.*, 2016). The toxic effects of cuprizone are demonstrated earliest (around one week of administration of chow) using gene expression assays that target markers of mature OLs (e.g. MBP, MOG). At a dose of 0.2% cuprizone, it takes about four to six weeks to see extensive demyelination by histologic methods (Matsushima and Morell, 2001). If cuprizone is removed at this point, it will take approximately four to five weeks to fully spontaneously remyelinate the demyelinated areas (Matsushima and Morell, 2001; Deshmukh *et al.*, 2013). The presence of microgliosis and astrogliosis in areas targeted by demyelination has been shown to likely be due to myelin debris clearance pathways (Clarner *et al.*, 2012; Skripuletz *et al.*, 2013). After 9-12 weeks of cuprizone administration at the same dose, the model transitions to

a more severe chronic version where neurons become secondarily damaged in addition to myelin damage.

Unlike the EAE and TMEV demyelination models, the acute cuprizone model does not exhibit gross motor deficits like paralysis. Animals treated with 0.2% cuprizone for acute length of time (~6 weeks) do not have overt changes in behavior (Skripuletz *et al.*, 2011). A few laboratories have demonstrated changes in more complex behavioral assays (e.g. slower wheel-running compared to control mice when wheel has fewer rungs) with cuprizone treatment, but these findings have not yet been replicated across other groups (Hibbits *et al.*, 2009). Animals treated with 0.2% cuprizone for chronic amounts of time exhibit seizures (Skripuletz *et al.*, 2011; Lapato *et al.*, 2017). The change in behavior after chronic treatment is suggested to be due to axonal loss.

ii. Known Therapeutic Agents That Impact Remyelination in In Vivo MS Models

Several therapeutic mechanisms have been tested for remyelination propensity in remyelination animal model paradigms after cuprizone and LPC demyelination. Below, a few recent studies are highlighted where therapeutic agents (compounds or biologics) have been tested in these models.

Deshmukh et al. dosed the muscarinic 1/3 receptor antagonist benztropine at 10 mg/kg by intraperitoneal administration for up to 5 weeks following 7 weeks of 0.2% cuprizone demyelination in C57BL6/J mice (Deshmukh *et al.*, 2013). Two

weeks after cuprizone withdrawal and administration of compound, they saw approximately a 10% increase in luxol fast blue stain (a histological stain for basic phospholipids in myelin) in the corpus callosum of the benztropine group compared to the spontaneous remyelination in the corpus callosum vehicle group (Deshmukh *et al.*, 2013). Additionally, they tested benztropine (2.5mg/kg) as a combination treatment along with an anti-inflammatory approved for MS [fingolimod or interferon-beta (Ransohoff *et al.*, 2015)], and found that the clinical severity score in EAE ($PLP_{139-151}$, CFA & pertussis toxin) model was reduced with both combination treatments compared to either anti-inflammatory or pro-remyelination treatment alone (Deshmukh *et al.*, 2013). Benztropine is currently approved for Parkinson's disease; and there is the potential for it to be dosed at concentrations that could provoke known adverse effects like tachycardia, anxiety, and depression (Hai *et al.*, 2008; Deshmukh *et al.*, 2013). Thus, despite its success in animal models of remyelination and inflammation-induced demyelination, benztropine itself is unlikely to be approved for MS. Another muscarinic receptor antagonist with a better safety profile would be more ideal.

Clemastine, a histamine 1 receptor antagonist marketed for allergies and that has high binding affinity for muscarinic receptors (Kubo *et al.*, 1987), has been assessed for remyelination potential using the LPC model of remyelination. Mei et al. injected lysolecithin into white matter of the dorsal funiculus and ventrolateral spinal cord (between thoracic vertebrae T12/13) in 8 week old

C57BL6/J mice, dosing clemastine 10 mg/kg/day starting before demyelination (Mei *et al.*, 2014). At 14 days post-lesion they found a 20% difference in myelinated axons compared to control; and a decrease in g-ratio (axon diameter / axon diameter + myelin sheath; all assessed using electron microscopy) indicating clemastine increased myelination with treatment (Mei *et al.*, 2014). In a separate experiment, the Chan laboratory also isolated OPCs from muscarinic or histamine receptor knockout mice, treated with clemastine & benztropine and saw the expected increase in mature OLs in every condition except the M1 receptor knockout, indicating that M1 mediates the effect for both compounds (Mei *et al.*, 2016).

The Chan laboratory also recently completed a small (n = 50) proof-of-concept clinical trial with clemastine where RRMS patients with chronic demyelinating optic neuropathy received 5.36 mg clemestine twice per day during the test portion of a double-blind, randomized, cross-over trial (Green *et al.*, 2017). Around 20% of the subjects demonstrated a 6 millisecond decrease in latency with visual-evoked potential conduction, which serves as an indirect measure of increased optic tract myelination (Green *et al.*, 2017). No effect was seen with treatment by MRI, which the authors attribute to variability.

Fingolimod, a RRMS FDA-approved anti-inflammatory that prevents T cell infiltration [and efficacious treatment in EAE models (Webb *et al.*, 2004)] by targeting sphingosine-1-phosphate, has been tested in both lysolecithin and

cuprizone models of remyelination. Hu et al injected sprague dawley rats with 1.5 µL of 1% LPC into the dorsal white matter of the spinal cord and treated 3 days later with 2 µL of 2 mg/mL fingolimod locally, then collected on day 10, and then stained with LFB for myelin (Hu *et al.*, 2011). Fingolimod increased the amount of demyelination area (lack of LFB stain) compared to LPC vehicle alone (Hu *et al.*, 2011). For the cuprizone demyelination study, Hu et al. treated C57BL6 mice with 0.3% cuprizone incorporated into chow for 4 weeks in combination with 10 mg/kg rapamycin [5 days/week, IP; to maximize demyelination (Sachs *et al.*, 2014)] whereupon the cuprizone chow was removed and animals received 1mg/kg fingolimod for 2 weeks (Hu *et al.*, 2011). No effect on remyelination was seen with fingolimod treatment compared to control in the corpus callosum using immunohistochemistry for MBP or by electron microscopy (Hu *et al.*, 2011). Thus, fingolimod did not show efficacy in either the LPC or cuprizone model of remyelination, which indicates it may only improve remyelination caused by an inflammatory mechanism.

Another study from a different laboratory demonstrated that fingolimod is protective of mature oligodendrocytes in the cuprizone model of demyelination if it is dosed within 3 days but not at 10 days into demyelination (Kim *et al.*, 2017). Thus, to the extent that oligodendrocyte damage in the cuprizone model is similar to MS oligodendrocyte damage, there is the potential fingolimod could protect

against new oligodendrocyte damage in MS. However, it will not enable repair or remyelination of axons.

LINGO-1(leucine rich repeat and Ig domain containing Nogo receptor interacting protein1) inhibits OL maturation which prevents myelination (Mi *et al.*, 2005). No anti-inflammatory effects of LINGO-1 antagonism are anticipated in rodent or humans (Ranger *et al.*, 2018). LINGO-1 antagonists to inhibit endogenous OL maturation inhibition have been tested in the remyelination models lysolechithin and cuprizone. Mi et al. injected sprague dawley rats with 1.5 µg of LINGO-1 antagonist 3 days post-injection of 250 g LPC in the spinal cord (Mi *et al.*, 2009). A twenty-fold reduction in lesion (lack of LFB stain) occurred with LINGO-1 antagonist compared to control in the LPC model; by EM there were ~50% more myelinated axons with treatment (Mi *et al.*, 2009). For assessment in the cuprizone model, LINGO-1 antagonist was stereotaxically injected into the corpus callosum at 2.5 and 3 weeks during cuprizone demyelination (% dosage not provided); animals were euthanized 4 and 6 weeks after treatment while still on cuprizone (Mi *et al.*, 2009). LINGO-1 antagonist treated animals had a 4-fold increase in myelinated axons by EM in the corpus callosum; qualitative immunohistochemistry staining for MBP demonstrated no stain in the cuprizone vehicle and moderate stain in the treated (Mi *et al.*, 2009). Thus, both LPC and cuprizone remyelination assays showed increased remyelination with LINGO-1 antagonist. However, the cuprizone assay is

somewhat confounded due to the fact that cuprizone was never removed from the model to test remyelination in the absence of demyelination.

A LINGO-1 antagonist (opicinumab, Biogen) has proceeded to a three phase 2 trials in demyelinating disease conditions so far. A 24-week trial in 82 newly-diagnosed optic neuritis patients did not reach its primary endpoint, reduction in conduction latency measured by visual-evoked potential (Cadavid *et al.*, 2017). However, patients that adhered to protocol actually had an average of 7.6 millisecond reduction in conduction latency of the optic nerve with opicinumab compared to control, but at $p = 0.050$, it missed the statistical significance threshold pre-set for the trial (Cadavid *et al.*, 2017). A follow-up VEP measure was taken 8 weeks later, outside of the primary endpoint parameters for pre-determined success of the clinical trial, where now patients on opicinumab had an average 9.1 millisecond reduction in latency and statistical significance was achieved with $p = 0.011$ (Cadavid *et al.*, 2017). In June of 2016, Biogen issued a press release that a combination therapy trial with interferon-beta-1a (Avonex) in largely RRMS did not meet primary endpoint of cognitive/neurophysical improvement defined by an aggregate score from several tests (ClinicalTrials.gov NCT01864148), but a complete written report is still pending. An unofficial report compiled largely from poster presentations at scientific meetings suggested that subgroup analyses showed that the two lower doses showed efficacy in patients younger than 40, patients with RRMS, or

disease duration of less than 8 years (Ruggieri *et al.*, 2017). Currently another combination therapy trial in largely RRMS is recruiting (ClinicalTrials.gov NCT03222973; any of the following anti-inflammatory treatments can be combined: interferon-beta, natalizumab, dimethyl fumarate).

Thus, the cuprizone and lysolecithin models of remyelination have been informative in developing therapeutics in several cases for human demyelinating diseases where addressing remyelination is a question.

iii. Kallikrein 6 in Animal Models of Oligodendrocyte Demyelination & Remyelination

Modulation of KLK6 (also known as protease M, neurosin, or myelencephalon-specific protease) expression has been characterized in several models of altered myelination. One study used the cuprizone model of mature oligodendrocyte toxicity to induce demyelinaton. This study demyelinated the corpus callosum for seven days with 0.7% cuprizone and then removed the toxin, allowing for seven days of remyelination (Bando *et al.*, 2006). KLK6 expression, along with mature oligodendrocyte gene MBP expression, decreased during the demyelination period and increased during the remyelination period (Bando *et al.*, 2006). While levels of KLK6 and MBP were similar in a non-demyelinated control cohort in their study, after 5-7 days of remyelination post-treatment with cuprizone, their data suggests KLK6 levels of expression are higher than MBP

levels (Bando *et al.*, 2006). It should be noted that this concentration of cuprizone is generally higher than typically used in the literature, and the duration of demyelination and remyelination are also shorter than typically examined.

Another study demonstrated that KLK6 itself can cause demyelination. KLK6 was injected in the dorsal funiculus of the spinal cord and induced a two-fold larger lesion and a 20% loss of oligodendrocytes over 72 hours compared vehicle injection (Burda *et al.*, 2013).

KLK6 expression has been characterized in EAE models of immune-induced demyelination. Terayama et al. demonstrated that expression of KLK6 was highest at the same time of highest clinical severity of behavioral symptoms in the EAE MOG_{35-55} model (Terayama *et al.*, 2005). They also noted that there was more expression of KLK6 around EAE lesions in spinal cord, but that it was not exclusive to white matter (Terayama *et al.*, 2005). In co-labeling experiments they saw that some KLK6 positive cells were of oligodendroglial lineage but that there were other cell types positive for KLK6 that they did not identify (Terayama *et al.*, 2005). Application of exogenous KLK6 in an EAE MOG_{35-55} model increased pro-inflammatory markers (e.g.IL-17, TNF), inhibited anti-inflammatory markers (e.g. IL-4, IL-5) and stimulated earlier onset of dysfunctional motor behavior compared to the EAE model on its own (Yoon and Scarisbrick, 2016).

Another group used a slightly different model, EAE $PLP_{139-151}$, but confirmed high endogenous KLK6 expression at a similar time after induction of

immune response as the MOG_{35-55} model (Blaber *et al.*, 2004; Terayama *et al.*, 2005). Additionally, they peripherally immunized animals with rat KLK6 either at the same time of EAE induction or prior to EAE induction. They found that KLK6 protein expression co-localized with T cell and macrophage markers in EAE mice 21 days after induction (higher clinical severity) but not at 12 days (lower clinical severity) (Blaber *et al.*, 2004). Immunization at either time point delayed manifestation of clinical symptoms 3-4 days, decreased symptom severity, and reduced white matter pathology and inflammation by histology (Blaber *et al.*, 2004). They also demonstrated that activation of T cells increases their KLK6 mRNA expression (Blaber *et al.*, 2004).

It has also been shown that induction of EAE MOG_{35-55} in KLK6 knockout mice have less severe clinical pathology (mostly tail weakness and not hind limb paralysis) and delayed onset of motor dysfunction, decreased BBB permeability (peripherally injected Evans blue dye did not extravasate) (Bando *et al.*, 2018). About 10% less demyelination in perivascular areas in EAE spinal cord was observed in KLK6 knockout mice induced using EAE MOG_{35-55} compared to EAE MOG_{35-55} induced wildtype animals (Bando *et al.*, 2018). Less peripheral infiltrating CD45+ cells were observed (Bando *et al.*, 2018). Further, treatment with a KLK6-neutralizing antibody reduced microgliosis and MMP9 expression in spinal cord that addition of exogenous KLK6 in the EAE MOG_{35-55} enhanced (Bando *et al.*, 2018).

One study characterized KLK6 levels in the TMEV model of inflammation-derived progressive demyelination. In brain, TMEV increased levels of KLK6 RNA expression by 2.5-fold seven days post-induction (acute phase), then returned to control levels until day 120 (where there was a 2-fold increase), but then returned to control levels by day 180 (Scarisbrick *et al.*, 2012b). In spinal cord, KLK6 levels were increased at day 7 post-induction (2-fold), then peaked around day 90 (5-fold), and returned back to control levels at day 180 (Scarisbrick *et al.*, 2012b). When they pre-administered KLK6-neutralizing antibody for 5 weeks before inducing the TMEV model of inflammation-derived progressive demyelination white matter pathology and microgliosis in spinal cord was reduced compared to control at 40 days post-induction, but there was no difference with treatment at 180 days (Scarisbrick *et al.*, 2012b).

The study of potential therapeutics via inhibition of the KLK6 pathway in animal models of MS has been limited to models in which inflammation drives myelin pathology. This presents difficulty in determining whether inhibition of the KLK6 pathway enables remyelination or if it prevents or hinders inflammation that leads to further demyelination. Chapter three of this work focuses on examining whether KLK6 pathway inhibition impacts remyelination following demyelination in the mouse corpus callosum using the toxin cuprizone. Small molecule inhibitors to KLK6 and PAR1 are used that have not been previously tested in

any animal model of MS. Histologic assessment of the anterior body of the corpus callosum is conducted to determine if KLK6 pathway inhibition after cuprizone demyelination alters myelin load or presence of cell types involved in the remyelination process, such as OPCs, microglia, and astrocytes.

b) Methods

i. KLK6 Inhibition Study in Cuprizone Demyelination Animal Model

1. Subjects

Eight to nine week-old male C57BL6 mice (#664, Jackson Laboratories) were treated for 7 weeks with 0.2% Cuprizone formulated as a custom mouse diet (TD.170070, Envigo) or vehicle (normal, Purina 5053) diet. After 7 weeks, half of the animals were perfused with phosphate-buffered saline; brains were collected and fixed with 4% paraformaldehyde (demyelination cohort). The remaining cohort (remyelination cohort) was divided into vehicle and KLK6 inhibitor groups and switched to normal chow (see below for osmotic minipump implantation and lateral ventricle cannulation). At the end of two weeks, samples were processed to paraffin block. In addition, plasma and brain samples collected for pharmacokinetic analysis. All procedures performed on these animals were in accordance with regulations and established guidelines and were reviewed and approved by the Institutional Animal Care and Use Committee.

2. Osmotic minipump delivery of KLK6 inhibitor via lateral ventricle cannulation

During the seventh week of cuprizone chow administration, mice were cannulated in the lateral ventricle (1.0 mm lateral from Bregma, -0.4 mm posterior from Bregma, and -2.2 mm ventral from skull). At the same time, an osmotic minipump (Alzet #2002; capable of delivering ~0.5 uL/hour for fourteen days) was implanted subcutaneously on the body and connected to the cannula via catheter (Brain infusion kit 3, Alzet). Pumps were pre-primed with vehicle [20% (v/v) PEG 400 / 80% (v/v) of 12.5% SBECD in deionized water, with pH between 6.6-7.4] or 7 mM (3.84 mg/mL) KLK6 inhibitor [table 1, item 5 within (Liang *et al.*, 2012a)] in vehicle overnight at 37 degrees Celsius the day prior to surgery. The final average concentration of the KLK6 inhibitor delivered to the brain is expected to be around 2.7 μM in the area of delivery based on exposure and estimated protein binding.

3. Histology

Brains were processed to paraffin (TissueTek VIP6, Sakura) and then sectioned at 5 μm thickness in the region of interest, the anterior body of corpus callosum, in a twenty microscope slide series (e.g. first slide contains 1st and 21st sections). The 5th and 15th slides (4 sections per animal) were selected for

staining with luxol fast blue (Acros Organics 212171000, CAS 1328-51-4). The luxol fast blue (LFB) staining solution was made with 0.1g LFB and 0.5mL glacial acetic acid per 100 mL 95% ethanol. The sections were hydrated to water through xylenes and graded alcohols, then incubated in this LFB staining solution for several hours at 42 degrees Celsius. Afterwards, the sections were rinsed in water followed by ~10 seconds in 50 mg lithium carbonate (Sigma-Aldrich 62470, CAS 554-13-2) per 100 mL distilled water. Sections were then dehydrated through gradient ethanol to xylene and coverslipped using a xylene-based mounting medium. Images were acquired using a Zeiss Axioscan Z1 microscope and analyzed by a binary assessment of pixels stained over area analyzed using a custom macro designed and run using the Visiopharm image analysis platform (version 6.9.2.3050; www.visiopharm.com). Statistical analysis was done by either an unpaired, two-tailed t-test (demyelination cohort) or a one-way ANOVA with Tukey post-hoc comparisons (remyelination cohort).

ii. PAR1 Inhibition Study in Cuprizone Demyelination Animal Model

1. Subjects

Eight to ten week-old male C57BL6 mice (#664, Jackson Laboratories) were treated for 7 weeks with 0.2% Cuprizone formulated as a custom mouse diet (TD.170070, Envigo) or vehicle (normal, Purina 5053) diet. After 7 weeks,

half of the animals were perfused with phosphate-buffered saline; brains were collected and fixed with 4% paraformaldehyde or frozen with liquid nitrogen for biochemical/gene expression experiments (demyelination cohort). The remaining cohort (remyelination cohort) was switched to normal chow. At the same time, they were divided and split to vehicle (5% DMSO, 5% Kolliphor, 0.9% w/v saline) or 50 mg/kg PAR1 inhibitor (Q94 hydrochloride, Tocris 4755) groups and dosed twice a day for 2 weeks, subcutaneously. At the end of two weeks, samples were processed the same as above, in addition to plasma and brain samples collected for pharmacokinetic analysis. All procedures performed on these animals were in accordance with regulations and established guidelines and were reviewed and approved by the Institutional Animal Care and Use Committee.

2. Histology

Brains were processed to paraffin (TissueTek VIP6, Sakura) and then sectioned at 5 µm thickness in the region of interest, the anterior body of the corpus callosum, in a twenty microscope slide series (e.g. first slide contains 1st and 21st sections). The 5th and 15th slides (4 sections per animal) were selected for staining with luxol fast blue (Acros Organics 212171000, CAS 1328-51-4). The luxol fast blue (LFB) staining solution was made with 0.1g LFB and 0.5mL glacial acetic acid per 100 mL 95% ethanol. The sections were incubated in this solution for several hours at 42 degrees Celsius. Then, sections were rinsed in

water followed by ~10 seconds in 50 mg lithium carbonate (Sigma-Aldrich 62470, CAS 554-13-2) per 100 mL distilled water. Sections were rinsed in water and then dehydrated quickly through gradient ethanol to xylene and coverslipped using a xylene-based mounting medium. Images were acquired using a Zeiss Axioscan and analyzed by binary assessment of pixels stained over area analyzed using a custom macro designed and run using the Visiopharm image analysis platform (version 6.9.2.3050; www.visiopharm.com). Statistical analysis was done by either an unpaired, two-tailed t-test (demyelination cohort) or an one-way ANOVA with Tukey post-hoc comparisons (remyelination cohort).

3. Immunohistochemistry

Four equally-spaced sections were chosen per immunohistochemical stain and hydrated from xylene through graded alcohols to water. Antigen retrieval was performed using a Biocare Decloaker (120 degrees Celsius for 30 seconds, 84.5 degrees Celsius for 10 seconds) in citrate buffer (Biogenex). Sections were blocked in normal serum raised to the host species of the secondary antibody for an hour, then incubated with primary antibody overnight (see **Table 4**) at 4 degrees Celsius. A fluorescent secondary antibody directed to the host species of the primary antibody (AlexaFluors, LifeTechnologies) was applied for 1.5 hours at room temperature following a few washes with phosphate-buffered saline, and counterstained with DAPI (LifeTechnologies). Images were acquired using a

Zeiss Axioscan Z1 microscope and analyzed using custom macros designed and run using the Visiopharm image analysis platform (version 6.9.2.3050; www.visiopharm.com). Statistical analysis was done by either an unpaired, two-tailed t-test (demyelination cohort) or a one-way ANOVA with Tukey post-hoc comparisons (remyelination cohort).

5. UPLC-MS/MS Pharmacokinetic Analysis of PAR1 and KLK6 Inhibitors

Plasma and brain samples were analyzed by liquid chromatography–tandem mass spectrometry (LC-MS/MS). Brain samples were prepared for analysis by adding four volumes of 60:40 isopropanol and homogenized using 2 mm zirconia beads (BioSpec) and 2 minutes of shaking in a bead beater (BioSpec). Analytical standards for each analyte were prepared by solubilizing powder stocks into 1:1 DMSO:ACN and standard curves were prepared in naïve animal plasma. Brain samples were prepared separately from plasma samples, using a mixed matrix approach where an equal volume of naïve brain homogenate was added to all standards and an equal volume of naïve plasma was added to samples. Samples were extracted using protein precipitation with ~5 volumes of an internal standard cocktail (verapamil at 2.5 ng/ml and terfenadine at 30 ng/ml) in acetonitrile. Sample blocks were vortexed for 30 seconds and centrifuged at 3,000 rpm for 5 minutes and ~50 µL of the

supernatant was diluted into three volumes of water containing 0.1% formic acid for injection onto the LC-MS.

Chromatography was performed on a Waters Acquity iClass UPLC System (Milford, MA). The autosampler and column were kept at at 10°C and 40°C, respectively. Separation was achieved with an Acquity UPLC HSS T3 column (2.1x50mm, 1.8 µm), and a gradient of 0.1% formic acid in water (Mobile Phase A) and 0.1% formic acid in acetonitrile (Mobile Phase B) at a flow rate of 0.600 mL/min. An initial mobile phase composition of 5% B was ramped to 95% over 2 minutes, held at 95% for 0.3 minutes, and then returned to initial 5% B for re-equilibration.

Data was collected on an AB Sciex API6500 mass spectrometer (Foster City, CA, USA) using positive Turbo IonSpray™ electrospray ionization (ESI) and multiple reaction monitoring (MRM) mode. Typical source conditions, heated capillary temperature, gas1, gas2, and curtain gas were set at 500ºC, 40, 60 and 30 respectively. MRM transitions for each analyte, including DP and CE, were as follows: KLK6 inhibitor 549→91 DP:110 CE:75; PAR1 inhibitor 333→125 DP:85 CE:36. Verapamil was used as the internal standard for the KLK6 inhibitor (MRM transitions = 455→165 DP:80 CE:30). Terfenadine was used as the internal standard for the PAR1 inhibitor (MRM transitions = 472→436 DP:80 CE:30). Data acquisition and processing was carried out with Analyst software version 1.6.2. (Applied Biosystems/MDS Sciex, Canada)

6. Determination of Compound Fraction Unbound via Equilibrium Dialysis

Equilibrium dialysis experiments were conducted in an HTD 96 device obtained from HTDialysis, LLC (Gales Ferry, CT). Prior to the experiment, cellulose dialysis membranes (HTDialysis, LLC, MWCO 12-14K) were soaked in de-ionized water for 15 minutes, 30% ethanol/de-ionized water for 15 minutes, and Dulbecco's phosphate buffered saline [DPBS; BioWhittaker, #17-512Q] for 15 minutes or overnight. CD-1 mouse plasma and Wistar-han rat brains were obtained from BioreclaimationIVT, LLC (Hicksville, NY). Mouse plasma was thawed at 37°C in a water bath or incubator then pH adjusted to 7.4 with 1 N hydrochloric acid. Rat brain tissue was homogenized prior to use in DPBS (1:10 tissue: PBS dilution) at RT with an Omni TH tissue homogenizer (Omni International, Kennesaw, GA). A probe (7 x 110 mm) was used for 30-second pulses at high speed. The dialysis device was assembled following the instructions from the manufacturer (http://www.htdialysis.com). Compound stock solutions were prepared at 4 mM in dimethylsulfoxide (DMSO) then diluted 200 µM in DMSO. Compound was added to matrices (1:100 dilution) and mixed well for a final test compound concentration of 2 µM and 1% DMSO. To calculate stability and recovery for each test compound, a T0 sample of each matrix (15 µL) was immediately collected into a 96-well plate, mixed with 45 µL of DPBS, and crashed with 200 µL of cold acetonitrile containing IS (IS; a cocktail of 5

ng/ml terfenadine and 0.5 ng/ml tolbutamide). For the fraction unbound determination, an aliquot (150 µL, n=4 per compound) of spiked matrix (plasma or brain homogenate) was added to the donor side of the membrane in the dialysis device and blank DPBS (150 µL) was added to the receiver side of the membrane. The dialysis device was sealed with Breathe-Easy Membranes (Sigma-Aldrich) before being incubated in a humidified incubator (75% relative humidity, 5% CO2/95% air) at 37°C for 6 hours at 200 rpm with an orbital shaker. Upon completion of the incubation, matrix samples (15 µL) from the donor wells were added to 45 µL of DPBS in a 96-well plate. Dialyzed DPBS (45 µL) from the receiver wells was added to the blank matrix (15 µL). Samples were crashed in acetonitrile as mentioned above for T0 recovery and stability samples. The samples were vortexed for 3 minutes (VWR) and centrifuged at 3000 rpm for 5 minutes at RT. The supernatant was transferred and analyzed by LC-MS/MS. Sertraline was used on every incubation plate for quality control. Chromatography was performed on a Waters Acquity iClass UPLC System (Milford, MA). Separation was achieved with an Acquity UPLC BEH C18 (2.1x50mm, 1.7 µm) [PAR1 inhibitor] , and kinetex C18 (30x 2.1mm, 2.6µm) [KLK6 inhibitor] and a gradient of 0.1% formic acid in water (Mobile Phase A) and 0.1% formic acid in acetonitrile (Mobile Phase B) at a flow rate of 0.500 mL/min. An initial mobile phase composition of 5% B was ramped to 95% over 2 minutes, held at 95% for 0.5 minutes, and then returned to initial 5% B for re-equilibration

for the PAR1 inhibitor. For the KLK6 inhibitor, it was ramped to 95% over 1.2 minutes, held at 95% for 0.4 minutes, and then returned to initial 5% B for re-equilibration. Data was collected on an AB Sciex API6500 mass spectrometer (Foster City, CA, USA) using positive Turbo IonSpray™ electrospray ionization (ESI) and multiple reaction monitoring (MRM) mode. Typical source conditions, heated capillary temperature, gas1, gas2, and curtain gas were set at 500 ºC, 40, 60 and 30 respectively. MRM transitions for each analyte, including DP and CE, were as follows: KLK6 inhibitor 549→91 DP:110 CE:50; PAR1 inhibitor 333→125 DP:85 CE:36. Data acquisition and processing was carried out with Analyst software version 1.6.2. (Applied Biosystems/MDS Sciex, Canada).

c. Results

Pharmacokinetic study of the KLK6 inhibitor used previously for *in vitro* experiments was done at 0.5, 2, 8, and 24 hours post-administration by subcutaneous injection in mouse. One key objective was to determine if the compound was likely to be brain penetrant following this administration route. Exposure levels of compound were measured in plasma and brain at two concentrations of the inhibitor: 10 mg/kg & 50 mg/kg. The KLK6 inhibitor was not readily brain penetrant at either concentration tested (**Figure 3 C-D**). The KLK6 inhibitor was also found to bind highly in brain (**Table 5**). Thus, to investigate the impact of the KLK6 inhibitor in an *in vivo* remyelination model, a chronic osmotic

pump delivery method cannulated into the lateral ventricle was used with the highest concentration with parameters compatible with the dosing paradigm (37 degrees C for 14 days). Pharmacokinetic analysis from lateral ventricle cannulated osmotic pump animals receiving KLK6 inhibitor for 14 days indicate the drug was present in brain (cerebellum), cerebrospinal fluid, and plasma (**Figure 3E**).

Next, a seven week paradigm of *ad libitum* 0.2% cuprizone chow administration was used to induce demyelination of the corpus callosum in C57BL6/J mice. During the seventh week, cuprizone chow was removed upon implantation of a subcutaneous osmotic pump pre-primed with KLK6 inhibitor (or vehicle) that was cannulated for intracerebroventricular delivery into the lateral ventricle. After 14 days of continuous administration the animals were euthanized and samples were collected for analysis. Demyelination was induced in the corpus callosum after seven weeks of cuprizone treatment, as indicated by a decrease in luxol fast blue staining (**Figure 4 A-B, G**). Cuprizone withdrawal and replacement with normal chow naturally spurred spontaneous remyelination in cuprizone/vehicle animals, as indicated by a smaller percentage change difference in luxol fast blue staining compared to animals that only received normal chow (**Figure 4 C-D, H**). Compared to cuprizone/vehicle, luxol fast blue staining in cuprizone/KLK6i treated animals demonstrated 16% more myelination in the corpus callosum (**Figure 4 D-F, H**). Immunohistochemical staining for the

CC1 clone of APC which stains mature oligodendrocytes demonstrated that 7 weeks of cuprizone decreases CC1 staining by 30% in mouse corpus callosum (**Figure 5 A-B, G**). The effects of spontaneous remyelination observed with luxol fast blue was corroborated by a large increase in corpus callosum CC1 staining in animals in which cuprizone chow was withdrawn compared to cuprizone naïve animals (**Figure 5 C-D, H**). Cuprizone/KLK6i treated animals demonstrated a 19% increase in corpus callosum CC1 staining compared to cuprizone/vehicle animals, but the result did not achieve statistical significance at $p = 0.11$ (**Figure 5 D-F, H**).

The cuprizone model paradigm employed also induced a significant neuroinflammation in the corpus callosum. Astrogliosis, indicated by gain in GFAP+ staining, was increased 660% with cuprizone treatment (**Figure 6 A-B, G**). Microgliosis, indicated by gain in Iba1+ staining, was increased by 25% with cuprizone treatment (**Figure 7 A-B, G**). Two weeks after cuprizone withdrawal, less inflammation was observed in the corpus callosum, via GFAP and Iba1 stain reductions, in the cuprizone/vehicle condition (**Figure 6 C-D, H**; **Figure 7 C-D, H**). Cuprizone/KLK6i treated animals had a further reduction in GFAP+ stain in corpus callosum, a 19% decrease, compared to cuprizone/vehicle (**Figure 6 D-F, H**). In contrast, no change was seen in the corpus callosum of curpizone/KLK6i treated animals compared to vehicle with Iba1+ staining (**Figure 7 D-F, H**). No differences in oligodendrocyte precursor cells were identified in the corpus

callosum upon cuprizone treatment or with KLK6i treated after cuprizone withdrawal (**Figure 8 A-H).**

Pharmacokinetic analysis of the PAR1 inhibitor was done in mouse at 0.5, 2, 8, and 24 hours after subcutaneous injection to determine if the compound was likely to be brain penetrant (measured by exposure levels in plasma and brain at two concentrations of the inhibitor- 10 mg/kg & 50 mg/kg). The PAR1 inhibitor was found to be brain penetrant at both concentrations tested (10 and 50 mg/kg), with an estimated duration of eight hours before drug concentration significantly diminishes (**Figure 5 A-B**). The PAR1 inhibitor was also found to bind highly in brain (**Table 5**).

A seven-week duration of 0.2% cuprizone administration to C57Bl6/J mice was used to establish demyelination and to test the remyelination potential of the brain penetrant PAR1 inhibitor. At seven weeks, a portion of the animals were collected as part of a demyelination cohort for analysis. The cohort for remyelination analysis discontinued cuprizone treatment at this time and began administration of vehicle or PAR1 antagonist (50mg/kg, BID, SC).

Data from the demyelination cohort of the cuprizone study demonstrates the baseline of demyelination at which drug administration began. Using luxol fast blue staining and a custom positive pixel per area analyzed algorithm, a forty-five percent reduction in myelinated fibers in the anterior body of the corpus callosum was seen in the seven-week, 0.2% cuprizone treated animals

compared to vehicle animals (**Figure 9 A ,B, G**). This indicates significant demyelination has occurred in the corpus callosum with the cuprizone paradigm. This model thus allows for a maximum of forty-five percent recovery of myelination from baseline before drug administration, excluding rate of spontaneous remyelination.

In the remyelination cohort, collected two weeks later after PAR1 or vehicle administration, only a twenty-five percent reduction in myelinated fibers in the anterior body of the corpus callosum existed between vehicle/naïve and cuprizone/vehicle-treated animals (representative images, **Figure 9 C-D, H**). This indicates, as expected for the model, spontaneous remyelination has taken place in the two weeks in which cuprizone was removed from the mouse diet during the vehicle or drug treatment portion of the remyelination study. No statistically significant changes in myelinated fibers were detected between the cuprizone/vehicle and cuprizone/PAR1 inhibitor treated animals in the anterior body of the corpus callosum (representative images, **Figure 9 D-F, H**). This suggests that the PAR1 inhibitor treatment paradigm did not have a larger impact on remyelination compared to the level of spontaneous remyelination in the model.

Immunohistochemical staining for NG2, a chondroitin sulfate proteoglycan present on later-stage oligodendrocyte precursor cells, also demonstrated no statistically significant differences in percent stained area across treatment

groups in the anterior body of the corpus callosum (**Figure 10 A-H**) or in the cingulate cortex (**Figure 10 I-M**).

Cuprizone treatment induced microgliosis and astrogliosis, as indicated by a 163% increase in Iba1 immunohistochemical stain (**Figure 11 A-B, G**) or 409% increase in GFAP immunohistochemical stain (**Figure 12 A-B, G**), respectively, in the corpus callosum. Two weeks of PAR1 inhibitor treatment paradigm did not result in a reduction of Iba1 or GFAP compared to vehicle treatment (**Figure 11 C-F, H; Figure 12 C-F, H**).

d. Discussion

Compared to other animal models of demyelination, the cuprizone model of demyelination is not etiologically created by immune dysfunction and allows for direct study of an agent on remyelination as opposed to inflammation. Chapter three of this work uses the cuprizone model of demyelination to examine the role of KLK6 pathway inhibition on remyelination in a mammalian species *in vivo* using specific inhibitors that have not previously been described with the cuprizone model.

Cuprizone administration in chow for seven weeks resulted in 30-45% demyelination in the rostral corpus callosum as assessed by luxol fast blue myelin stain. Pharmacological intervention in the cuprizone model has been previously demonstrated to have the largest window for efficacy at 2-3 weeks post-withdrawal of cuprizone using very similar demyelination parameters

(Deshmukh *et al.*, 2013; Li *et al.*, 2015). Spontaneous remyelination continues to occur as time passes post-cuprizone withdrawal (reducing dynamic range to see an efficacious impact). As expected, during the two weeks post-demyelination in which treatment was evaluated compared to vehicle, animals treated with cuprizone experienced some degree of spontaneous remyelination. Thus, in order to be efficacious in the model, the treatments need to be more efficient or faster at inducing myelination compared to spontaneous remyelination due to cuprizone withdrawal and an acute cuprizone treatment paradigm.

In order to evaluate brain penetrance and clearance, pharmacokinetic evaluation was conducted using subcutaneous administration for the KLK6 inhibitor and the PAR1 inhibitor used in *in vitro* oligodendrocyte maturation assays in chapter 2. Pharmacokinetic analysis of the PAR1 inhibitor demonstrated plasma and brain exposure following subcutaneous administration. The profile of clearance over time suggested a minimum of twice a day dosing at the highest concentration tested to engage the target for the majority of a given day. Pharmacokinetic analysis of the KLK6 inhibitor following subcutaneous administration demonstrated plasma exposure but virtually no brain exposure at the concentrations tested. Thus, the PAR1 inhibitor is easily incorporated into an evaluation of remyelination using the cuprizone model of demyelination. However, evaluating the effect of KLK6 inhibition on remyelination via cuprizone model of demyelination is more complicated. While the KLK6 inhibitor increased

oligodendrocyte maturation with direct application *in vitro*, it would not be able to reach the target cell types in the brain using conventional dosing methods. Given the lack of KLK6 inhibitor brain penetrance, options for administering the KLK6 inhibitor directly into the central nervous system under subchronic conditions were researched. Options were assessed for feasibility based on compound properties such as solubility and stability. A chronic intracerebroventricular infusion method via cannulated osmotic minipump (Alzet) was selected to deliver the KLK6 inhibitor into the lateral ventricle within the brain in a continuous, subchronic fashion. Direct-into-the-brain injection was ruled out due to the length of dosing (14 days) and the potential for the cannula to clog if situated directly in brain tissue due to tissue remodeling and the lipid-rich region of interest. One caveat with ICV injection delivery is that the compound will still need to cross from the cerebrospinal fluid into the brain to reach the target cells. Although stereotaxic surgery involved in this method of administration (cannula implantation) creates acute disruption in the blood-brain barrier, it is unlikely to impact demyelination and remyelination outcomes (Tejedor *et al.*, 2017). However, administration of opioids and non-steroidal anti-inflammatories, used for surgical treatment-related comfort of the animal, may have the potential to induce remyelination (Eschenroeder *et al.*, 2012; Preisner *et al.*, 2015).

The concentration of KLK6 inhibitor was maximized according to solubility in an osmotic-pump compatible vehicle where it would be also stable for >14

days at 37 degrees Celsius (data not shown) and to account for non-specific protein binding estimates. At the end of a seven week demyelination period using 0.2% cuprizone chow, animals were equipped with an osmotic pump filled with KLK6 inhibitor or vehicle which was catheterized to a lateral ventricle cannula. After 14 days of treatment, pharmacokinetic analysis of plasma, CSF, and cerebellum indicated that exposure was achieved in all compartments and even in brain tissue far away from the injection site. Due to protein binding estimates, it is expected that the compound is at higher concentration closer to the injection site.

Assessment of myelin by luxol fast blue staining demonstrated a 16% increase in corpus callosum myelination after two weeks cuprizone withdrawal/concurrent KLK6 inhibitor treatment when compared to vehicle. This degree of remyelination is similar to levels previously published with alternate mechanisms (Deshmukh *et al.*, 2013). Additionally, KLK6 inhibitor treatment resulted in 19% decreased GFAP-positive astrocyte stained area in the corpus callosum compared to vehicle treatment after cuprizone. CC1 staining for mature oligodendrocytes post-cuprizone withdrawal reflected an increase with spontaneous remyelination/oligodendrocyte differentiation, but the 19% increase between cuprizone/vehicle and cuprizone/KLK6i treatments did not reach statistical significance ($p = 0.11$). No changes were seen in Iba1-positive

microglia stained area or NG2-positive OPC stained area in the corpus callosum with KLK6 inhibitor treatment post-cuprizone withdrawal.

Thus, this experiment is the first example of a small molecule KLK6 inhibitor to demonstrate enhanced myelination following the non-immune mediated cuprizone model of demyelination. Further, the reduction in astrocyte but not microglia staining suggests a dual effect of KLK6 inhibition on oligodendrocytes and astrocytes, or may signify a role for astrocytic regulation of myelination via KLK6. Previous work has demonstrated that KLK6 protein is found within reactive, hypertrophied astrocytes in a variety of diseases (Scarisbrick *et al.*, 2012a). This is in contrast to *in vitro* RNA sequencing data which suggests KLK6 is only present in oligodendrocytes, and not astrocytes (Zhang *et al.*, 2014; Zhang *et al.*, 2016). However, the latter work was done on cells in their basal state, not an activated state.

To investigate whether the inhibition of downstream signaling molecule activated by KLK6 could also enhance myelination *in vivo* post-cuprizone treatment, a brain-penetrant PAR1 inhibitor was also tested. The PAR1 inhibitor was dosed subcutaneously at 50 mg/kg concentration, dosed twice a day for 14 days following cuprizone withdrawal. No difference in myelination was seen by luxol fast blue staining in the corpus callosum of animals treated with a PAR1 inhibitor compared to vehicle treatment for 2 weeks post-cuprizone withdrawal.

Further, no difference was also seen with KLK6 inhibitor treatment related to NG2-positive OPCs. Cuprizone treatment itself is not expected to impact OPC population, which was corroborated with our data. However, if the remyelination was not complete enough to be seen by LFB but currently in progress when the samples were collected, it is reasonable to expect an increase in OPCs around the callosal region (corpus callosum and cingulate cortex above corpus callosum were analyzed) in the PAR1 inhibitor treatment group but not the vehicle treated group. In both regions there were similar levels of NG2-positive percent area stain per area measured in the PAR1 inhibitor treatment group as vehicle. This evidence corroborates the luxol fast blue results and similarly conveys that the PAR1 inhibitor did not accelerate maturation leading to successful myelination differentially vehicle. No difference was also seen with GFAP-positive astrocyte staining or Iba1-positive microglial staining upon KLK6 inhibition.

This overall result is somewhat surprising given previous findings that PAR1 inhibition can mature OPCs *in vitro (Yoon et al., 2015)*, however, the results of this experiment corroborate the *in vitro* result in chapter 2 of this work.

Based on our pharmacokinetic profile, it is confirmed that the PAR1 inhibitor is brain penetrant and thus has access to the brain to mediate direct mechanisms of therapeutic intervention in the brain. No overt adverse events were associated with this concentration, exposure, and duration of treatment with PAR1 inhibitor in mice in this study. This is the first attempt of *in vivo*

administration of this particular PAR1 inhibitor (IC_{50} = 10-100nM), which is expected to have better brain penetration than PAR1 inhibitors used *in vitro (Burda et al., 2013)* or *in vivo* (Bogovyk *et al.*, 2017) based on chemical structure. It is possible that exposure was not consistently high enough to see the hypothesized effect on remyelination and the drug should have been dosed three times per day. The process of generating myelin sheaths after differentiation has been shown to be restricted to a timeframe as short as five hours post-maturation for oligodendrocytes in zebrafish (Czopka *et al.*, 2013). A gap of time longer than this existed between each day of treatment. In addition, the amount of protein binding estimated to exist in brain may have reduced the amount of compound that made it to target cells in the brain. Future studies should focus on comparison of SCH79797 and the PAR1 inhibitor used in this study to understand the different properties that could impact function.

The cuprizone model has previously been used to determine whether therapeutic mechanisms are purely related to dampening inflammation or also exert direct effects on myelin repair (Hu *et al.*, 2011). It is possible that PAR1 inhibition may still be beneficial in treating inflammatory components associated with disorders of myelin loss like MS, whether or not it directly enhances remyelination. Overly active, infiltrating cytotoxic T lymphocytes secrete granzyme B in MS, which induces cell death (Neumann *et al.*, 2002; Frischer *et al.*, 2009; Bien *et al.*, 2012). PAR1 inhibition has also been shown to prevent T

lymphocyte granzyme B neurotoxicity (Lee *et al.*, 2017) and improve recovery after spinal cord injury by reducing associated inflammation (Radulovic *et al.*, 2016).

In summary, a novel KLK6 inhibitor was shown to increase remyelination in the corpus callosum after cuprizone-mediated demyelination. A reduction in astrogliosis in the corpus callosum was also seen with KLK6 inhibition post-cuprizone. Understanding of current data suggests that perhaps an effect of KLK6 inhibition on both cell types could be related to similar lineage origin of astrocytes and oligodendrocytes. In this case KLK6 inhibition may be both an anti-inflammatory and a pro-myelinating treatment. Another interpretation is that the reduction in astrogliosis is reflective of astrocyte modulation of oligodendrocytes/myelination and thus the mechanism by which myelination is increased with KLK6 treatment. A PAR1 inhibitor, thought to be another method of inducing downstream KLK6 inhibition, was not effective at enhancing myelination in the corpus callosum post-cuprizone withdrawal. It is suspected that despite brain penetrance, other properties of the small molecule may have been problematic.

Future directions include furthering current understanding of the relationship between myelination in response to KLK6 inhibition and reduction in astrogliosis in response to KLK6 inhibition. Additionally, this KLK6 inhibitor, or one with improved chemical properties, should be tested in a model of

progressive demyelination (such as TMEV) by itself and in combination with an anti-inflammatory treatment to explore its efficacy in a model most similar to human MS.

Full Name	Short Name	Vendor	Catalog Code	Host Species	Tissue Tested Species
CC-1 clone / Adenomatus Polyposis Coli	CC1	Millipore	OP80	Mouse	Mouse, Human
Glial Fibrillary Acidic Protein	GFAP	Dako North America	Z0034	Rabbit	Mouse, Human
Ionized calcium-binding adapter molecule 1	Iba1	Wako Chemicals	019-19741	Rabbit	Mouse, Human
Myelin Basic Protein	MBP	AbD Serotec	MCA409S	Rat	Mouse, Human
Neural/Glial proteoglycan antigen 2	NG2	Millipore	AB5320	Rabbit	Mouse, Human

Table 4. Chapter 3 Antibody Information

Free, unbound fraction of/in:	Mouse Plasma	Rat Brain
KLK6 inhibitor	0.0081	0.00038
PAR1 inhibitor	0.0053	0.0017

Table 5. Free, unbound fractions of small molecule inhibitors in plasma and brain

Figure 3. Pharmacokinetic Assessment of Small Molecule Inhibitors

A-B: PAR1 inhibitor concentration in mouse plasma and brain after subcutaneous administration of 10mg/kg (red) or 50 mg/kg (blue) at 0.5, 2, 8, or 24 hours post-injection. The PAR1 inhibitor was determined to be brain penetrant and a dose of 50 mg/kg was selected for an *in vivo* remyelination model study.
C-D: The KLK6 inhibitor used for *in vitro* experimentation is not readily brain penetrant when dosed peripherally in a study with same design as described in A-B, as demonstrated by pharmacokinetic study in plasma and brain.
E: KLK6 inhibitor is detectable in brain (cerebellum), cerebrospinal fluid, and plasma after 14 days of lateral ventricle cannulated osmotic pump continuous delivery (~0.5 µL/hour). All graphs within the figure represent the data as mean plus or minus the standard error of the mean.

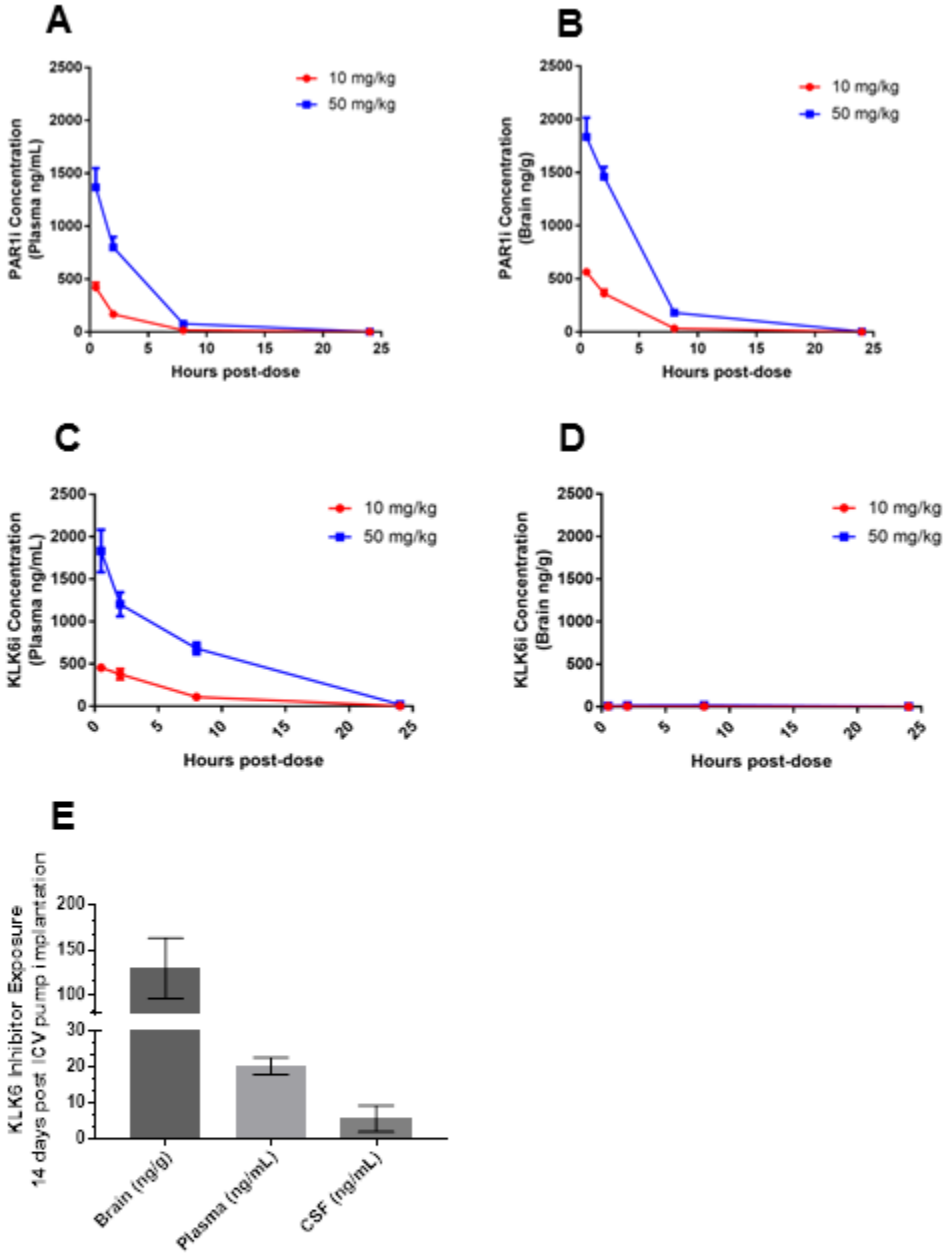
A
PAR1i Concentration (Plasma ng/mL)
10 mg/kg
50 mg/kg
Hours post-dose
B
PAR1i Concentration (Brain ng/g)
10 mg/kg
50 mg/kg
Hours post-dose
C
KLK6i Concentration (Plasma ng/mL)
10 mg/kg
50 mg/kg
Hours post-dose
D
KLK6i Concentration (Brain ng/g)
10 mg/kg
50 mg/kg
Hours post-dose
E
KLK6 Inhibitor Exposure
14 days post ICV pump implantation
Brain (ng/g)
Plasma (ng/mL)
CSF (ng/mL)

Figure 4. The Effects of KLK6 Inhibition on In Vivo Remyelination

A-B, G: A 30% reduction in corpus callosum myelinated fibers (Luxol Fast Blue) is seen in mouse brain after 7 weeks 0.2% cuprizone treatment (cuprizone/naïve, C/N) versus normal chow vehicle (normal chow/naïve, N/N). This was quantified using a custom algorithm designed in Visiopharm. Statistical analysis was done using an unpaired, two-tailed t-test.

C-F, H: Following 7 weeks 0.2% cuprizone treatment administration, normal vehicle chow was resumed for 2 weeks concurrent with continuous administration of a KLK6 inhibitor or vehicle via subcutaneously implanted osmotic pump cannulated to the lateral ventricle of the brain. Naïve animals that never received cuprizone treatment (Normal/Naïve, N/N) were carried along as sample processing comparison. Compared to naïve, a 22% reduction was seen two weeks post-cuprizone withdrawal in the vehicle group. There was a 16% statistically significant increase in myelinated fibers during this time in this portion of the corpus callosum between Cuprizone/Vehicle (C/V) and Cuprizone/KLK6i (C/P) inhibitor treatment. Representative images from one to two animals per group are shown. Quantification was done using a custom algorithm designed in Visiopharm. Statistical analysis was done using a one-way ANOVA with Tukey post hoc comparisons. Scale bar = 100 µm. All graphs within the figure represent the data as mean plus or minus the standard error of the mean.

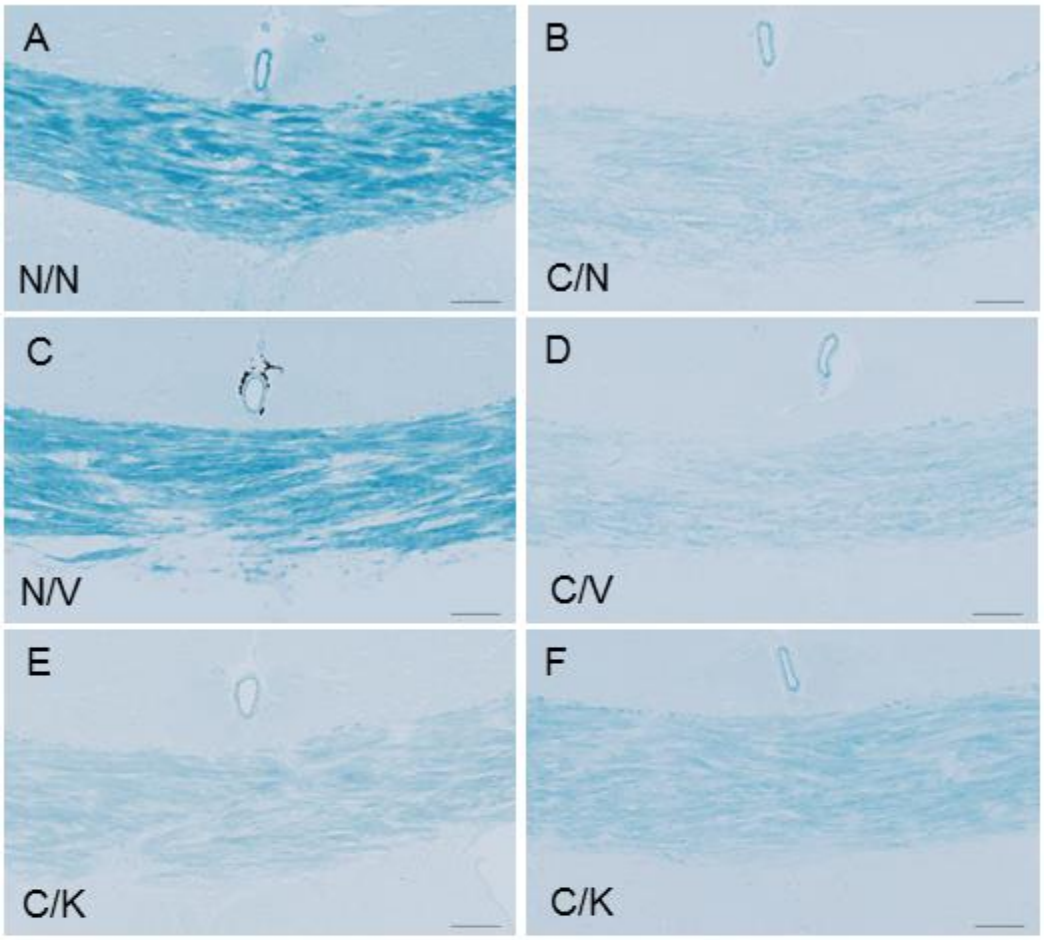
A
N/N
B
C/N
C
N/V
D
C/V
E
C/K
F
C/K

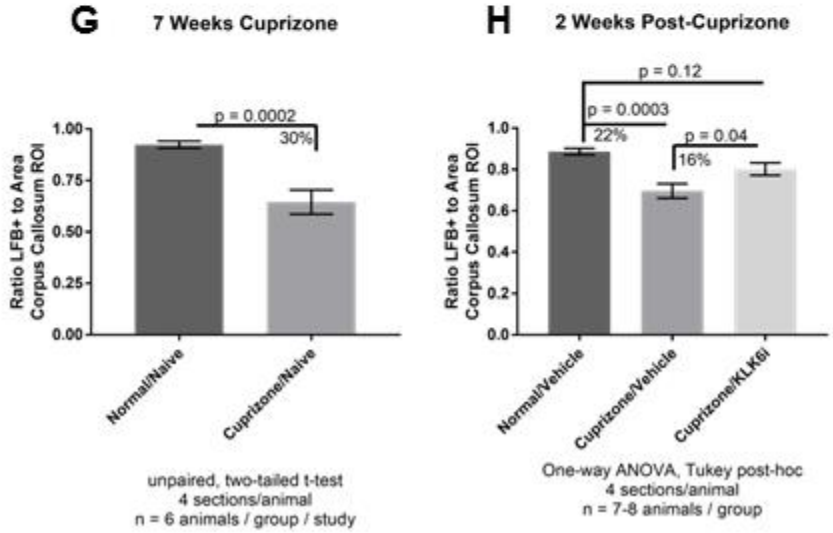
G
7 Weeks Cuprizone
p = 0.0002
30%
Ratio LFB+ to Area Corpus Callosum ROI
1.00
0.75
0.50
0.25
0.00
Normal/Naive
Cuprizone/Naive
unpaired, two-tailed t-test
4 sections/animal
n = 6 animals / group / study
H
2 Weeks Post-Cuprizone
p = 0.12
p = 0.0003
22%
p = 0.04
16%
Ratio LFB+ to Area Corpus Callosum ROI
1.0
0.8
0.6
0.4
0.2
0.0
Normal/Vehicle
Cuprizone/Vehicle
Cuprizone/KLK6i
One-way ANOVA, Tukey post-hoc
4 sections/animal
n = 7-8 animals / group

Figure 5. KLK6i Treatment Post-Cuprizone Results in Trend Increase of CC1+ Mature Oligodendrocytes

A-B, G: Seven weeks treatment with 0.2% cuprizone induced a 30% decrease in area stain of mature oligodendrocytes immunohistochemically detected in the corpus callosum using CC1 clone of APC antigen. Quantification was done using a custom algorithm designed in Visiopharm. Statistical analysis was done using an unpaired, two-tailed t-test.

C-F, H: Two weeks after the withdrawal of cuprizone administered via the above described paradigm, there was a 150% increase in area stained by CC1 in the corpus callosum (N/V to C/V), that is likely the result of increased mature oligodendrocyte differentiation related to spontaneous remyelination in this model. There is a 19% increase in CC1 area stain in corpus callosum between cuprizone/vehicle and cuprizone/KLK6i-treated animals, but it did not reach statistical significance ($p = 0.11$). Quantification was done using a custom algorithm designed in Visiopharm. Statistical analysis was done using a one-way ANOVA with Tukey post-hoc.

CC1 = red; DAPI = blue. Scale bar = 100 µm. All graphs within the figure represent the data as mean plus or minus the standard error of the mean.

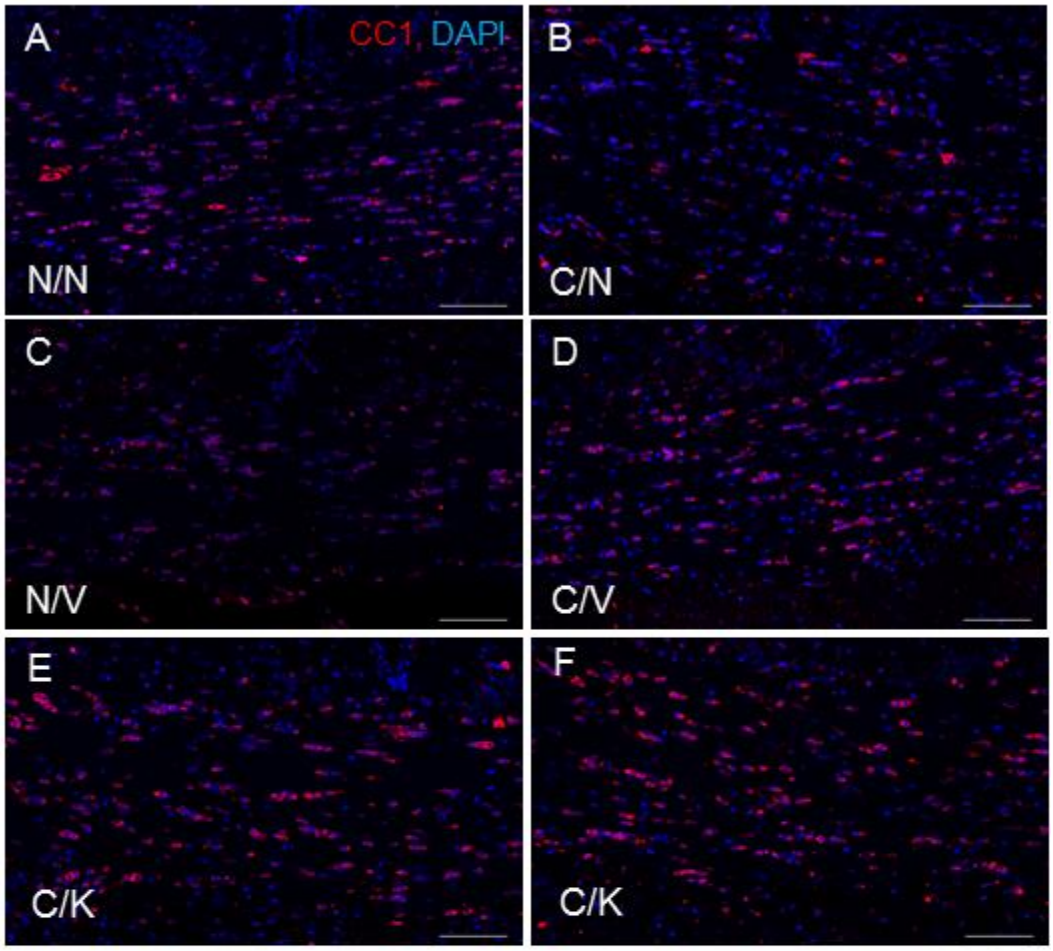
A
CC1, DAPI
N/N
B
C/N
C
N/V
D
C/V
E
C/K
F
C/K

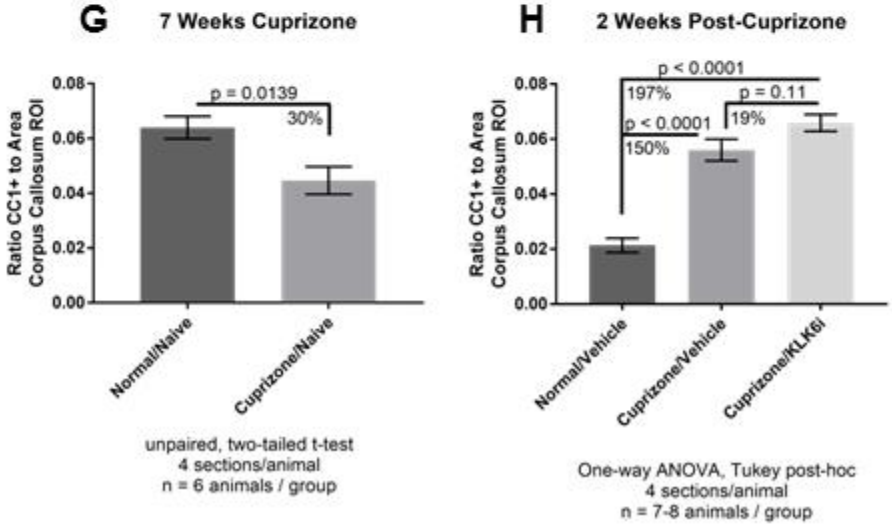
G
7 Weeks Cuprizone
Ratio CC1+ to Area Corpus Callosum ROI
0.08
0.06
0.04
0.02
0.00
p = 0.0139
30%
Normal/Naive
Cuprizone/Naive
unpaired, two-tailed t-test
4 sections/animal
n = 6 animals / group
H
2 Weeks Post-Cuprizone
p < 0.0001
197%
p = 0.11
19%
p < 0.0001
150%
Normal/Vehicle
Cuprizone/Vehicle
Cuprizone/KLK6i
One-way ANOVA, Tukey post-hoc
4 sections/animal
n = 7-8 animals / group

Figure 6. KLK6i Treatment Post-Cuprizone Reduces Astrogliosis

A-B, G: Seven weeks of 0.2% cuprizone treatment induced 660% increase in astrogliosis (defined by GFAP+ stain area per area analyzed) in the corpus callosum compared to normal/naïve mice. Quantification was done using a custom algorithm designed in Visiopharm. Statistical analysis was done using an unpaired, two-tailed t-test.

C-F, H: Two weeks post-cuprizone withdrawal, less astrogliosis was present relative to just after 7 weeks of cuprizone treatment. However, there was still a 223% increase in GFAP+ stain in cuprizone/vehicle compared to normal/vehicle animals. After 14 days continuous administration of a KLK6 inhibitor into the lateral ventricle, a 19% decrease in GFAP+ stain was seen compared to vehicle-treated cohort. Quantification was done using a custom algorithm designed in Visiopharm. Statistical analysis was done using a one-way ANOVA with Tukey post-hoc.

GFAP = red; DAPI = blue. Scale bar = 100 µm. All graphs within the figure represent the data as mean plus or minus the standard error of the mean.

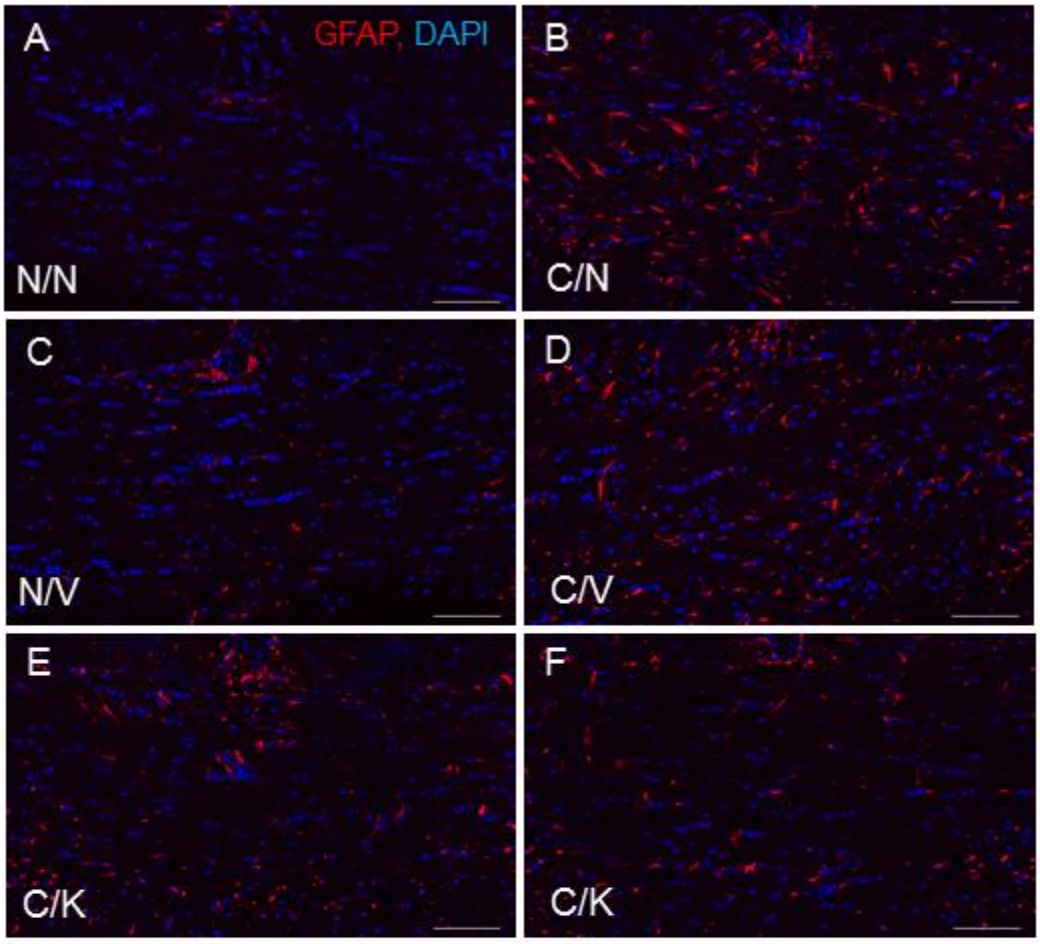
A
GFAP, DAPI
N/N
B
C/N
C
N/V
D
C/V
E
C/K
F
C/K

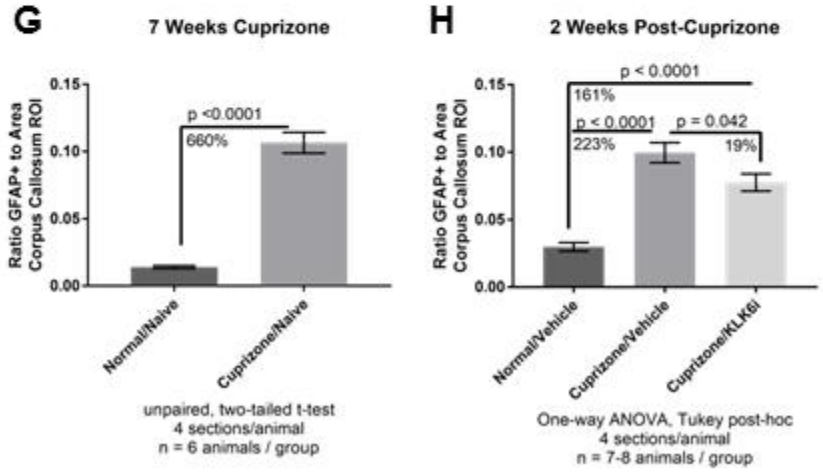
G
7 Weeks Cuprizone
Ratio GFAP+ to Area Corpus Callosum ROI
0.15
0.10
0.05
0.00
p <0.0001
660%
Normal/Naive
Cuprizone/Naive
unpaired, two-tailed t-test
4 sections/animal
n = 6 animals / group
H
2 Weeks Post-Cuprizone
p < 0.0001
161%
p < 0.0001
223%
p = 0.042
19%
Normal/Vehicle
Cuprizone/Vehicle
Cuprizone/KLK6i
One-way ANOVA, Tukey post-hoc
4 sections/animal
n = 7-8 animals / group

Figure 7. KLK6i Treatment Post-Cuprizone Does Not Alter Microgliosis

A-B, G: Compared to normal/naïve mice, a 25% increase in Iba1+ stain/area was induced with seven weeks 0.2% cuprizone administration in mouse corpus callosum. Quantification was done using a custom algorithm designed in Visiopharm. Statistical analysis was done using an unpaired, two-tailed t-test.

C-F, H: Two weeks after cuprizone withdrawal, an 18% increase in microgliosis (defined by Iba1+ stain/area) persisted in the corpus callosum of cuprizone/vehicle treated animals compared to normal/naïve treated. No statistically significant difference in Iba1+ stain was found between cuprizone/vehicle treated and cuprizone/KLK6i treated animals. Quantification was done using a custom algorithm designed in Visiopharm. Statistical analysis was done using a one-way ANOVA with Tukey post-hoc.

Iba1 = green; DAPI = blue. Scale bar = 100 µm. All graphs within the figure represent the data as mean plus or minus the standard error of the mean.

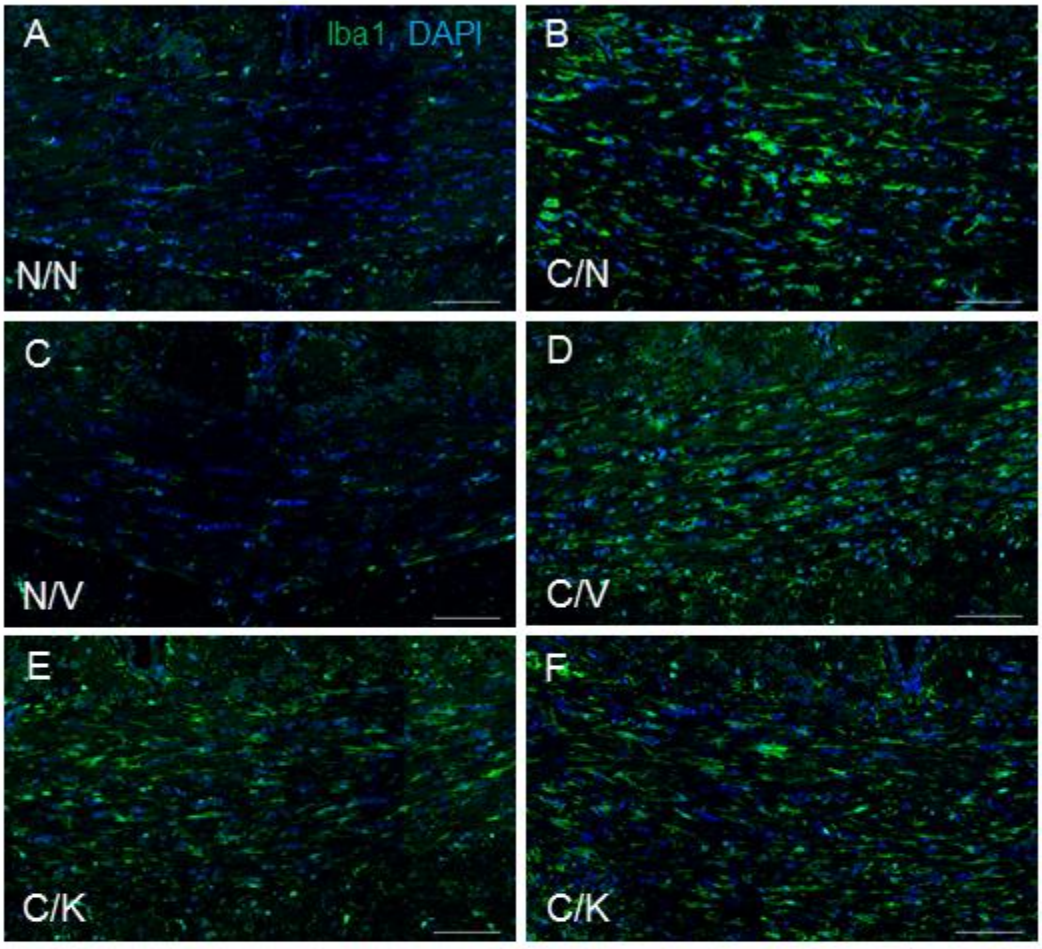
A
Iba1, DAPI
N/N
B
C/N
C
N/V
D
C/V
E
C/K
F
C/K

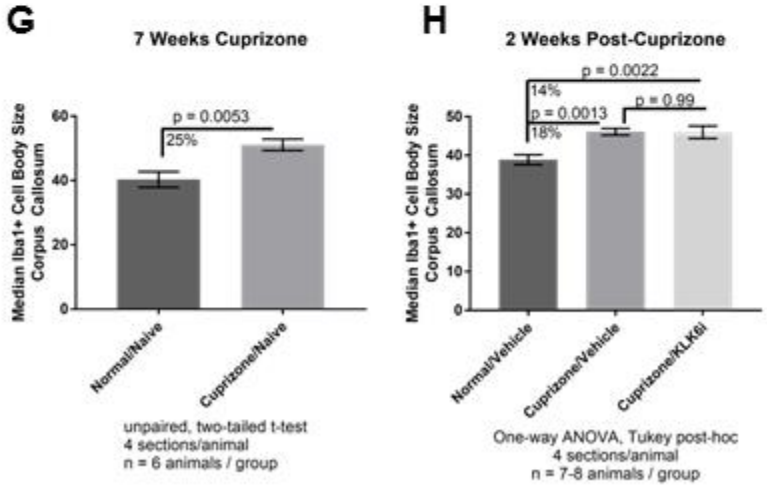
G
7 Weeks Cuprizone
Median Iba1+ Cell Body Size Corpus Callosum
p = 0.0053
25%
Normal/Naive
Cuprizone/Naive
unpaired, two-tailed t-test
4 sections/animal
n = 6 animals / group
H
2 Weeks Post-Cuprizone
p = 0.0022
14%
p = 0.0013
p = 0.99
18%
Normal/Vehicle
Cuprizone/Vehicle
Cuprizone/KLK6i
One-way ANOVA, Tukey post-hoc
4 sections/animal
n = 7-8 animals / group

Figure 8. Oligodendrocyte Precursor Cells Are Not Altered by Cuprizone, KLK6i Treatment

A-B, G: No statistically significant changes in NG2, a marker of oligodendrocyte precursor cells, immunohistochemical staining were present in the corpus callosum following seven weeks of 0.2% cuprizone treatment. Quantification was done using a custom algorithm designed in Visiopharm. Statistical analysis was done using an unpaired, two-tailed t-test.

C-F, H: No statistically significant changes in NG2 immunohistochemical staining in the corpus callosum were observed two weeks after cuprizone withdrawal or with continuous KLK6 inhibitor infusion into the lateral ventricle. Quantification was done using a custom algorithm designed in Visiopharm. Statistical analysis was done using a one-way ANOVA with Tukey post-hoc.

NG2 = green; DAPI = blue. Scale bar = 100 μm. All graphs within the figure represent the data as mean plus or minus the standard error of the mean.

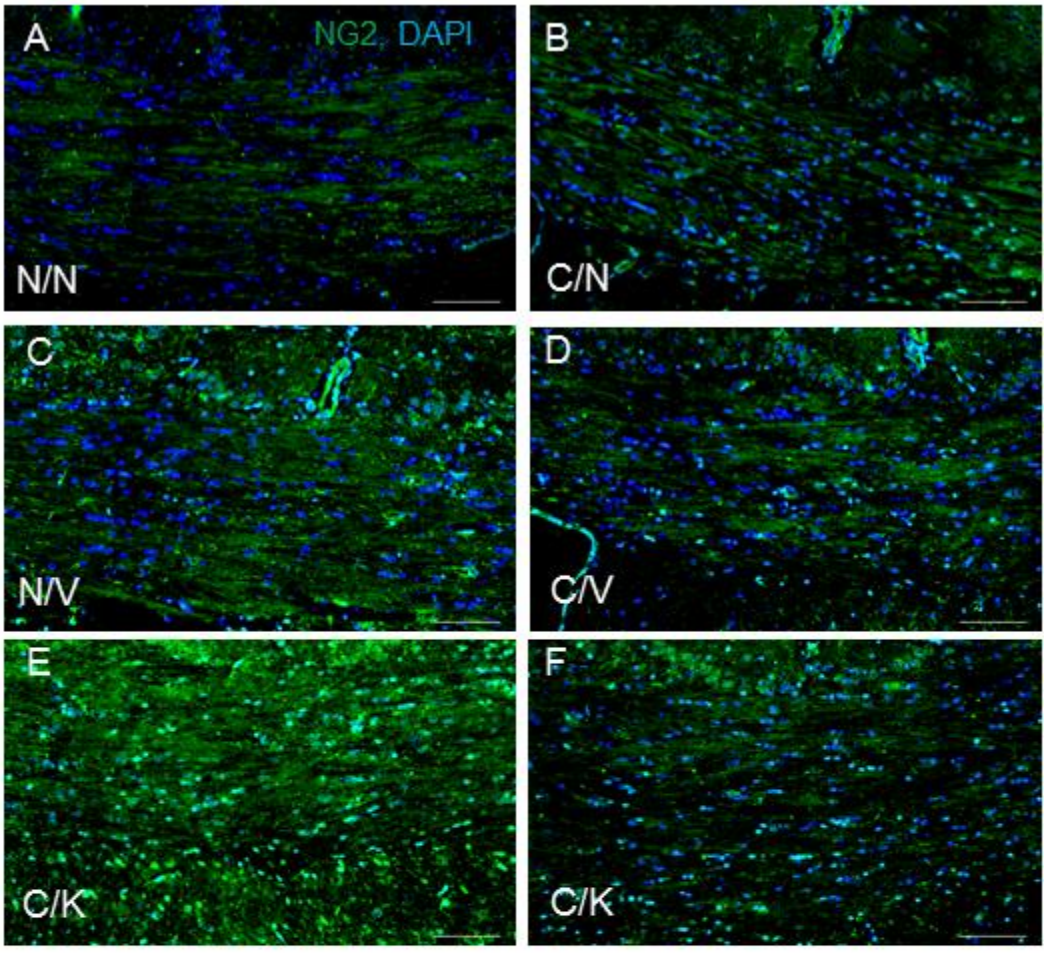
A
NG2, DAPI
N/N
B
C/N
C
N/V
D
C/V
E
C/K
F
C/K

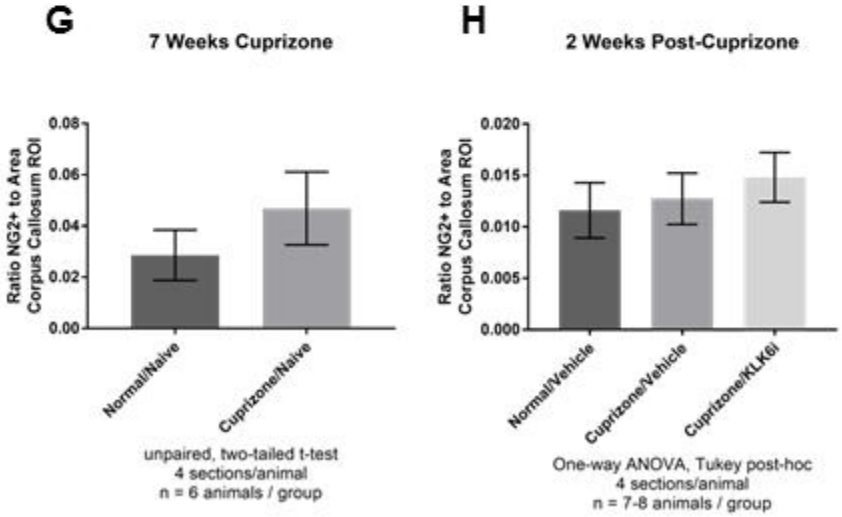
G
7 Weeks Cuprizone
Ratio NG2+ to Area
Corpus Callosum ROI
0.08
0.06
0.04
0.02
0.00
Normal/Naive
Cuprizone/Naive
unpaired, two-tailed t-test
4 sections/animal
n = 6 animals / group
H
2 Weeks Post-Cuprizone
Ratio NG2+ to Area
Corpus Callosum ROI
0.020
0.015
0.010
0.005
0.000
Normal/Vehicle
Cuprizone/Vehicle
Cuprizone/KLK6i
One-way ANOVA, Tukey post-hoc
4 sections/animal
n = 7-8 animals / group

Figure 9. The Effects of PAR1 Inhibition on In Vivo Remyelination

A-B, G: A 45% reduction in corpus callosum myelinated fibers (Luxol Fast Blue) is seen in mouse brain after 7 weeks 0.2% cuprizone treatment (cuprizone/naïve, C/N) versus normal chow vehicle (normal/naïve, N/N), quantified using a custom algorithm designed in Visiopharm. Statistical analysis was done using an unpaired, two-tailed t-test.

C-F, H: Following 7 weeks 0.2% cuprizone treatment administration, normal vehicle chow was resumed for 2 weeks concurrent with subcutaneous administration of a PAR1 inhibitor (50mg/kg) or Vehicle. Naïve animals that never received cuprizone treatment (Normal/Naïve, N/N) were carried along as sample processing comparison. Compared to naïve, a 25% reduction was seen 2 weeks post-cuprizone withdrawal in the vehicle group. There was no statistically significant change in myelinated fibers during this time in this portion of the corpus callosum between Cuprizone/Vehicle (C/V) and Cuprizone/PAR1 (C/P) inhibitor treatment. Representative images from one to two animals per group are shown. Quantification was done using a custom algorithm designed in Visiopharm. Statistical analysis was done using a one-way ANOVA with Tukey post hoc comparisons. Scale bar = 100 µm. All graphs within the figure represent the data as mean plus or minus the standard error of the mean.

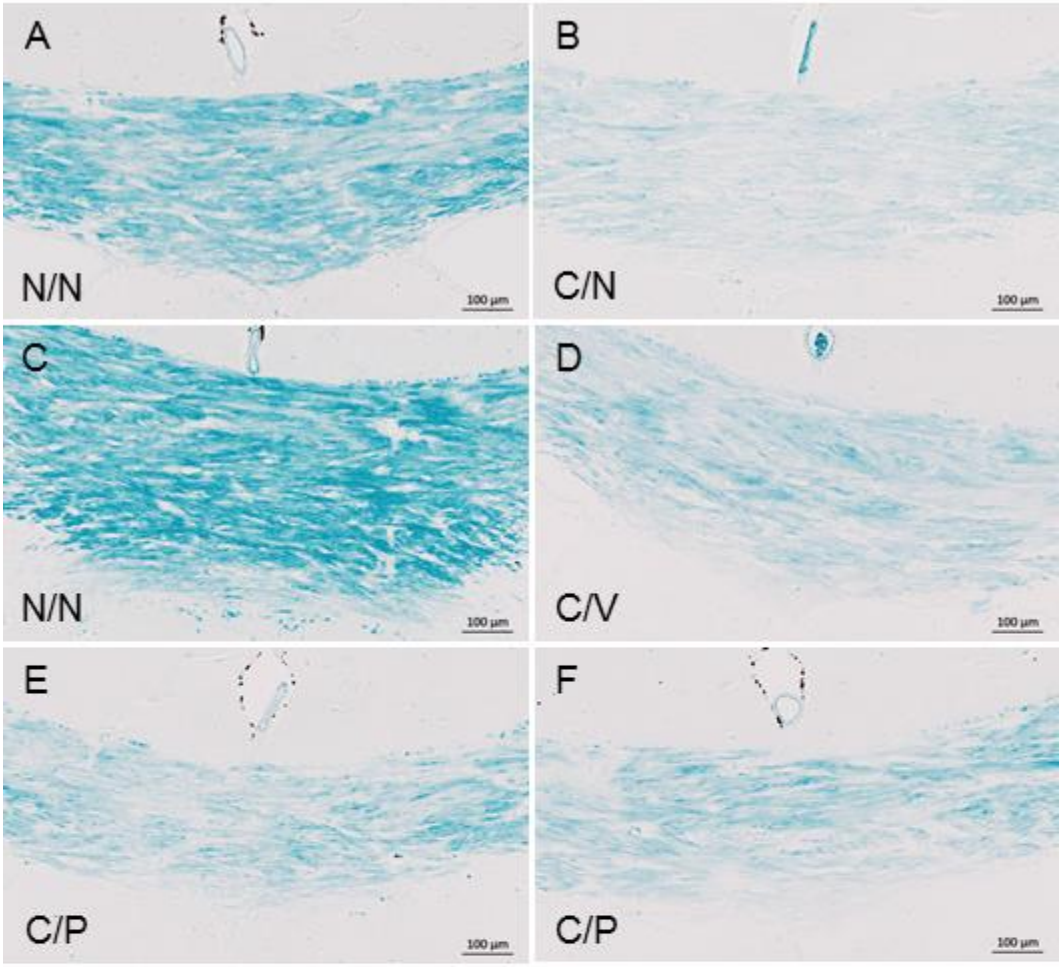

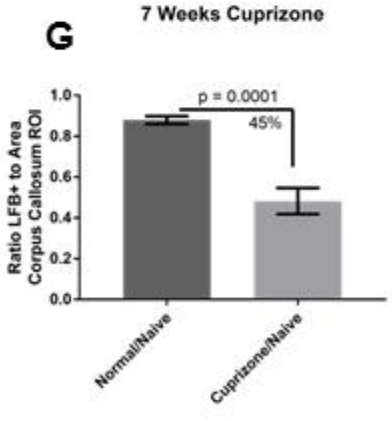

unpaired, two-tailed t-test
4 sections/animal
n = 6 animals/group

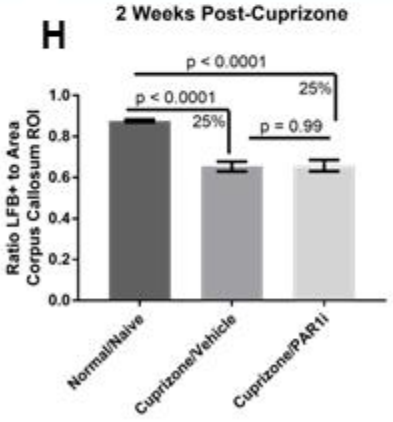

One-way ANOVA, Tukey post-hoc
4 sections/animal
n= 5-6 animals/group

Figure 10: Oligodendrocyte Precursor Cells Are Not Impacted By Cuprizone, PAR1i Treatment

Oligodendrocyte precursor cells (labeled by the chondroitin sulfate proteoglycan protein NG2) in the corpus callosum (**A-H**) and cingulate cortex (**I-M**) are not impacted by cuprizone treatment nor altered upon PAR1 inhibitor treatment. Cuprizone (0.2%) was administered in chow for seven weeks, then withdrawn for the 2 week period of remyelination during which a 50 mg/kg PAR1 inhibitor or vehicle was administered. A custom algorithm (Visiopharm) was used to assess percentage of stained NG2-positive pixels per area over the region of interest (cingulate cortex or anterior body of the corpus callosum). Statistical analysis was done with either an unpaired, two-tailed t-test or a one-way ANOVA with Tukey post-hoc comparisons.

NG2 = green; DAPI = blue. Scale bar = 100 μm. All graphs within the figure represent the data as mean plus or minus the standard error of the mean.

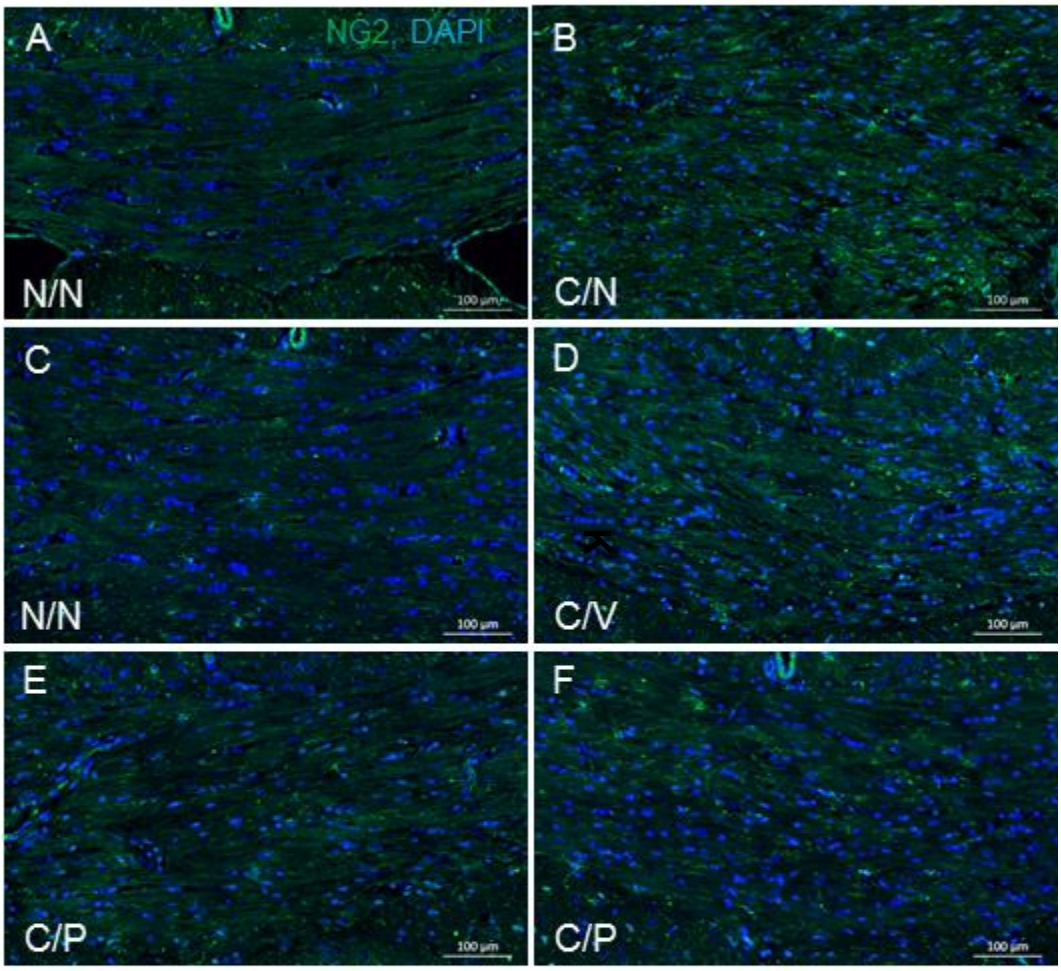

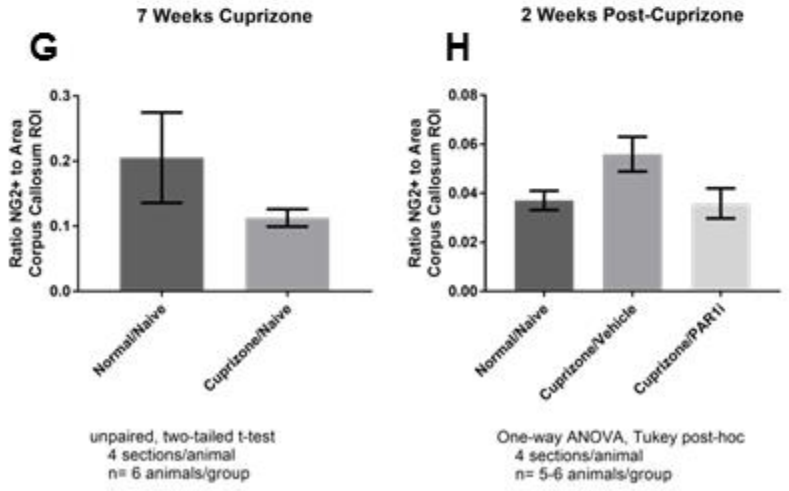

unpaired, two-tailed t-test
4 sections/animal
n= 6 animals/group

One-way ANOVA, Tukey post-hoc
4 sections/animal
n= 5-6 animals/group

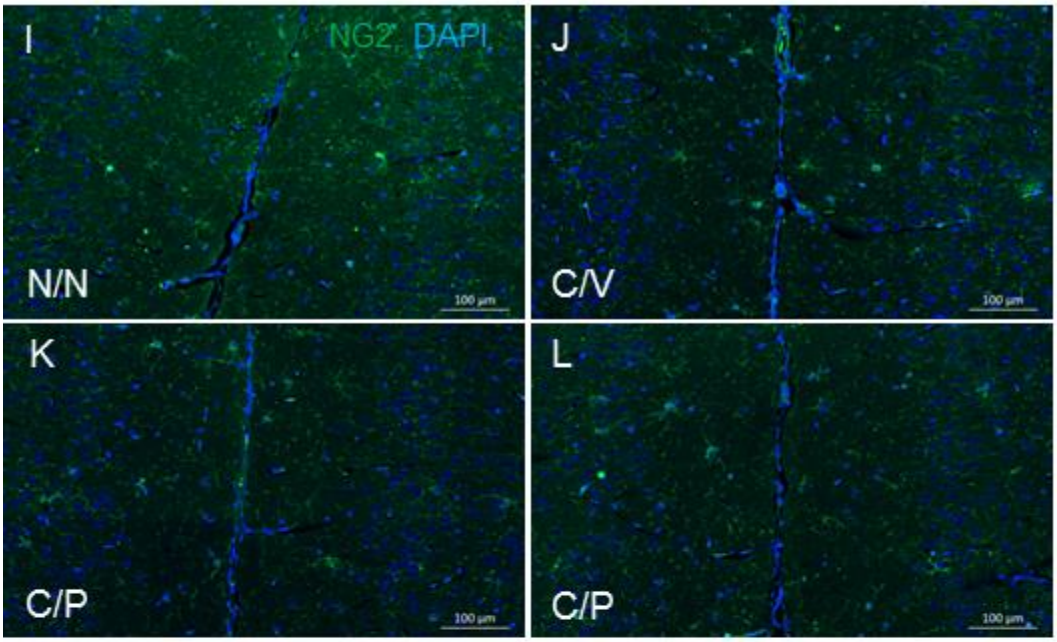

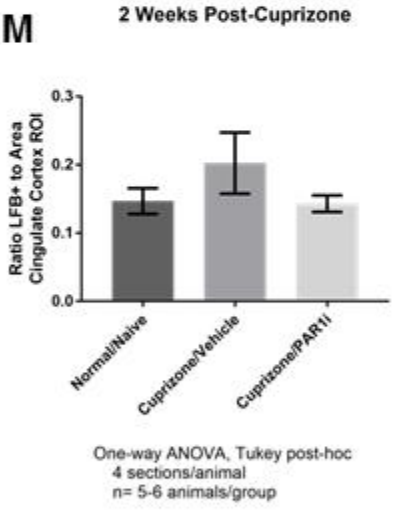

One-way ANOVA, Tukey post-hoc
4 sections/animal
n= 5-6 animals/group

Figure 11: Astrogliosis Is Induced With Cuprizone Treatment but Is Not Modulated Upon Treatment with A PAR1 Inhibitor

A-B, G: An above 400% increase in astrogliosis (as measured by GFAP immunoreactivity, red, per area analyzed) was seen in the corpus callosum in mouse brain after 7 weeks 0.2% cuprizone treatment (cuprizone/naïve, C/N) versus vehicle (vehicle/naïve, V/N), quantified using a custom algorithm designed in Visiopharm. Statistical analysis was done using an unpaired, two-tailed t-test. **C-F, H:** Following 7 weeks 0.2% cuprizone treatment administration, vehicle chow was resumed for 2 weeks concurrent with subcutaneous administration of a PAR1 inhibitor (50mg/kg) or Vehicle. Naïve animals that never received cuprizone treatment (Vehicle/Naïve, V/N) were carried along as sample processing comparison. A continued above 400% increase in astrogliosis was present 2 weeks post-cuprizone withdrawal in the vehicle group compared to naive. There was no statistically significant change in astrogliosis in the corpus callosum with Cuprizone/PAR1 (C/P) inhibitor treatment compared to Cuprizone/Vehicle (C/V). Representative images from one to two animals per group are shown. Quantification was done using a custom algorithm designed in Visiopharm. Statistical analysis was done using a one-way ANOVA with Tukey post hoc comparisons.

GFAP = red; DAPI = blue. Scale bar = 100 μm. All graphs within the figure represent the data as mean plus or minus the standard error of the mean.

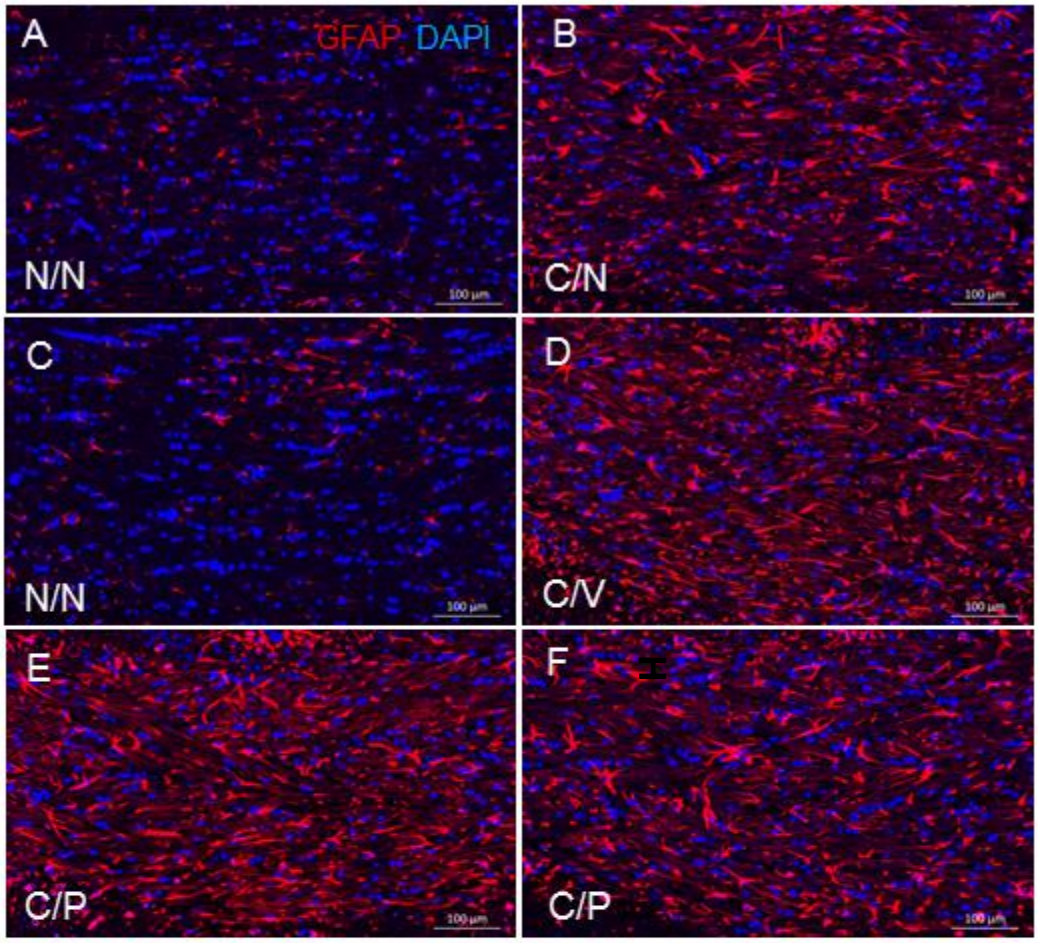

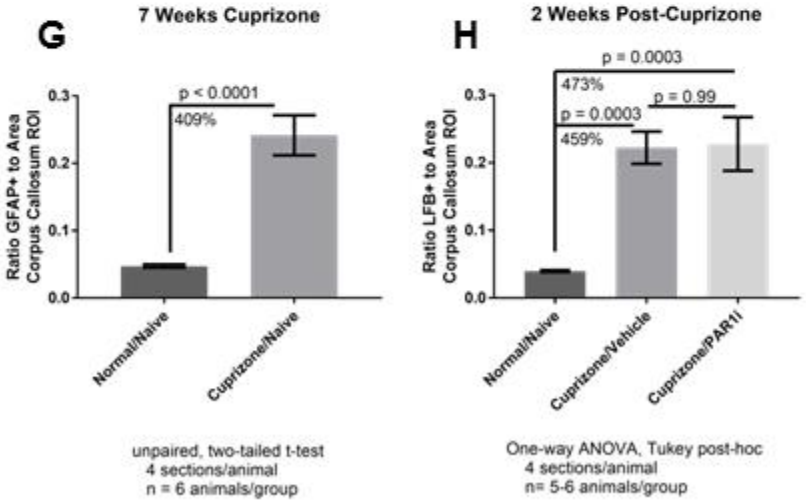

unpaired, two-tailed t-test
4 sections/animal
n = 6 animals/group

One-way ANOVA, Tukey post-hoc
4 sections/animal
n= 5-6 animals/group

Figure 12: Microgliosis Is Induced With Cuprizone Treatment but Is Not Modulated Upon Treatment with A PAR1 Inhibitor

A, B, G: An 160% increase in microgliosis (as measured by Iba1 immunoreactivity) in the corpus callosum is seen in mouse brain after 7 weeks 0.2% cuprizone treatment (cuprizone/naïve, C/N) versus vehicle (vehicle/naïve, V/N), quantified using a custom algorithm designed in Visiopharm. Statistical analysis was done using an unpaired, two-tailed t-test.

C-F, H: Following 7 weeks 0.2% cuprizone treatment administration, vehicle chow was resumed for 2 weeks concurrent with subcutaneous administration of a PAR1 inhibitor (50mg/kg) or Vehicle. Naïve animals that never received cuprizone treatment (Vehicle/Naïve, V/N) were carried along as sample processing comparison. A continued above 100% increase in microgliosis was present 2 weeks post-cuprizone withdrawal in the vehicle group compared to naive. There was no statistically significant change in microgliosis in the corpus callosum with Cuprizone/PAR1 (C/P) inhibitor treatment compared to Cuprizone/Vehicle (C/V). Representative images from one to two animals per group are shown. Quantification was done using a custom algorithm designed in Visiopharm. Statistical analysis was done using a one-way ANOVA with Tukey post hoc comparisons.

Iba1 = red; DAPI = blue. Scale bar = 100 µm. All graphs within the figure represent the data as mean plus or minus the standard error of the mean.

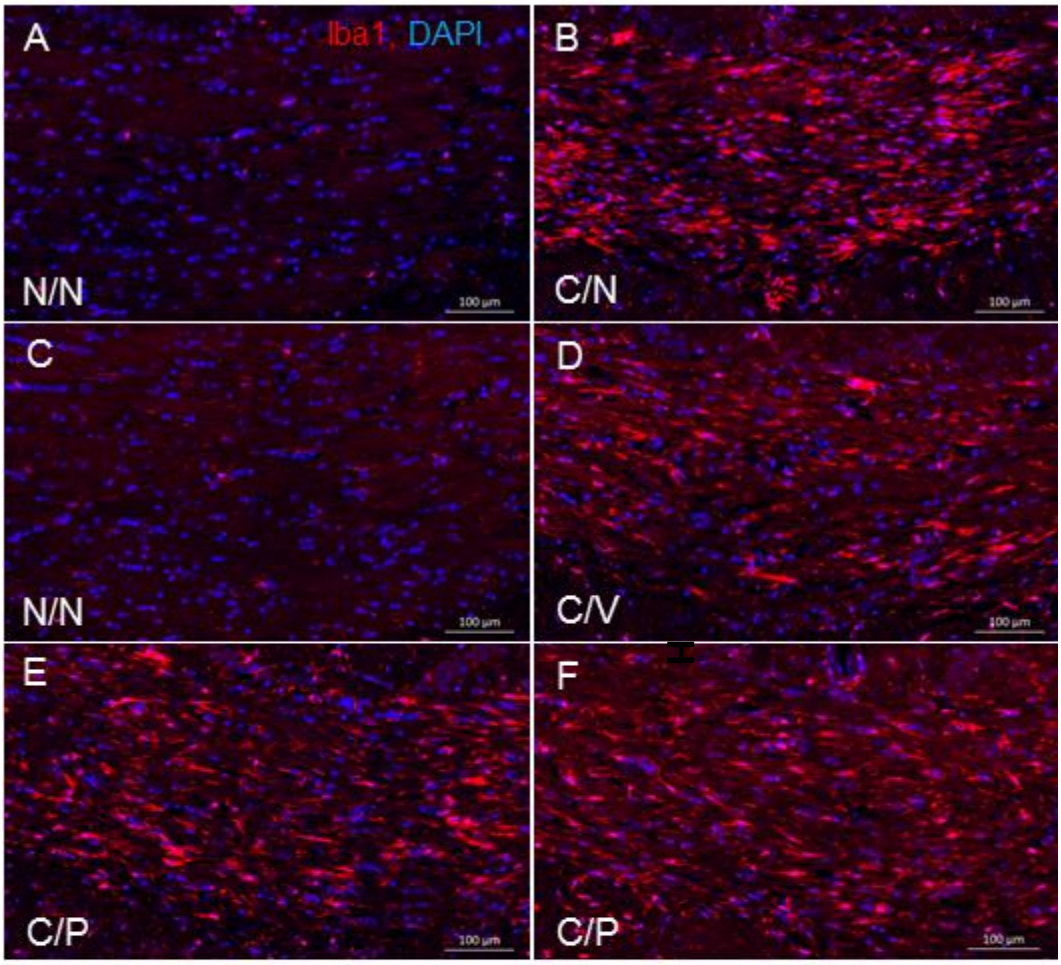

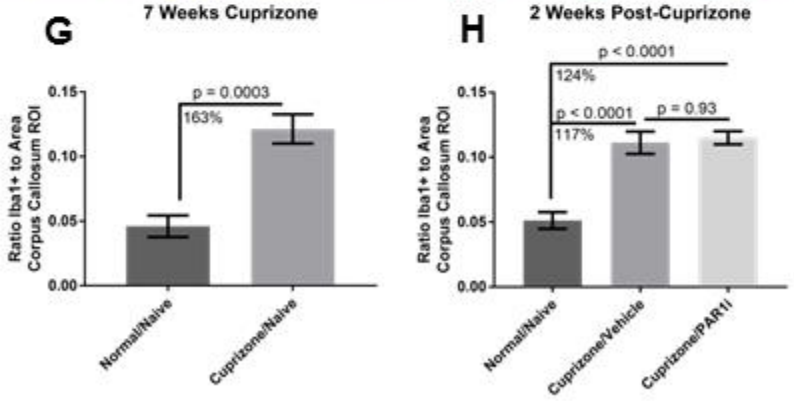

unpaired, two-tailed t-test
4 sections/animal
n= 6 animals/group

One-way ANOVA, Tukey post-hoc
4 sections/animal
n= 5-6 animals/group

CHAPTER FOUR

Kallikrein 6 in Multiple Sclerosis

a) Introduction

Multiple sclerosis (MS) is a heterogeneous disorder, with patients manifesting various combinations of symptoms to varying levels of severity over different periods of time. Sub-classification types of MS exist in an attempt to further define the patient experience and behavioral representation of disease pathology. Relapsing-remitting MS (RRMS) patients cycle through phases of disability and remission while progressive MS patients (secondary or primary; SPMS, PPMS) increase in disability over time (Stadelmann and Bruck, 2008). Diagnosis of MS and characterization of a patient within a sub-classification of the disease is based largely on clinical history and assessment by the neurologist (Katz Sand, 2015; Thompson *et al.*, 2017). Currently, there are no biomarkers available that can specifically assess degree of MS pathology or define subsets of MS (Siva, 2018). Magnetic resonance imaging is generally done to examine the presence of white matter lesions in the brain, although it does not exclude other white matter-affecting disorders (Katz Sand, 2015; Siva, 2018). Through T2 MRI (with or without gadolinium-contrast agent), gross white matter pathology in the brain and spinal cord can be visualized (Katz Sand, 2015). Although this measure is not generally used to determine the primary endpoint of clinical efficiency in therapeutic-directed clinical trials, perhaps due to current imaging

limitations, it is often a measure observed to see if progress has been made. Clinical MRI methods are continuously evolving to become more sensitive and to have higher resolution (Kilsdonk *et al.*, 2016).

Although these measures do not diagnose MS, assessment of CNS pathology in MS can be examined in more detail using cerebrospinal fluid and blood product samples as well as histological/immunohistochemical analysis of brain and spinal cord collected post-mortem (Katz Sand, 2015; Siva, 2018). Researchers are currently investigating potential biomarkers in MS CSF and plasma/serum (Housley *et al.*, 2015).

Kallikrein 6 (KLK6; also known as protease M, neurosin, or myelencephalon-specific protease), is a serine protease that has been proposed as a biomarker in cancer and neurodegenerative disease (Ruckert *et al.*, 2008; Petraki *et al.*, 2012; Seiz *et al.*, 2012; Dukic *et al.*, 2016). Recently, it has been found to be increased in MS patients. One study has shown that MS patients (with unspecified sub-classification) have around 4 ng/mL higher levels of KLK6 in their CSF (Hebb *et al.*, 2010). Another has demonstrated that SPMS patient serum has ~0.5 µg/L higher KLK6 than in control patients; this same study also tested RRMS patients but variability was high across patients (Scarisbrick *et al.*, 2008). A separate study found an increase in KLK6 of RRMS patient CSF versus control when they examined active KLK6 levels (Bando *et al.*, 2018). They also reported that MS patients that had received a pulse of steroid treatment (broad

anti-inflammatory treatment) had lower levels of KLK6 in CSF compared patients who hadn't (Bando *et al.*, 2018).

The presence of KLK6 has also been generally noted within MS plaques and around their borders using immunohistochemistry (Scarisbrick *et al.*, 2002). RNA sequencing data from rodents and patients without MS suggests that expression is primarily in oligodendrocytes out of common cells found within the brain in their basal state (Zhang *et al.*, 2014; Zhang *et al.*, 2016). However, other cells may express KLK6 in activated states which is supported by reports that KLK6 aids in T lymphocyte cell survival and causes astrocytes to become reactive (Scarisbrick *et al.*, 2011; Scarisbrick *et al.*, 2012a). In animal models, KLK6 has been noted in macrophages and T cells in addition to cells of oligodendroglial cell lineage (Blaber *et al.*, 2004; Terayama *et al.*, 2005).

The cellular pathology at the level of MS plaque is another diverse aspect of the disease and has been categorized into general subgroups in sometimes slightly different ways by different researchers. Kuhlmann et al. have recently proposed a single system aimed at unifying these scales for ease of comparison across patients and studies (Kuhlmann *et al.*, 2017). This scale varies across the amount of macrophage/microglia activity (active, mixed, or inactive) within the lesion and whether the lesion is demyelinating or post-demyelinating (Kuhlmann *et al.*, 2017). Active lesions can contain reactive microglia/macrophages, astrocytes, and T cells. They are more commonly found in RRMS patients and

decrease with length of disease (Kuhlmann *et al.*, 2017). Mixed active lesions have an outer border of activated microglia/macrophages and are more common in patients with longer disease duration and/or progressive types of MS (Kuhlmann *et al.*, 2017). Inactive lesions have few microglia or T cells but may haven axonal damage or loss, and an astrocytic glial scar; these lesions are found in even longer duration of disease patients and progressive types of MS (Kuhlmann *et al.*, 2017). Demyelinating lesions are characterized by a lack of myelin debris whereas post-demyelinating lesions do have debris; either state can be present with any inflammatory activity state (Kuhlmann *et al.*, 2017). Lesion location appears to be associated with spontaneous remyelination; periventricular lesions have less remyelination than subcortical white matter lesions (Lassmann, 2013). Remyelination is less common in lesions of patients with longer disease duration (Stangel *et al.*, 2017).

Limited data exists on KLK6 expression in specific cell types in MS brain, as well as between subtypes of lesions and across sub-classifications of the disease. The scope of execution on these tasks within this work was limited based on availability of postmortem MS patient brain tissue and number of lesion present within tissue obtained. Chapter four of this work focuses on the characterization of KLK6 expression in human postmortem tissue. Existing RNA sequencing information databases containing normal adult human tissue samples from various regions of the body were examined to determine KLK6

expression relative to the CNS and amongst other serine hydrolases. Postmortem MS patient brain lesions in subcortical white matter were examined for KLK6 expression using immunohistochemistry after immunocytochemical validation of the antibody to detect the human KLK6 protein.

b) Methods

i. Analysis of Adult Human Tissue Expression of KLK6

The Genotype-Tissue Expression (GTEx) Consortium database profiles gene expression by RNA sequencing across 449 adult human donors, within 42 distinct biological tissues spanning the subregions of the brain and body (Consortium *et al.*, 2017). The GTEx dataset (http://www.gtexportal.org) was utilized to examine the distribution and expression level of two-hundred and thirty-two serine hydrolases. A heat map was generated to demonstrate expression levels of the top 50 serine hydrolases (y-axis) at the genetic level that are enriched in brain compared to other tissues (x-axis). The scale (4 to -4) reflects a weighted average expression across tissues, where 4 (dark red) equals a 16-fold (2^4) increase in expression and -4 (dark blue) is a 16-fold decrease in expression. Additionally, a transcripts per million (tpm) graph was generated to illustrate and compare KLK6 expression levels in different subregions of the brain and body across multiple subjects.

ii. Validation of Human KLK6 Antibody by Immunocytochemistry

To determine specificity of KLK6-directed human antibodies, Chinese hamster ovary cells were transfected with full length human KLK6 (NM_002774) C-terminally tagged with myc and FLAG in the pCMV6-Entry plasmid (Origene RC218647) using Lipofectamine 2000 (Thermofisher Scientific). For each treatment condition (Naïve, Non-template control transfected, KLK6 transfected), at least 6 ninety-six wells were run. Following transfection, cells were fixed using 4% paraformaldehyde. Immunocytochemical staining was then done. Briefly, cells were permeabilized for 15 minutes with 0.5% triton-X-100, and then blocked for 1 hour in 10% normal donkey serum (Jackson ImmunoResearch) in PBS. Primary antibodies were incubated at 4 degree Celsius for 24 hours (**Table 7**). Then, samples were rinsed with PBS, incubated in donkey host species secondary antibodies with 568, Cy3, or 647-conjugated fluorophores (Thermofisher Scientific or Jackson ImmunoResearch) for 2 hours, and then counterstained with DAPI (Thermofisher Scientific). Full wells were imaged using a CellDiscoverer7 (Zeiss).

iii. Multiple Sclerosis Patient Tissue

Formalin-fixed, post-mortem human brain tissue was obtained from the Rocky Mountain Multiple Sclerosis Center Tissue Bank and National Multiple Sclerosis Society (**Table 6**). Tissue was blocked and processed to paraffin wax using a VIP6 Tissue Processor (Sakura), and sectioned at 5μm thickness using a microtome (Leica RM2145).

iv. Immunohistochemistry

Sections were hydrated from paraffin wax using xylene, and gradient ethanol solutions to water. Citrate antigen retrieval (Biogenex) was performed in a pressurized decloaking chamber (BioCare Medical) for 30 seconds at 120 degrees Celsius, then 10 seconds at 84.5 degrees Celsius. Afterwards, sections were stained using fluorescent immunohistochemistry. Briefly, sections were incubated with 0.5% tritonX-100 for 15 minutes, then with 10% normal serum of secondary antibody host species for 20 minutes, then primary antibody for ~48 hours at 4 degree Celsius (**Table 7**). After PBS washes, secondary antibodies (AlexaFluor, Thermofisher Scientific) directed against the primary antibody host species were applied for 1.5 hours, and then counterstained with DAPI (Thermofisher Scientific). Sections were imaged using a Zeiss Axioscan Z1 microscope and qualitatively examined.

c) Results

Two hundred and thirty-two serine hydrolases were profiled to determine those that are enriched in brain compared to peripheral tissues using the GTEx RNA sequencing database of adult human post-mortem tissue. KLK6 was determined to be the top serine hydrolase in that it has the highest expression in the largest number of CNS tissues compared to peripheral tissues **(Figure 13A)**. The GTEx database was also used to visualize expression levels of KLK6 in transcripts per million across CNS and peripheral tissues in post-mortem adult human tissue. KLK6 expression was shown to be elevated in brain, spinal cord, and epithelia of peripheral tissues such as skin, esophagus, and reproductive organs (**Figure 13B**). Other kallikrein family members (KLK7, KLK5, KLK8, KLK10, KLK14) were also found in the top 50 serine hydrolases with enriched brain expression compared to peripheral tissue expression (**Figure 13A**).

To study KLK6 at the protein level, an antibody reactive to human kallikrein 6 was validated using immunocytochemistry following transient transfection of CHO cells with lipofectamine and a FLAG-conjugated vector containing the full-length human KLK6 gene. FLAG (**Figure 14**, red) and KLK6 (**Figure 14**, green) co-localized using the human KLK6 abcam ab191281 antibody (**Figure 14**, Merge). No stain was apparent from either antibody with a non-transfected control (NTC) cell cohort (**Figure 14**).

Formalin-fixed post-mortem brain tissue was obtained from patients with a variety of MS subtypes for immunohistochemical analysis of KLK6 expression (**Table 6**), including PPMS, SPMS, and RRMS. White matter plaques were visible in the majority of samples across the subclassifications using an antibody to MBP. In general, most plaques were located in rostral telencephalic subcortical white matter and/or in close proximity to the ventricular system (**example, Figure 15A-B**). Cellular KLK6 staining was noted within several plaques, but absent in others. Images from a SPMS patient demonstrate two adjacent plaques [absence of MBP stain (red)], where the plaques have different levels of KLK6 (green) protein expression (**Figure 15C)**. KLK6 staining was found in nearly all of the cases studied, regardless of MS behavioral subclassification. Aside from heterogeneous localization of KLK6 in plaques, cellular KLK6 staining was found in some cortical regions across MS subclassifications. In some instances cellular KLK6 staining was also found close to ventricular spaces even in the absence of MBP-negative plaques. The majority of KLK6 cells across all cases and brain regions exhibited a hypertrophied stellate morphology. To investigate cell type classification of staining given this profile, immunohistochemical co-labeling was done with astrocyte marker GFAP and microglia/macrophage marker Iba1. It was confirmed that the majority of KLK6 staining co-localized with astrocytic marker GFAP across the cases and

regions of the brain (**Figure 15D-E**). In contrast, cellular KLK6 staining did not co-localize with microglial marker Iba1 (**Figure 15F-G**).

d) Discussion

Previous reports indicate that KLK6 gene expression is restricted to oligodendrocytes versus other major cell types in rodent and human brain such as neurons, microglia, and astrocytes (Zhang *et al.*, 2014; Zhang *et al.*, 2016). However, elevated levels of KLK6 protein have been identified in patients with MS, a CNS autoimmune disease that results in deterioration of myelin, and thus, the oligodendrocytes whose processes myelinate axons. Several studies have been done using MS patient biological fluids, such as CSF or serum. Specifically, MS patients showed higher KLK6 levels in CSF compared to controls (Hebb *et al.*, 2010). Active KLK6 has also been found to be increased in RRMS patient CSF compared to controls (Bando *et al.*, 2018). SPMS patient serum has been demonstrated to contain higher KLK6 than control patients (Scarisbrick *et al.*, 2008). High expression in CSF and serum could indicate that KLK6 is being cleared from the brain via dural venous sinuses and into the bloodstream. Still, it is unclear why KLK6 is elevated in MS brain, CSF or blood products. Data presented in this work using the GTEx database illustrates that KLK6 is normally enriched in the CNS compared to peripheral tissues in adult humans, and has the distinction of being the most abundant serine hydrolase in the CNS. The

enrichment of KLK6 in CNS compared to peripheral tissues also makes it an attractive therapeutic target for neurological disease in that it might be expected to have less off-target side effects. Because KLK6 is found to be elevated in MS patients compared to disease, a potential therapeutic avenue might be to lower KLK6 levels in MS. However, further characterization is needed to understand KLK6 expression in normal and MS brain.

Limited work has been done to characterize overall KLK6 expression at the protein level in human tissues. It has been shown that besides brain, peripheral nerves, choroid plexus and other glandular epithelia related tissue has high protein expression of KLK6 (Petraki *et al.*, 2001). These findings appear in line with GTEx gene expression KLK6 dataset results.

In MS brain, KLK6 has been shown to be associated with plaques using immunohistochemistry (Scarisbrick *et al.*, 2002). Here I have shown that KLK6 is not expressed equally in all plaques in MS brain tissue. Further, that its expression does not correspond to only a particular subclassification of MS such as SPMS or RRMS. In addition, cellular KLK6 staining can also be seen close to the ventricular system or in cortical regions despite the absence of plaques.

Based on the heterogeneous pattern within MS plaques, it seemed likely that KLK6 staining might be related to cellular composition of the plaque and whether active, mixed, or inactive state. MS plaque activity status is weighted on involvement of inflammatory cells, but particularly microglia/macrophages

(Kuhlmann *et al.*, 2017). Additionally, there is some evidence that KLK6 is present in activated astrocytes in multiple neurological indications such as spinal cord injury, glioblastoma multiforme, and MS (Scarisbrick *et al.*, 2012a).

I found that that cells immunoreactive for KLK6 in the MS cases tested were not likely to be macrophages or microglia due to lack of co-localization with Iba1. Instead, many KLK6 positive cells in the MS patient brains (in plaques and beyond) tested co-localized with astrocytic marker GFAP. Further, their stellate and hypertrophied morphology suggested their status as reactive astrocytes. The high correspondence of KLK6 to GFAP-positive cells makes it appear that very few KLK6-positive cells could also be oligodendrocytes.

Despite this, there may still be a connection between KLK6 expression and oligodendrocyte biology that include astrocytes. Astrocytes are influential in oligodendrocyte maturation and myelination. Astrocytes secrete factors such as PDGF, bFGF2, and LIF that promote oligodendrocyte maturation and myelination (Domingues *et al.*, 2016). Additionally, oligodendrocytes primarily obtain lipids to synthesize myelin from astrocyte lipid synthesis (Camargo *et al.*, 2017). Astrocytes can also negatively regulate oligodendrocyte maturation and myelination through mechanisms such as secretion of tenascin C, bone morphogenetic proteins, hyaluronan, and ET-1 (Silver and Miller, 2004; Domingues *et al.*, 2016). These latter types of mechanisms are used by astrocytes involved in glial scar formation, which is important in isolating damage

one might see in spinal cord injury or in restoring blood-brain barrier breaches (Silver and Miller, 2004; Domingues *et al.*, 2016). Also reflecting their dual nature and importance in control of regulation of processes, astrocytes can secrete pro-inflammatory or anti-inflammatory factors to influence microglia/macrophage activity (Poutiainen *et al.*, 2016). It has recently been shown that astrocytes are able to phagocytose myelin debris using receptor-mediated endocytosis (Ponath *et al.*, 2017). The precise roles in which astrocytes can impact neurological disease such as MS are unclear. However, recent work from multiple disease areas has highlighted the need to understand the role of astrocytes in neurologic disease and the potential of this work to lead to new therapeutic treatments (Rostami *et al.*, 2017; Hirase and Koizumi, 2018; Ponath *et al.*, 2018). Live imaging methods are in development which could help clarify the role of astrocytes in MS (Poutiainen *et al.*, 2016).

It has been previously reported that exogenous application of KLK6 on to cultured astrocytes results in a hypertrophied, stellate shape and thus, astrogliosis (Scarisbrick *et al.*, 2012a). This suggests that in addition to oligodendrocytes, astrocytes are also responsive to KLK6. Taken together with the genetic evidence that KLK6 is found in oligodendrocytes and negatively associated with maturation, and that it is also a secreted protein which is found on astrocytes, this may suggest that oligodendrocytes regulate astrocytes via

KLK6 to then regulate maturation of oligodendrocytes/myelination by oligodendrocytes.

Further study is warranted to access the relationship between high KLK6 mRNA expression in oligodendrocytes, and protein staining that associates KLK6 immunoreactivity with GFAP-positive astrocytes. This study demonstrated that the antibody used is reactive to human KLK6, ruling out a potential technical explanation. Another explanation could be that genetic expression was assessed in previous cell profiling experiments only during basal state, and that activated astrocytes do express high levels of KLK6. Thirdly, it may be that oligodendrocytes regulate their development by modulating astrocyte signaling with KLK6, as proposed above.

An additional consideration warranting further research is that it is unlikely that all KLK6 represented by immunohistochemical staining is all enzymatically active. It is unknown how protein expression levels of KLK6 correlate with KLK6 enzymatic activity. Methods do not currently exist to profile enzymatic activity at the level of individual cells in human post-mortem tissue.

Due to the limited availability of control tissue processed in a similar manner as MS cases and limited clinical information on patients, comparisons of KLK6 expression across MS and control brain were not described. However, this should be a focus in future studies. Since KLK6 appears to be present in various diseases with reactive astrocytes, it might be that all reactive astrocytes stain for

KLK6, which would include the increase in astrogliosis that occurs with age (Santoro *et al.*, 2018). Additional work should be done using a larger set of plaques of different activity stages from a range of MS patients to confirm a relationship between KLK6 expression and activity level within plaque.

In summary, expression of KLK6 is enriched in the adult human brain compared to peripheral organs and is the most highly expressed serine hydrolase in the CNS. Heterogeneous expression of KLK6 is found in MS plaques and seems more dependent on the activity state of plaques rather than subclassification of MS disease. However, KLK6 is also found outside of plaque regions defined by lack of MBP staining. KLK6 co-localizes with GFAP-positive cells, or astrocytes in MS brain. This suggests a role of KLK6 in astrocyte and oligodendrocyte biology. The consequences of this are relevant for understanding the potential of therapeutic efficacy in MS patients with a KLK6 or KLK6 pathway inhibitor treatment. Further study is needed to understand the relationship between KLK6, astrocytes, oligodendrocytes, and MS.

RMMSC#	Sample Type	Sex	Age	PMI (hours)	Slice
561	PPMS	F	53	19	6
566	PPMS	F	67	22	6
316	SPMS	F	53	N	9
471	SPMS	F	74	24	6
501	Progressive*	M	63	9	6
550	Progressive*	M	42	5.5	6
540	CSLT-MS	M	60	18	8
521	CSLT-MS	F	69	10	7
414	CSLT-MS	M	79	N	7
425	CSLT-MS	F	75	12	6
411	RRMS	M	42	12	6
477	RRMS	F	66	15	5
465	RRMS	M	56	41	7
526	RRMS	M	61	20	6
401	RRMS	M	58	30	7
C113	Control	M	62	24	9

CSLT-MS = Chronic-Severe-Long-term MS (description, not official subclassification); N = Not given; Progressive*= Progressive was described by the family but no medical record confirmation was obtained.

Table 6. Human Brain Tissue Information

Full Name	Short Name	Vendor	Catalog Code	Host Species	Tissue Tested Species
FLAG tag, M2 clone	FLAG	Sigma Aldrich	F9291	Mouse	Human
Myelin Basic Protein	MBP	AbD Serotec	MCA409S	Rat	Mouse, Human
Kallikrein 6	KLK6	Abcam	ab191281	Goat	Human
Glial Fibrillary Acidic Protein	GFAP	Dako North America	Z0034	Rabbit	Mouse, Human
Ionized calcium-binding adapter molecule 1	Iba1	Wako Chemicals	019-19741	Rabbit	Mouse, Human

Table 7. Chapter 4 Antibody Information

Figure 13. Expression of KLK6 in Adult Human Tissues

A large effort by the Genotype-Tissue Expression (GTEx) Consortium profiled gene expression by RNA sequencing across 449 adult human donors, within 42 distinct biological tissues spanning the subregions of the brain and body (Consortium *et al.*, 2017).

A: The GTEx dataset was utilized to examine the distribution and expression level of two-hundred and thirty-two serine hydrolases. KLK6 was one of the highest expressed serine hydrolyses throughout the brain compared to peripheral tissues. This heat map demonstrates expression levels of the top 50 serine hydrolases (y-axis) at the genetic level that are enriched in brain compared to other tissues (x-axis). The scale (4 to -4) reflects a weighted average expression across tissues, where 4 (dark red) equals a 16-fold (2^4) increase in expression and -4 (dark blue) is a 16-fold decrease in expression.

B: Localization of KLK6 expression is shown in transcripts per million (tpm) across multiple adult human tissues. Enriched expression is found in brain, spinal cord, and epithelia of other peripheral tissues including skin, esophagus, and reproductive organs.

A

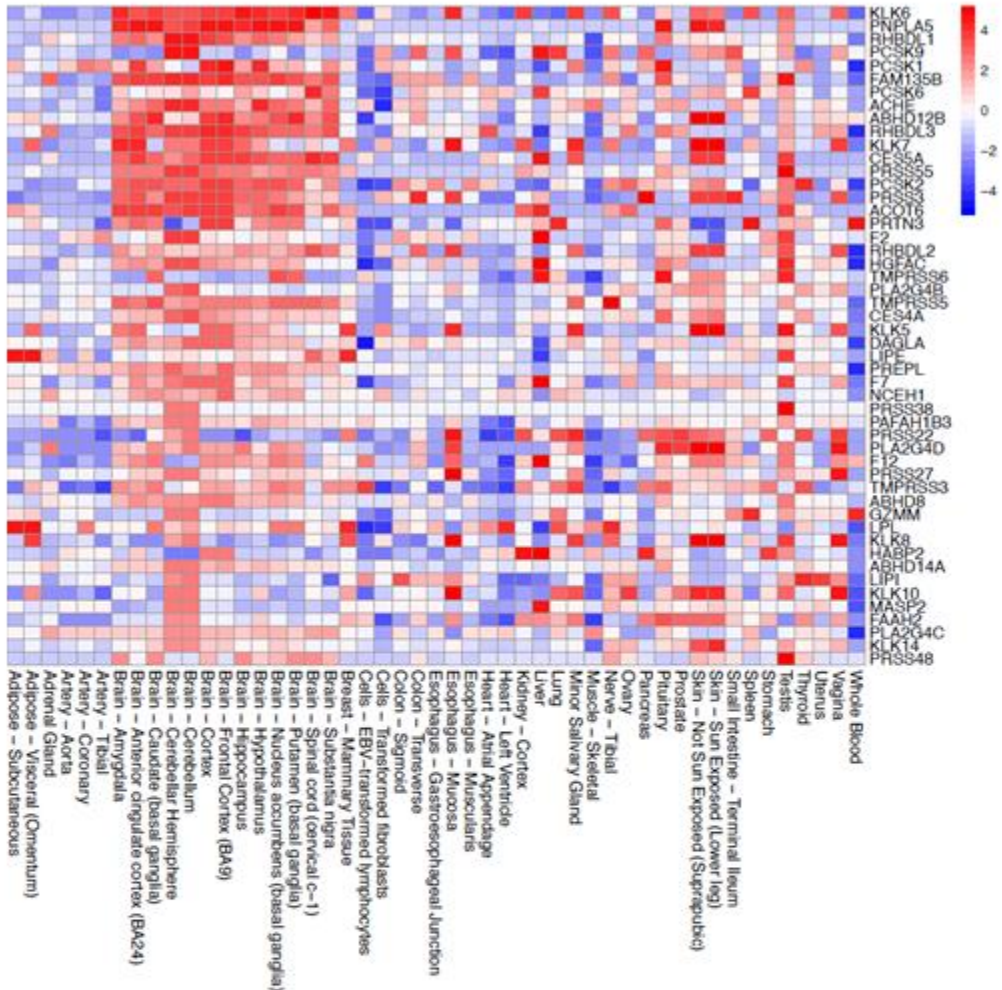
KLK6
PNPLA5
RHBDL1
PCSK9
PCSK1
FAM135B
PCSK6
ACHE
ABHD12B
RHBDL3
KLK7
CES5A
PRSS55
PCSK2
PRSS3
ACOT8
PRTN3
F2
RHBDL2
HGFAC
TMPRSS6
PLA2G4B
TMPRSS5
CES4A
KLK5
DAGLA
LIPE
PREPL
F7
NCEH1
PRSS38
PAFAH1B3
PRSS22
PLA2G4D
F12
PRSS27
TMPRSS3
ABHD8
GZMM
LPL
KLK8
HABP2
ABHD14A
LIPI
KLK10
MASP2
FAAH2
PLA2G4C
KLK14
PRSS48
4
2
0
−2
−4
Whole Blood
Vagina
Uterus
Thyroid
Testis
Stomach
Spleen
Small Intestine – Terminal Ileum
Skin – Sun Exposed (Lower leg)
Skin – Not Sun Exposed (Suprapubic)
Prostate
Pituitary
Pancreas
Ovary
Nerve – Tibial
Muscle – Skeletal
Minor Salivary Gland
Lung
Liver
Kidney – Cortex
Heart – Left Ventricle
Heart – Atrial Appendage
Esophagus – Muscularis
Esophagus – Mucosa
Esophagus – Gastroesophageal Junction
Colon – Transverse
Colon – Sigmoid
Cells – Transformed fibroblasts
Cells – EBV–transformed lymphocytes
Breast – Mammary Tissue
Brain – Substantia nigra
Brain – Spinal cord (cervical c–1)
Brain – Putamen (basal ganglia)
Brain – Nucleus accumbens (basal ganglia)
Brain – Hypothalamus
Brain – Hippocampus
Brain – Frontal Cortex (BA9)
Brain – Cortex
Brain – Cerebellum
Brain – Cerebellar Hemisphere
Brain – Caudate (basal ganglia)
Brain – Anterior cingulate cortex (BA24)
Brain – Amygdala
Artery – Tibial
Artery – Coronary
Artery – Aorta
Adrenal Gland
Adipose – Visceral (Omentum)
Adipose – Subcutaneous

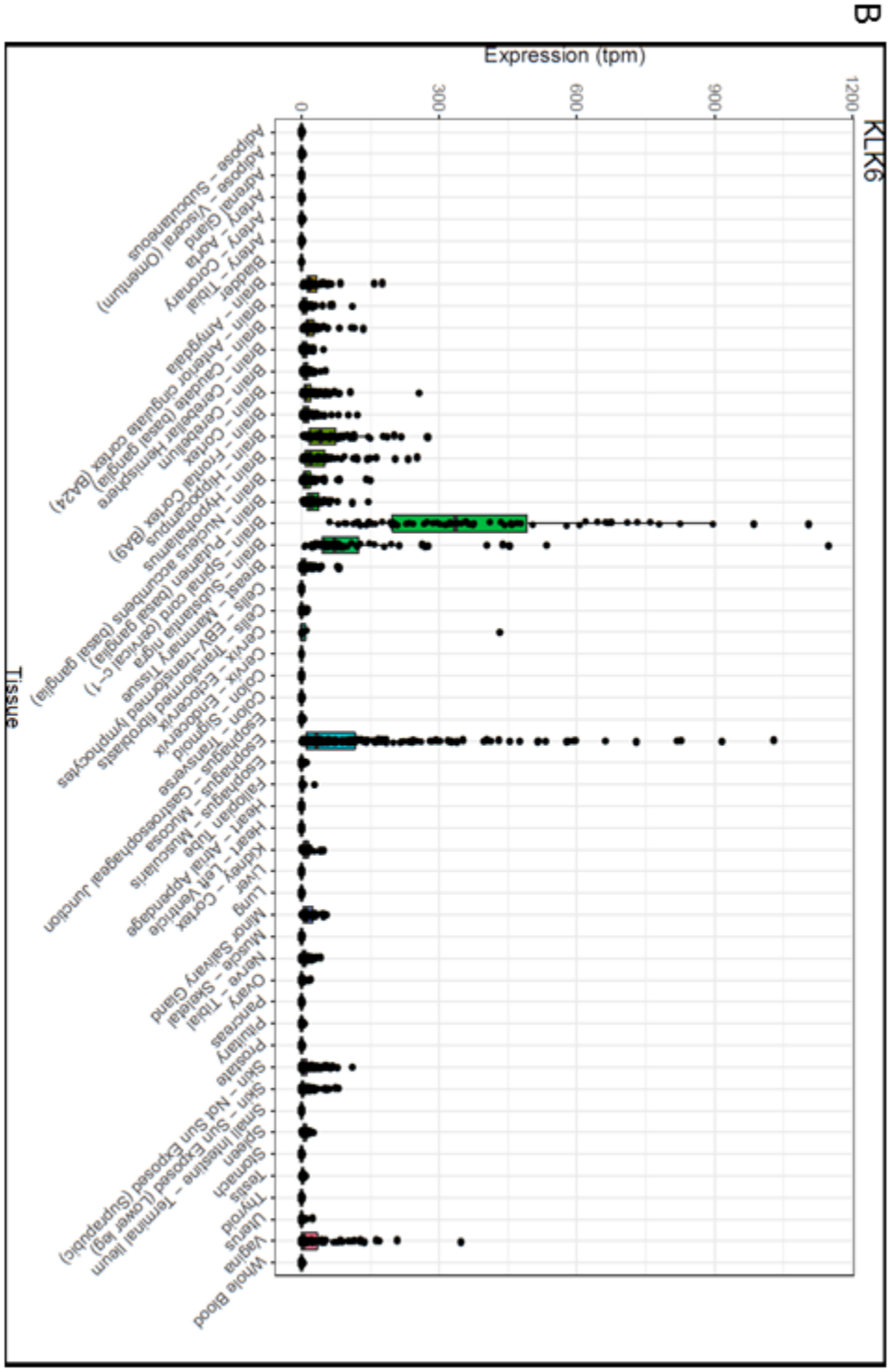
B
KLK6
Expression (tpm)
0
300
600
900
1200
Tissue
Whole Blood
Vagina
Uterus
Thyroid
Testis
Stomach
Spleen
Small Intestine – Terminal Ileum
Skin – Sun Exposed (Lower leg)
Skin – Not Sun Exposed (Suprapubic)
Prostate
Pituitary
Pancreas
Ovary
Nerve – Tibial
Muscle – Skeletal
Minor Salivary Gland
Lung
Liver
Kidney – Cortex
Kidney – Left Renal Appendage
Heart – Atrial Appendage
Heart – Left Ventricle
Fallopian Tube
Esophagus – Mucosa
Esophagus – Gastroesophageal Junction
Esophagus – Transverse
Esophagus – Muscularis
Cervix – Ectocervix
Cervix – Endocervix
Colon – Sigmoid
Colon – Transverse
Breast – Transformed fibroblasts
Cells – EBV–transformed lymphocytes
Cells – Leukemia cell line (CML)
Cells – Cultured fibroblasts
Brain – Substantia nigra
Brain – Spinal cord (cervical c–1)
Brain – Putamen (basal ganglia)
Brain – Nucleus accumbens (basal ganglia)
Brain – Hypothalamus
Brain – Hippocampus
Brain – Frontal Cortex (BA9)
Brain – Cortex
Brain – Cerebellum
Brain – Cerebellar Hemisphere
Brain – Caudate (basal ganglia)
Brain – Cortex (BA24)
Brain – Anterior cingulate cortex
Brain – Amygdala
Bladder
Artery – Tibial
Artery – Coronary
Artery – Aorta
Adrenal Gland
Adipose – Visceral (Omentum)
Adipose – Subcutaneous

Figure 14. Validation of KLK6 Antibody

To determine specificity of KLK6-directed human antibodies, Chinese hamster ovary cells were transfected with human KLK6 (NM_002774) C-terminally tagged with myc and FLAG in the pCMV6-Entry plasmid. Representative images demonstrate immunocytochemical staining for FLAG (red) and KLK6 (green) co-localized for the human KLK6 abcam ab191281 antibody (Merge, yellow). No stain was apparent from either antibody with a non-transfected control (NTC) cell cohort.

FLAG = red, KLK6 = green, DAPI = blue. Scale bar = 200 µm.

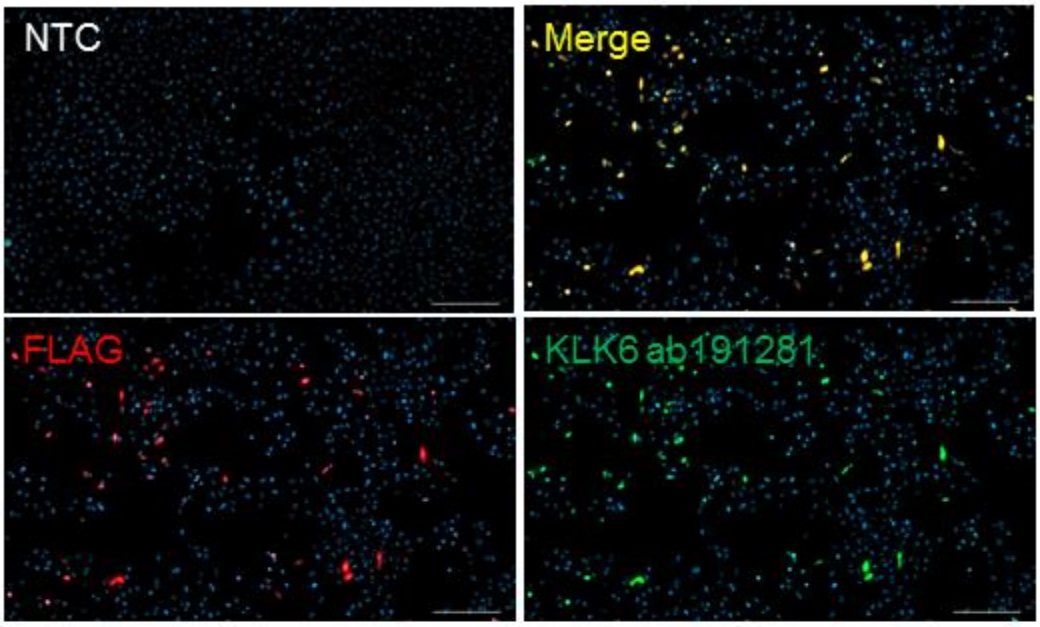
NTC
Merge
FLAG
KLK6 ab191281

Figure 15. Heterogeneous Expression of KLK6 in Multiple Sclerosis Plaques

A-B: Location of MS plaques in telencephalic white matter near the corpus callosum and cingulum bundle is depicted using a coronal view of the rostral aspect of the brain. The yellow box outline in **A** demonstrates the area shown in **B**. The white box in **B** demonstrates the area shown in **C**. Post-mortem brain tissue was obtained from the Rocky Mountain Multiple Sclerosis Center and National Multiple Sclerosis Society. **C**: Two plaques (lack of red, MBP) present in post-mortem brain tissue from a secondary progressive multiple sclerosis patient (RMMSC 316) demonstrate different levels of expression of KLK6 (green), as shown by merge and separation of three channels (KLK6 = green, MBP = red, DAPI = blue). Scale bar = 500 µm (C), 2000 µm (B).

D-E: Several KLK6 and GFAP immunoreactive co-localized cells in a demyelinated area (MBP stain absent) near the lateral ventricle are shown in two images from secondary progressive multiple sclerosis patient brain. GFAP = green, KLK6 = red, MBP = purple, DAPI = blue. Scale bar = 50 µm.

F-G: KLK6 does not co-localize with cells that are Iba1 immunoreactive in a demyelinated area (devoid of MBP stain) near the lateral ventricle in multiple sclerosis patient brain. Iba1 = green, KLK6 = red, MBP = purple, DAPI = blue. Scale bar = 50 µm.

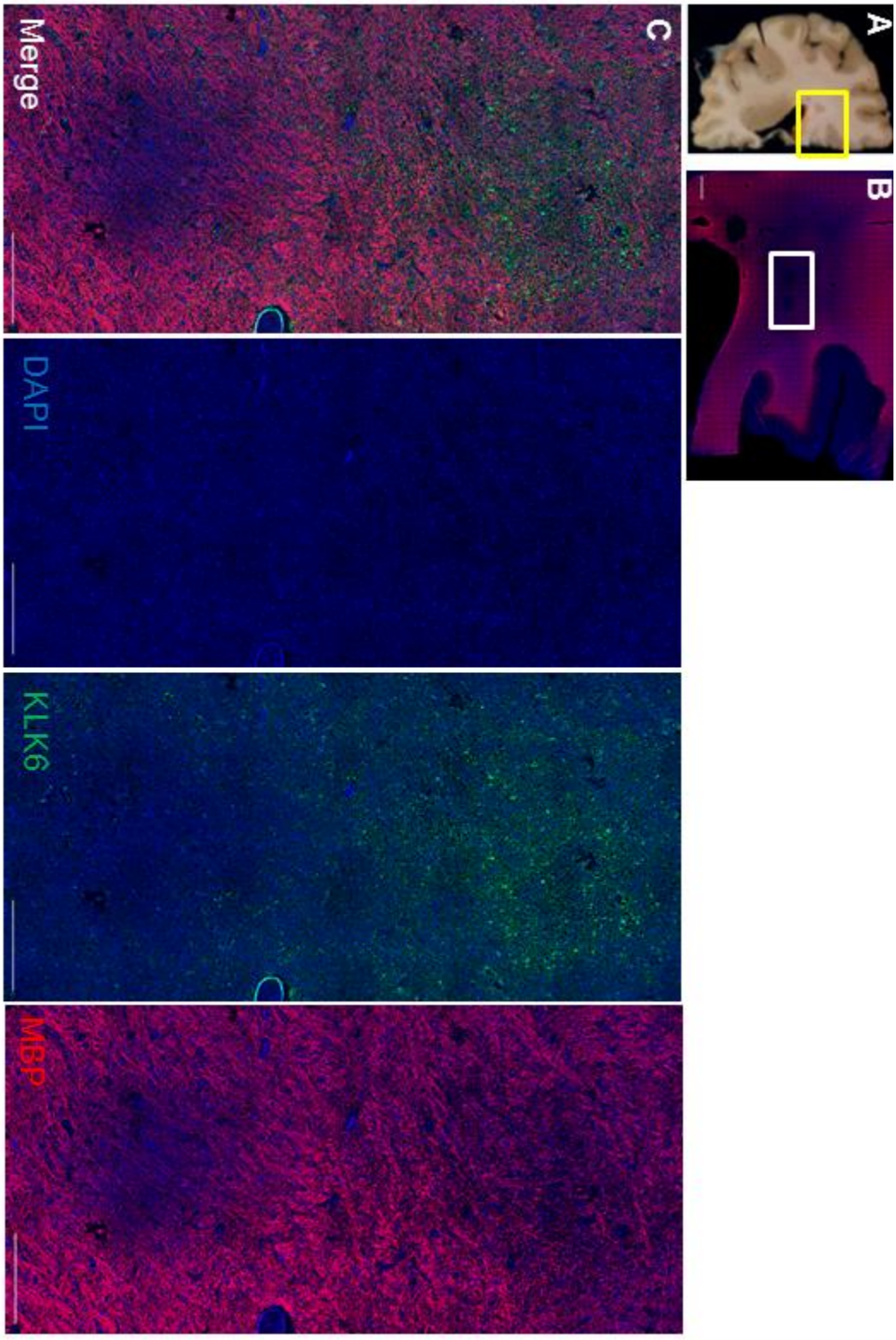
A
B
C
Merge
DAPI
KLK6
MBP

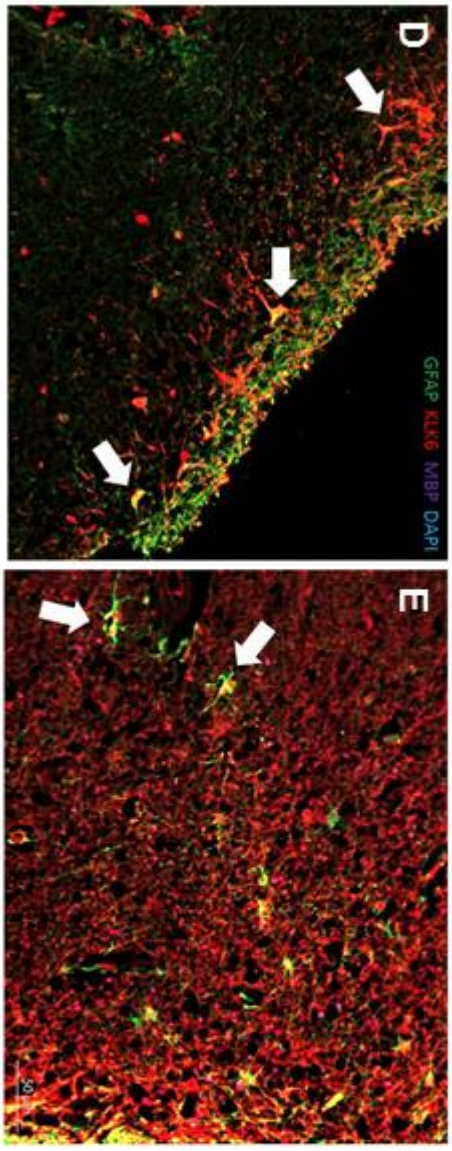
D
GFAP KLK6 MBP DAPI
E

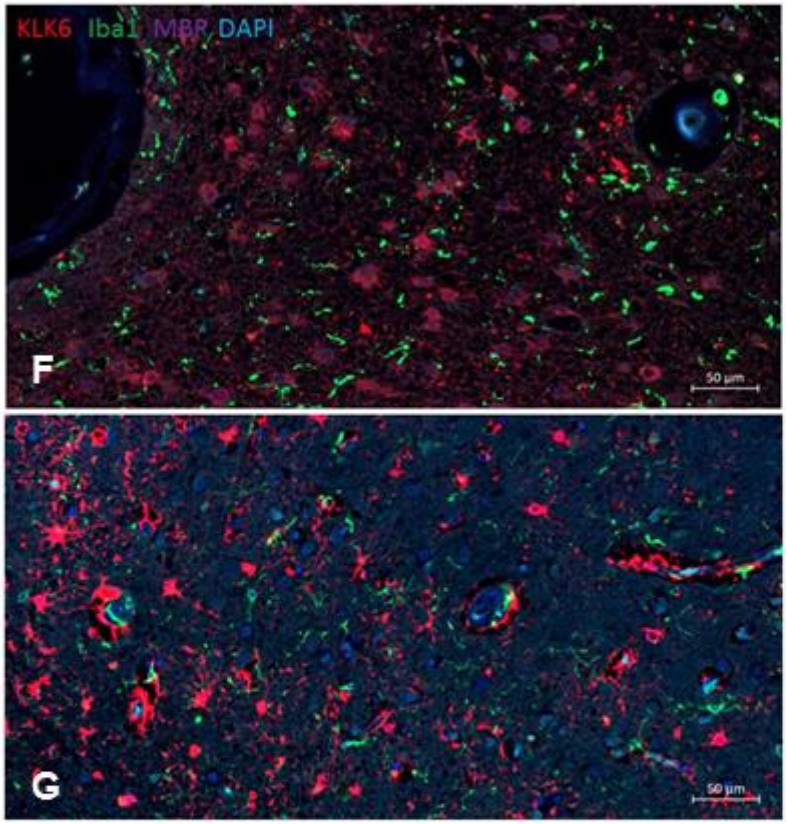
KLK6 Iba1 MBP DAPI
F
50 µm
G
50 µm

CHAPTER FIVE

Discussion and Future Directions

a) Discussion

Several therapeutic treatments exist to address the neuroinflammatory aspects of MS that drive pathology in the disease. However, treatment is often of limited therapeutic effectiveness and many treatments are only directed at RRMS, a single subclassification of MS clinical presentation (Ransohoff *et al.*, 2015). No current FDA-approved treatments address repairing the damage secondary to this inflammation- the demyelinated axons which impede normal neuronal signal conduction through the central nervous system. One of the current ongoing areas of research in MS is how remyelination could be enabled and whether it could help alleviate symptoms of the disease. An ideal treatment for MS might address both aspects known to contribute to MS pathology: an anti-inflammatory to limit damage to the myelin sheath and a promotor of remyelination to restore damage to myelin. This treatment paradigm might also expand the clinical subclassifications that can benefit from therapeutic treatment to include progressive forms of the disease. Progressive patients could benefit from remyelination as they are more likely to have lost endogenous myelin repair activities seen in RRMS patients and to have plaques without ongoing inflammation (Harlow *et al.*, 2015). However, there may still be advanced progressive MS patients to which myelin repair treatment is not therapeutic. They

may need neuroregenerative agents to be restorative, due to neuronal cell loss as a consequence of previous, prolonged demyelination (Bradl and Lassmann, 2009; Criste *et al.*, 2014).

The myelin sheath surrounding neuron axons that becomes damaged in MS is composed of oligodendrocyte processes. Kallikrein 6 (KLK6) is a serine protease found upregulated in MS that has been characterized to be expressed mainly by oligodendrocytes under basal conditions. It is currently unknown whether this upregulation is a contributor to MS pathology or if it is part of a compensatory response upregulated to enhance efforts to establish remyelination around demyelinated regions.

Evidence for its role as a pathogenic agent includes the fact that myelin basic protein, a key structural protein in the CNS myelin sheath, is a substrate of the KLK6 enzyme which preferentially cleaves proteins with basic amino acid chains (Prassas *et al.*, 2015). Evidence for that it is a part of normal oligodendrocyte biology includes the fact that KLK6 knockout mice exhibit decreased major myelin proteins (such as MBP) up to postnatal day 14 in spinal cord, although by adulthood the levels are similar to control (Murakami *et al.*, 2013).

The studies in this dissertation have been directed at elucidating the role of KLK6 in oligodendrocyte maturation and myelination. In addition, efforts are undertaken to further characterize KLK6 expression in human biological tissues

and in MS patient post-mortem brain tissue. The specific goal of this research is to address whether KLK6 inhibition could be beneficial in oligodendrocyte maturation and remyelination. The overarching goal driving this research is to identify potential mechanisms of remyelination that could be therapeutically relevant in MS.

In chapter two of this work, I show that KLK6 mRNA expression is at its highest point when MBP mRNA expression levels peak during maturation of OPCs to oligodendrocytes in an embryonic brain-based, neurosphere-derived, cell maturation assay. MBP is a gene expressed by mature oligodendrocytes. A marker of more mature oligodendrocytes, MOG, is shown to peak later in maturation compared to MBP and KLK6. Additionally, the application of exogenous KLK6 or a reported downstream KLK6 pathway mediator (PAR1-AP) on neural stem cell-derived OPCs decreases the number of MBP-positive cells per well and/or total length of MBP-positive cell processes. While this could indicate induction of cell death rather than a lack of maturation, I did not find evidence of increased cell death with KLK6 application. A study in the literature also indicates that although exogenous KLK6 can make OLs more susceptible to ATP excitotoxicity, it does not induce cell death on its own (Burda *et al.*, 2013).

When a novel KLK6 inhibitor (KLK6i) identified during a virtual screen (Liang *et al.*, 2012a) was applied to neural stem cell-derived OPCs, it was found that the KLK6i increased the number of oligodendrocytes and OPCs in culture

compared to control treatment. When KLK6i treatment was combined with a T3 maturation agent, the mechanisms appeared to be synergistic; they increase the number of OLs and their total branch length more than either treatment alone. Thus, these findings suggest that KLK6 is a negative modulator of OL maturation and KLK6 inhibition is a positive modulator of OL maturation. Using RNAseq analysis, the combination treatment of KLK6i and T3 was found to upregulate several pathways of genes involved in cholesterol synthesis more significantly than either treatment alone. Because cholesterol synthesis is predominately accomplished by astrocytes in the CNS (Kiray *et al.*, 2016; Camargo *et al.*, 2017), this implicates astrocytes in modulation of OL maturation via KLK6

Animal models of demyelination and remyelination have been helpful in understanding whether and how potential therapeutics will alter outcomes in human MS. FDA-approved anti-inflammatories natalizumab, glatiramer acetate previously showed efficacy in the EAE model (Baxter, 2007). There are currently no FDA-approved remyelination therapies for MS. Potential remyelination therapies like muscarinic 1 receptor antagonists have succeeded in cuprizone and lysolecithin animal models of demyelination, and look promising in human MS patients in the clinic (Deshmukh *et al.*, 2013; Mei *et al.*, 2014; Mei *et al.*, 2016; Green *et al.*, 2017). In chapter three of this work, I assess the potential of KLK6 inhibition to increase CNS myelination *in vivo*. KLK6i was delivered ICV in mice for 14 days post-demyelination with 0.2% cuprizone to measure the ability

of KLK6i to aid in remyelination. This model was chosen specifically because it tests the ability of the compound to promote remyelination rather than neuroinflammatory aspect of demyelination.

Samples from CSF, plasma, and cerebellum were all found to contain KLK6i after 14 days of infusion into the lateral ventricle at the anatomical level of the anterior horn. This demonstrates delivery of the inhibitor was ongoing at the end of the study and shows distribution of the inhibitor in brain tissue as well as in fluid compartments. The mammalian ventricular system where CSF is produced (by the choroid plexus and ependymal cells), circulates CSF based on blood pressure gradients (Mortazavi *et al.*, 2014; Simon and Iliff, 2016; Stratchko *et al.*, 2016). Humans produce ~500 µL of CSF per minute, changing over total CSF volume (approximately 150 mL) four times a day (Simon and Iliff, 2016). Mice produce 0.35 µL per minute, changing over total CSF volume (~30-40 µL), twelve times per day (Simon and Iliff, 2016). In humans, CSF travels from the lateral ventricle through the interventricular foramen of Monro to the third ventricle near the hypothalamus, then through the cerebral aqueduct of Sylvius to the fourth ventricle which is ventral to the cerebellum. It exits the fourth ventricle through either the foramen of Magendie or the foramina of Luschka to surround the CNS in the subarachnoid space (Mortazavi *et al.*, 2014). CSF is then reabsorbed into the blood stream through arachnoid granulations and the dural venous system (Simon and Iliff, 2016; Stratchko *et al.*, 2016). The anatomy of the

mouse ventricular system is similar to human, but mice lack a foramen of Magendie (Simon and Iliff, 2016; Snyder *et al.*, 2018).

The cuprizone model of demyelination decreases myelin fiber density most notably in the corpus callosum, a large white matter tract which interconnects the cerebral hemispheres of the brain (Skripuletz *et al.*, 2011). The corpus callosum is composed of several main anatomical regions; from rostral to caudal aspect they are the rostrum, genu, body, and splenium (Nieuwenhuys *et al.*, 2008). Generally, the topography of the corpus callosum is such that the more rostral aspects are involved in connecting association areas of more rostral aspects of the cerebral cortex, such as frontal cortex. More caudal aspects of the corpus callosum, such as the splenium, are associated with more posterior aspects of the cerebral cortex, such as the occipital lobe (Nieuwenhuys *et al.*, 2008). Myelination of the corpus callosum is thought to occur from posterior aspect to anterior (Fabri *et al.*, 2014). Studies with cuprizone have demonstrated regional differences in extent of corpus callosum demyelination and remyelination based on the rostrocaudal axis position (Blakemore and Franklin, 2008; Steelman *et al.*, 2012; Tagge *et al.*, 2016). The extent in which cuprizone reduces demyelination depends on a variety of factors related to experimental paradigm. Animals treated with 0.2% cuprizone for 6 weeks do not have overt changes in behavior (Skripuletz *et al.*, 2011). It has been reported that cuprizone elicits changes in more complex behavior (e.g. slower wheel-running in wheels

with further spaced rungs), but this has not yet been replicated across multiple groups (Hibbits *et al.*, 2009). Animals treated with 0.2% cuprizone for greater than 9 weeks start to exhibit seizures (Skripuletz *et al.*, 2011; Lapato *et al.*, 2017).

The corpus callosum is anatomically close in proximity to the lateral ventricle. The cannulation of mice at the anterior horn of the lateral ventricle puts delivery of KLK6i close to the genu / anterior portion of the body of the corpus callosum. This is where analysis for remyelination was conducted using histological methods. Due to the sample processing for histology to assess myelination and due to the low number of subjects per group related to the complicated nature of the surgical manipulation, the corpus callosum and adjacent tissue were not directly measured for KLK6i. However, it is expected that KLK6i exposure would be highest at the site of delivery compared to distal sites (drug exposure was measured in cerebellum, where it was expected to be less concentrated) due to protein binding estimates of the compound.

Cuprizone/KLK6i treated animals demonstrated an increase in myelination of the corpus callosum by luxol fast blue staining compared to cuprizone/vehicle treated mice. This result was corroborated by a trend increase with mature oligodendrocyte marker CC1 in the same region. Further, KLK6i treatment reduced the amount of GFAP-positive astrocyte staining in the corpus callosum compared to the induction seen after cuprizone treatment.

This work demonstrates that a novel small molecule inhibitor of KLK6 can increase OL maturation and increase corpus callosum remyelination after cuprizone demyelination. This is the first time a KLK6i has been tested in the cuprizone model of demyelination. This is also the first example of a small molecule KLK6i being used to induce remyelination in an *in vivo* model. This data builds on previous data that suggests KLK6i could be useful in treating MS. Previously, exogenous KLK6 had been shown to increase white matter pathology when injected in normal mouse spinal cords and to increase motor disability in a mouse EAE model (Burda *et al.*, 2013; Yoon and Scarisbrick, 2016). Contrariwise, a KLK6 knockout mouse was shown to have delayed onset and decreased motor disability using an EAE model paradigm (Bando *et al.*, 2018). Additionally, a KLK6-neutralizing antibody was shown to delay motor disability and severity of symptoms in an EAE mouse model (Blaber *et al.*, 2004; Bando *et al.*, 2018). A KLK6-neutralizing antibody has also been shown to reduce progressive MS-like pathology at 40 days post-induction of pathology in the TMEV model of progressive demyelination but this was not sustained at 180 days post-induction (Scarisbrick *et al.*, 2012b).

Thus, I have demonstrated that a small molecule KLK6i can aid in remyelination in a toxin based MS animal model while others have shown a KLK6i can limit pathology in immunologic-based MS animal models. These experiments which assess the impact of KLK6i from different angles have

demonstrated that KLK6 inhibitors may have the potential to be therapeutic in MS patients. The limited effectiveness in immune-based animal models of MS may reflect that KLK6i may have limited anti-inflammatory ability. However, it may also suggest that combination with an anti-inflammatory treatment is needed for this remyelination therapy to combat continuing damage to myelin by inflammation. Currently there are no FDA-approved therapeutic agents for MS that improve remyelination. In order to run effective clinical trials in the area of remyelination, more work is likely needed to detect remyelination at high resolution, potentially including the establishment of upstream biomarkers.

Similarly, more work is needed to understand KLK6 expression and function in human health and disease. In chapter four of this work, I demonstrate that KLK6 is one of the highest expressed serine hydrolases in the adult human CNS using the GTEx RNAseq database. It is also relatively selective for CNS expression compared to peripheral tissue expression, which could make it an attractive target for treating neurological diseases. However, this highlights the lack of complete understanding around what KLK6 does in the adult CNS. Further, are there consequences to lowering KLK6 beyond the amount in which it is elevated in a disease state? One limitation of this dataset is that it provides a general view of adult “non-diseased” human gene expression; individual demographics and clinical history of patients are not easily searchable to understand if KLK6 is higher in some individuals compared to others. It is also

possible that KLK6 has other roles besides negatively impacting oligodendrocyte maturation and myelination. Additionally, besides OLs, previous work has identified the presence of KLK6 in activated states of certain cell types such as T lymphocytes, macrophages and astrocytes (Blaber *et al.*, 2004; Terayama *et al.*, 2005; Scarisbrick *et al.*, 2011; Scarisbrick *et al.*, 2012a). RNAseq data that determined KLK6 was exclusively expressed in OLs was done on cells in their basal state, which could be the reason this was not described in that dataset (Zhang *et al.*, 2014; Zhang *et al.*, 2016).

Limited work has been done to characterize KLK6 expression at the protein level in the human CNS. A single study has done an expansive investigation into KLK6 protein expression using tissues spanning throughout the whole body. The results of this work suggest that choroid plexus and glial cells in brain (no region specified, no co-localization done) had the most KLK6 out of all of the CNS by immunohistochemistry (Petraki *et al.*, 2001). Outside of the CNS, peripheral nerves and organs with epithelia had high expression by immunohistochemistry (Petraki *et al.*, 2001). Although cell resolution is not available with the GTEx dataset, the overall finding that brain and peripheral epithelial tissues are positive for KLK6 is corroborated across both studies.

In MS patients, KLK6 has been shown to be at higher levels than control in *CSF* (Hebb *et al.*, 2010; Bando *et al.*, 2018), serum (Scarisbrick *et al.*, 2008), and brain (Scarisbrick *et al.*, 2002). The data on KLK6 protein expression in brain

suggests that KLK6 is generally located within and around the borders of MS plaques in discrete cells, but the cell type was not directly identified through co-labeling (Scarisbrick *et al.*, 2002).

In chapter four of this work, I used immunohistochemistry to examine MS post-mortem brain tissue from several patients with different subclassifications of the disease to characterize what is known about MS KLK6 expression in more detail. The numbers of plaques in the tissue obtained were relatively sparse, but there were no overt differences in KLK6 expression across patients with different subclassifications of MS. It was found that individual MS plaques even within the same patient and same region of brain had differential expression of KLK6 by immunohistochemistry. This finding makes sense because MS plaques are heterogeneous in nature; different cell types, particularly immune cell types, are present in different types of MS plaques (Kuhlmann *et al.*, 2017). There are several different categorization schemes for classifying MS plaques, but they all largely currently depend on microglia/macrophage/astrocytic/T cell infiltration and whether the plaque is post-myelinating (Kuhlmann *et al.*, 2017).

Co-labeling of KLK6-positive cells with astrocytic marker GFAP and microglia/macrophage marker Iba1 elucidated that the majority of KLK6-positive cells in MS plaques were astrocytes. There were also examples of reactive astrocytes outside of clear MS plaques that were positive for KLK6.

Another group has reported that astrocytes assume reactive, hypertrophied morphology upon treatment with exogenous KLK6 (Scarisbrick *et al.*, 2012a). Further, they demonstrate that reactive astrocytes from a few neurological conditions can contain KLK6; a chronically active MS plaque is shown to contain KLK6 in reactive astrocytes (Scarisbrick *et al.*, 2012a). Together, this data supports that astrocytes may play a role in KLK6 impact on OL maturation and myelination, but more work is needed to further understand this relationship. Further study of KLK6 in MS should profile KLK6 expression in a larger number of MS plaques scored for various levels of microglia and astrocyte activity, as well as myelination status. Since the majority of positive KLK6 staining appears to be in astrocytes, not OLs, it is possible that the elevation of KLK6 seen previously in the literature with MS patient samples is due to an increase in reactive astrogliosis compared to control patients. A limitation of many studies that profile KLK6 protein expression by immunohistochemistry, including this work, is that the activation status of KLK6 is unknown. A potential method to investigate expression levels and activity levels in histological samples might be to use click chemistry methods combined with immunohistochemistry. Bando et al. use an antibody that only labels the active form of KLK6 and find expression to be in OLs (Bando *et al.*, 2018). Future studies should explore whether the KLK6 present in astrocytes is active KLK6 and whether activated astrocytes all secrete KLK6.

Notably, three different experiments across this dissertation connect astrocyte involvement to KLK6 signaling related to oligodendrocytes. First, an antibody to KLK6 stains reactive astrocytes in human MS patient brain tissue. Second, KLK6 inhibition lowers GFAP-positive astrocyte staining post-cuprizone withdrawal in mouse corpus callosum. Third, KLK6 inhibition combined with maturation agent T3 significantly increases several cholesterol biogenesis pathways compared to either treatment alone. Cholesterol in the brain largely comes from astrocytes (Ferris *et al.*, 2017). Thus, putatively, it may be that KLK6 inhibition increases astrocyte-related cholesterol synthesis which in turn enhances remyelination by oligodendrocytes. One limitation of this hypothesis is the decrease in astrocyte marker GFAP stain seen with KLK6 inhibition concurrent with a proposed increase in astrocyte cholesterol synthesis. It seems unlikely a decrease in number of astrocytes could increase cholesterol synthesis, if they are responsible for the cholesterol synthesis. It is also unlikely that astrocytes were removed from the site of remyelination because the literature has demonstrated that ablating astrocytes inhibits myelin debris cleanup after cuprizone and delays remyelination (Skripuletz *et al.*, 2013).

A possible explanation could be that the GFAP antibody is not detecting all astrocytes and that a different population of cholesterol-synthesizing astrocytes is increasing. Although GFAP was at one point thought to label all astrocytes, now

Aldh1L1 is considered the most inclusive marker (Zhang and Barres, 2010). In addition, multiple isoforms of GFAP exist. The antibody used for this study does not have information on the isoforms it detects. The literature suggests that different types of reactive astrocytes are selective for different GFAP isoforms (Kamphuis *et al.*, 2014). It seems most likely that GFAP is a sensitive measure for reactive astrocytes, and the decrease in GFAP is due to dynamic regulation of intermediate filaments being restored to basal astrocyte state in response to KLK6 inhibition. It may also be that reactive astrocytes produce less cholesterol. In the literature, a study used alpha-synuclein peptide to cause human primary astrocytes in culture to exhibit morphological characteristics of reactivity. They found that these reactive astrocytes had higher levels of GFAP staining but had decreased levels of cholesterol in the membrane fraction of the homogenate compared to control treatment (Koob *et al.*, 2010). More work is needed to determine if this is what happens with exogenous KLK6 application to astrocytes, and if the reverse occurs in response to KLK6 inhibition.

Astrocytes perform a variety of roles within the CNS: they maintain and regulate the environment by secreting growth factors, lactate, cholesterol, thrombospondins, and extracellular matrix proteins; they help form the blood-brain barrier which protects the brain from peripheral insults; they can also secrete cytokines and chemokines to which can then direct downstream immunological cascades (Kiray *et al.*, 2016; Li *et al.*, 2016). Generally, there are

two main types of astrocytes have been described in the brain which are largely defined based on morphology and location (Barres, 2008). Protoplasmic astrocytes are large with many branches and are located in gray matter (Li *et al.*, 2016). Fibrous astrocytes are smaller with fewer processes, but those processes are longer in length (Li *et al.*, 2016). Fibrous astrocytes are located in white matter (Li *et al.*, 2016). It is currently not well-understood whether astrocytes are incredibly dynamic, performing a variety of functions, or whether specific types of astrocytes, which we have been unable to clearly define, have unique capabilities and functions. Continued work is needed to further understand astrocytes heterogeneity and function (Zhang and Barres, 2010).

Astrocytes influence myelination in several known ways. They promote OPC proliferation and development through secretion of growth factors PDGF and bFGF (Kiray *et al.*, 2016). Their secretion of growth factors leukemia inhibitory factor and ciliary neurotrophic factor helps promote maturation and survival of OLs (Kiray *et al.*, 2016; Li *et al.*, 2016). Other factors they secrete such as bone morphogenetic proteins, interleukin 6, or hyaluronan inhibit OPC maturation and/or OL maturation and myelination (Li *et al.*, 2016).

Reactive astrocytes are present in several neurologic diseases, including MS (Li *et al.*, 2016; Hirase and Koizumi, 2018; Ponath *et al.*, 2018). However, relatively little is known about whether astrocytes are more part of compensatory mediation as a result of disease or contributors to disease pathology. In MS,

reactive astrocytes can perpetuate pro-inflammatory signaling which contributes to demyelination (Li *et al.*, 2016; Ponath *et al.*, 2018). They can also form a glial scar to prevent peripheral cell invaders from further damaging the CNS (Li *et al.*, 2016; Ponath *et al.*, 2018). Further work to understand and regulate astrocyte diversity and function may help development of therapeutic interventions for MS and other neurologic diseases.

In contrast to the KLK6i used in this work, a previously untested brain penetrant PAR1 inhibitor did not demonstrate increased OL maturation *in vitro* or increased remyelination over spontaneous remyelination two weeks post-withdrawal of cuprizone in a mouse model of corpus callosum demyelination. The PAR1 pathway is expected to be downstream of KLK6 (Burda *et al.*, 2013). It was thought that PAR1 inhibition could be another method to test KLK6 inhibition should properties of the KLK6 inhibitor be unfavorable to testing. The PAR1 inhibitor selected for the studies in this dissertation had good brain exposure and target selectivity, which was ideal for *in vivo* testing and differentiated it from other commercially-available PAR1 inhibitors. Results in the literature with genetic PAR1 knockout models suggest that the reason for failure of this compound in both the *in vitro* and *in vivo* assays is due to poor drug properties (Burda *et al.*, 2013), such as protein binding. Additionally, a different PAR1 inhibitor (SCH79797) has been shown to increase OL maturation in primary OPCs (Yoon *et al.*, 2015). The SCH79797 compound was not selected for study

in this dissertation because it was determined unlikely to be brain penetrant (based on structure). While the two compounds have very different chemical structures, they have similar IC_{50} values and are both expected to be selective for PAR1 compared to other PARs. Future work should be done to confirm efficacy of the two compounds head-to-head in an OPC maturation assay. Additionally, brain penetrance, receptor binding selectivity, and potency should be confirmed experimentally. Although the compounds were assessed based on available information, they were not compared head-to-head. This act could have provided additional information. One explanation for the discrepancy between compounds could be related to compound potency and the mechanism of PAR1 modulation. PAR1 signaling is expected to be mediated through downstream calcium ion activity (Burda *et al.*, 2013). It is known that differential patterns of calcium ion signaling elicit different effects on oligodendrocytes and myelination (Baraban *et al.*, 2018). Perhaps one compound has higher potency and was administered in a manner that created an alternative calcium signaling pattern that was not conducive to OPC maturation or myelination by OLs. Another explanation could be that although the compounds are both selective for PAR1, one is more selective than the other.

At the time the *in vitro* OPC maturation assay work was done with the PAR1 inhibitor, it was unclear whether the *in vitro* assay results would directly predict remyelination efficacy *in vivo*. Based on the two compounds profiled in

this work, it appears that the *in vitro* OPC maturation assay was predictive for determining remyelination efficacy *in vivo* following cuprizone demyelination. This may or may not be true with different mechanisms of OL maturation due to the limitations of the *in vitro* assay, which does not include all cell types.

b) Future Directions

i. Further Development of KLK6 Inhibitors for Remyelination

While the KLK6 inhibitor used in this work was able to inhibit KLK6, it was not readily brain penetrant. Future small molecule KLK6 inhibitors should be developed with increased brain penetrance when administered using a peripheral route of administration. This would avoid complicated delivery techniques, such as invasive surgery, to allow the drug to be useful as a CNS remyelination therapeutic in humans. Specificity for KLK6 should also be tested at escalating concentrations compared to other kallikrein family members or other serine proteases due to similarity of their protein cleavage mechanism (Di Cera, 2009). Additionally, compounds will need to be assessed for exposure and adverse events throughout the body during acute and chronic administration paradigms. Specific areas in the body where adverse events might be expected are in reproductive tissue and epithelium of other various organs (e.g. esophagus), as

moderate levels of KLK6 expression have been detected in these regions (Petraki *et al.*, 2001).

Therapies combining anti-inflammatory and remyelination properties are expected to be the most effective treatment for MS due to the inflammation-directed damage of myelin and the decreasing propensity of remyelination over time in the disease (Stangel *et al.*, 2017). Thus, groups in both the preclinical and clinical space are beginning to test potential remyelination therapies alongside anti-inflammatory treatments. For example, benztropine, a muscarinic antagonist shown to increase myelination, was combined with anti-inflammatories and this combination was found to reduce behavioral manifestations of pathology in an EAE ($PLP_{129-151}$) preclinical model more than either agent on its own (Deshmukh *et al.*, 2013). Further, an ongoing clinical trial with a myelination-promoting LINGO-1 antagonist is testing the antagonist in combination with anti-inflammatory treatments without a LINGO-1 only treatment arm (ClinicalTrials.gov NCT03222973). Similarly, KLK6 inhibitors should be tested in combination with anti-inflammatory agents in progressive animal models such as the TMEV model of demyelination to see if combined therapy is more effective in enhancing remyelination and decreasing disease progression than either alone.

In order to more effectively measure remyelination in human clinical trials to evaluate therapeutics, further development is needed to identify or enhance

clinical measures or biomarkers indicative of remyelination. Currently, MR methods of the brain and EVP of optic nerve are our best measurements available (Kilsdonk *et al.*, 2016; Cadavid *et al.*, 2017; Green *et al.*, 2017). Increased resolution of clinical measures of remyelination would provide more precise measurements of clinical outcomes. For example, clinical measurements could be based on molecular and cellular pathways that manifest earlier than end-stage behavior consequences of decreased myelination. This could also lead to a reduction in length of clinical trials.

ii. The Impact of Remyelination in Disease

There is some debate about whether remyelination therapies will be able to significantly ameliorate disease pathology in neurological diseases with demyelination. Some argue that remyelination is not the same as original myelination, particularly focusing on that it is “thinner” (Prineas and Connell, 1979). Others say that this is an artifact of time-dependence when measuring myelin thickness (Powers *et al.*, 2013). In either case, the main concern is that thinner remyelination is not optimally performing compared to the original myelin, for whatever length of time for which it is thinner.

Regarding whether remyelination can ever reach original myelin thickness levels, studies in zebrafish suggest that remyelination can be achieved at optimal original myelin thickness in younger fish, but not in older fish (Munzel *et al.*,

2014). This suggests that there may be factors changing in aging that may be useful to target to enhance remyelination so that it can be as thick as the original myelin. Regarding the properties of thinner remyelination, a recent longitudinal study in a small number of dogs and cats indicates that thinner remyelination after demyelination persists over years and is adequately functional compared to original myelin (Duncan *et al.*, 2017). More longitudinal studies combining functional outcomes as well as structural are needed to confirm whether thinner remyelination has functional limitations compared to original myelination or if it is perfectly adequate. If it is determined that thinner myelin is actually functionally limited in conduction capacity, research should be pursued to increase the speed in which optimally-functioning thicker myelin can be re-created.

While remyelination therapies aim to restore myelin in diseases in which they have been lost, there may be some types of patients where remyelination is not possible. For example, remyelination therapy would not be effective in patients who no longer have neuronal axons/neurons that can be myelinated, as can occur in progressive MS patients (Criste *et al.*, 2014). Further, it may be that remyelination therapies have synergistic effects when combined with a sustained propensity to remyelinate, such as was seen *in vitro* with a KLK6 inhibitor and T3 maturation agent. This may suggest that a remyelination therapy would be more effective in patients such as RRMS patients that still have remyelination capacity compared to progressive patients with diminished remyelination capacity. Thus,

perhaps remyelination therapy would be restorative in RRMS, but would merely put the brakes on further deterioration in progressive forms of MS. This type of treatment would still be very impactful for progressive patients.

Historically, clinical demonstration of remyelination in response to treatment has been limited to MR imaging which lacks ideal resolution. Recently, techniques to clinically demonstrate remyelination have expanded to include EVP analysis of optic nerve myelination (Kilsdonk *et al.*, 2016; Cadavid *et al.*, 2017; Green *et al.*, 2017). EVPs may currently be the most promising measure to rapidly test remyelination efficacy in clinical trials (Cadavid *et al.*, 2017; Green *et al.*, 2017). Better clinical imaging methods are needed in order to better assess remyelination potential in live humans throughout the brain and spinal cord (Kilsdonk *et al.*, 2016).

Identifying mechanisms in which CNS myelination or remyelination could be therapeutically enhanced could be beneficial to several disorders in which CNS demyelination is present. The most obvious example is MS, a demyelinating disease. However, there is some evidence for decreased myelination in developmental disorders. Patients with autistic disorders may also have less myelination than normally developing peers (Deoni *et al.*, 2015) and/or auto-antibodies to myelin proteins (Gonzalez-Gronow *et al.*, 2015). Several disorders involving psychosis, such as schizophrenia, are reported to exhibit aberrant myelination in frontal/prefrontal cortical regions of the brain (Mighdoll *et*

al., 2015). Further, perhaps enhancement of myelination might be helpful in boosting normal cognition and reducing dementia generally associated with myelin loss in aging (Peters *et al.*, 1996; Rivera *et al.*, 2016).

iii. Aberrant KLK6 Signaling in Other Neurological Diseases

Dysregulation of KLK6 has been implicated in several other neurodegenerative diseases besides MS including: Alzheimer's disease (Sun *et al.*, 2017), Parkinsonism disorders (Iwata *et al.*, 2003; Tatebe *et al.*, 2010; Spencer *et al.*, 2013; Spencer *et al.*, 2015; Pampalakis *et al.*, 2017), and spinal cord injury (Murakami *et al.*, 2013; Radulovic *et al.*, 2013). KLK6 expression has also been shown to be correlated with low survival rate in glioblastoma multiforme patients; it is expressed at higher levels in grade IV compared to grade III gliomas (Drucker *et al.*, 2015).

Although direct KLK6 dysregulation has not been identified in all disorders with aberrant myelination, if KLK6 inhibition can increase production of oligodendrocytes, these disorders might also be able to benefit from treatment.

iv. KLK6 Modulation in the Peripheral Nervous System

While the central and peripheral nervous systems both myelinate axons the ways in which this is accomplished are not completely the same. However, it

is reasonable to entertain whether KLK6 has a role in peripheral myelination and/or Schwann cell maturation because KLK6 has a role in oligodendrocyte maturation and CNS myelination. There is not currently much known about the role of KLK6 in the peripheral nervous system. The literature has reported that peripheral nerves demonstrate expression of KLK6 by immunohistochemistry (Petraki *et al.*, 2001). Still, the presence of a molecule is not necessarily indicative of a similar function across peripheral and central nervous systems. For example, neuregulin 1 has varying importance and roles in peripheral myelination and CNS myelination (Taveggia *et al.*, 2008; Feltri *et al.*, 2016). Further study is warranted to confirm presence and determine involvement of KLK6 in the myelination of peripheral nerves.

v. KLK6 Modulation in Non-Neurological Diseases

KLK6 has been recently shown to be upregulated in prostate cancer, in addition to other kallikrein family members (Oikonomopoulou *et al.*, 2010; Bayani and Diamandis, 2011). It has also been shown to be increased in ovarian cancer (Korbakis *et al.*, 2017). Currently, KLK6 is being proposed or used as a biomarker in these cancers. The mechanism that leads to upregulation in these cancers is unknown. One potential explanation for increased KLK6 expression is that KLK6 has been shown to be upregulated by increases in estrogen and progestins that are elevated in some cancers (Yousef *et al.*, 1999). At the same

time, hormones elevated during pregnancy appear to decrease symptomatic relapses in MS (Miller *et al.*, 2014). Levels of KLK6 have been shown to be high in general in MS, but have not been specifically examined in pregnant MS patients compared to non-pregnant MS patients. Learning more about the underlying mechanisms driving KLK6 elevation in one disease may be informative for other diseases. Additional work should be done to clarify the mechanism of KLK6 upregulation in reproductive organ cancers and whether peripheral treatment of epithelial cancers with high levels of KLK6 could be effectively treated with peripheral KLK6 inhibitors.

BIBLIOGRAPHY

Akkermann R, Beyer F, Kury P. Heterogeneous populations of neural stem cells contribute to myelin repair. Neural Regeneration Research 2017; 12(4): 509-17.

Asteriti S, Daniele S, Porchia F, Dell'Anno MT, Fazzini A, Pugliesi I*, et al.* Modulation of PAR(1) signalling by benzimidazole compounds. British Journal of Pharmacology 2012; 167(1): 80-94.

Auricchio F, Scavone C, Cimmaruta D, Di Mauro G, Capuano A, Sportiello L*, et al.* Drugs approved for the treatment of multiple sclerosis: review of their safety profile. Expert Opinion on Drug Safety 2017; 16(12): 1359-71.

Bajic G, Degn SE, Thiel S, Andersen GR. Complement activation, regulation, and molecular basis for complement-related diseases. EMBO Journal 2015; 34(22): 2735-57.

Bando Y, Hagiwara Y, Suzuki Y, Yoshida K, Aburakawa Y, Kimura T*, et al.* Kallikrein 6 secreted by oligodendrocytes regulates the progression of experimental autoimmune encephalomyelitis. Glia 2018; 66(2): 359-78.

Bando Y, Ito S, Nagai Y, Terayama R, Kishibe M, Jiang YP*, et al.* Implications of protease M/neurosin in myelination during experimental demyelination and remyelination. Neuroscience Letters 2006; 405(3): 175-80.

Baraban M, Koudelka S, Lyons DA. Ca (2+) activity signatures of myelin sheath formation and growth in vivo. Nature Neuroscience 2018; 21(1): 19-23.

Barres BA. The mystery and magic of glia: a perspective on their roles in health and disease. Neuron 2008; 60(3): 430-40.

Barres BA, Raff MC. Proliferation of oligodendrocyte precursor cells depends on electrical activity in axons. Nature 1993; 361(6409): 258-60.

Baumann N, Pham-Dinh D. Biology of oligodendrocyte and myelin in the mammalian central nervous system. Physiological Reviews 2001; 81(2): 871-927.

Baxter AG. The origin and application of experimental autoimmune encephalomyelitis. Nature Reviews: Immunology 2007; 7(11): 904-12.

Bayani J, Diamandis EP. The physiology and pathobiology of human kallikrein-related peptidase 6 (KLK6). Clinical Chemistry and Laboratory Medicine 2011; 50(2): 211-33.

Ben-Zacharia AB. Therapeutics for multiple sclerosis symptoms. Mount Sinai Journal of Medicine 2011; 78(2): 176-91.

Benetti F, Ventura M, Salmini B, Ceola S, Carbonera D, Mammi S*, et al.* Cuprizone neurotoxicity, copper deficiency and neurodegeneration. Neurotoxicology 2010; 31(5): 509-17.

Bennett ML, Bennett FC, Liddelow SA, Ajami B, Zamanian JL, Fernhoff NB*, et al.* New tools for studying microglia in the mouse and human CNS. Proceedings of the National Academy of Sciences of the United States of America 2016; 113(12): E1738-46.

Bercury KK, Macklin WB. Dynamics and mechanisms of CNS myelination. Developmental Cell 2015; 32(4): 447-58.

Bergsland N, Horakova D, Dwyer MG, Uher T, Vaneckova M, Tyblova M*, et al.* Gray matter atrophy patterns in multiple sclerosis: A 10-year source-based morphometry study. Neuroimage Clinics 2018; 17: 444-51.

Bien CG, Vincent A, Barnett MH, Becker AJ, Blumcke I, Graus F*, et al.* Immunopathology of autoantibody-associated encephalitides: clues for pathogenesis. Brain 2012; 135(Pt 5): 1622-38.

Blaber SI, Ciric B, Christophi GP, Bernett MJ, Blaber M, Rodriguez M*, et al.* Targeting kallikrein 6 proteolysis attenuates CNS inflammatory disease. FASEB Journal 2004; 18(7): 920-2.

Blaber SI, Scarisbrick IA, Bernett MJ, Dhanarajan P, Seavy MA, Jin Y*, et al.* Enzymatic properties of rat myelencephalon-specific protease. Biochemistry 2002; 41(4): 1165-73.

Blaber SI, Yoon H, Scarisbrick IA, Juliano MA, Blaber M. The autolytic regulation of human kallikrein-related peptidase 6. Biochemistry 2007; 46(17): 5209-17.

Blakemore WF, Franklin RJ. Remyelination in experimental models of toxin-induced demyelination. Current Topics in Microbiology and Immunology 2008; 318: 193-212.

Bogovyk R, Lunko O, Fedoriuk M, Isaev D, Krishtal O, Holmes GL*, et al.* Effects of protease-activated receptor 1 inhibition on anxiety and fear following status epilepticus. Epilepsy & Behavior 2017; 67: 66-9.

Braak H, Alafuzoff I, Arzberger T, Kretzschmar H, Del Tredici K. Staging of Alzheimer disease-associated neurofibrillary pathology using paraffin sections and immunocytochemistry. Acta Neuropathologica 2006; 112(4): 389-404.

Braak H, Del Tredici K, Rub U, de Vos RA, Jansen Steur EN, Braak E. Staging of brain pathology related to sporadic Parkinson's disease. Neurobiology of Aging 2003; 24(2): 197-211.

Bradl M, Lassmann H. Progressive multiple sclerosis. Seminars in Immunopathology 2009; 31(4): 455-65.

Brennan MS, Patel H, Allaire N, Thai A, Cullen P, Ryan S*, et al.* Pharmacodynamics of Dimethyl Fumarate Are Tissue Specific and Involve NRF2-Dependent and -Independent Mechanisms. Antioxidants and Redox Signaling 2016; 24(18): 1058-71.

Brown MA, Wallace CS, Anamelechi CC, Clermont E, Reichert WM, Truskey GA. The use of mild trypsinization conditions in the detachment of endothelial cells to promote subsequent endothelialization on synthetic surfaces. Biomaterials 2007; 28(27): 3928-35.

Burda JE, Radulovic M, Yoon H, Scarisbrick IA. Critical role for PAR1 in kallikrein 6-mediated oligodendrogliopathy. Glia 2013; 61(9): 1456-70.

Buttermore ED, Thaxton CL, Bhat MA. Organization and maintenance of molecular domains in myelinated axons. Journal of Neuroscience Research 2013; 91(5): 603-22.

Cadavid D, Balcer L, Galetta S, Aktas O, Ziemssen T, Vanopdenbosch L*, et al.* Safety and efficacy of opicinumab in acute optic neuritis (RENEW): a randomised, placebo-controlled, phase 2 trial. Lancet Neurology 2017; 16(3): 189-99.

Calabrese M, Rinaldi F, Grossi P, Gallo P. Cortical pathology and cognitive impairment in multiple sclerosis. Expert Review of Neurotherapeutics 2011; 11(3): 425-32.

Camargo N, Goudriaan A, van Deijk AF, Otte WM, Brouwers JF, Lodder H*, et al.* Oligodendroglial myelination requires astrocyte-derived lipids. PLoS Biology 2017; 15(5): e1002605.

Cantorna MT, Waddell A. The vitamin D receptor turns off chronically activated T cells. Annals of the New York Academy of Sciences 2014; 1317: 70-5.

Clarner T, Diederichs F, Berger K, Denecke B, Gan L, van der Valk P*, et al.* Myelin debris regulates inflammatory responses in an experimental demyelination animal model and multiple sclerosis lesions. Glia 2012; 60(10): 1468-80.

Coetzee T, Fujita N, Dupree J, Shi R, Blight A, Suzuki K*, et al.* Myelination in the absence of galactocerebroside and sulfatide: normal structure with abnormal function and regional instability. Cell 1996; 86(2): 209-19.

Cole KLH, Early JJ, Lyons DA. Drug discovery for remyelination and treatment of MS. Glia 2017; 65(10): 1565-89.

Consortium GT, Laboratory DA, Coordinating Center -Analysis Working G, Statistical Methods groups-Analysis Working G, Enhancing Gg, Fund NIHC*, et al.* Genetic effects on gene expression across human tissues. Nature 2017; 550(7675): 204-13.

Constantinescu CS, Farooqi N, O'Brien K, Gran B. Experimental autoimmune encephalomyelitis (EAE) as a model for multiple sclerosis (MS). British Journal of Pharmacology 2011; 164(4): 1079-106.

Cottrell GS, Coelho AM, Bunnett NW. Protease-activated receptors: the role of cell-surface proteolysis in signalling. Essays in Biochemistry 2002; 38: 169-83.

Coutu JP, Goldblatt A, Rosas HD, Salat DH, Alzheimer's Disease Neuroimaging I. White Matter Changes are Associated with Ventricular Expansion in Aging, Mild Cognitive Impairment, and Alzheimer's Disease. Journal of Alzheimer's Disease 2016; 49(2): 329-42.

Crawford AH, Chambers C, Franklin RJ. Remyelination: the true regeneration of the central nervous system. Journal of Comparative Pathology 2013; 149(2-3): 242-54.

Criste G, Trapp B, Dutta R. Axonal loss in multiple sclerosis: causes and mechanisms. Handbook of Clinical Neurology 2014; 122: 101-13.

Czopka T, Ffrench-Constant C, Lyons DA. Individual oligodendrocytes have only a few hours in which to generate new myelin sheaths in vivo. Developmental Cell 2013; 25(6): 599-609.

Dargahi N, Katsara M, Tselios T, Androutsou ME, de Courten M, Matsoukas J*, et al.* Multiple Sclerosis: Immunopathology and Treatment Update. Brain Scien 2017; 7(7).

Demerens C, Stankoff B, Logak M, Anglade P, Allinquant B, Couraud F*, et al.* Induction of myelination in the central nervous system by electrical activity. Proceedings of the National Academy of Sciences of the United States of America 1996; 93(18): 9887-92.

Dendrou CA, Fugger L, Friese MA. Immunopathology of multiple sclerosis. Nature Reviews: Immunology 2015; 15(9): 545-58.

Denic A, Johnson AJ, Bieber AJ, Warrington AE, Rodriguez M, Pirko I. The relevance of animal models in multiple sclerosis research. Pathophysiology 2011; 18(1): 21-9.

Deoni SC, Zinkstok JR, Daly E, Ecker C, Consortium MA, Williams SC*, et al.* White-matter relaxation time and myelin water fraction differences in young adults with autism. Psychological Medicine 2015; 45(4): 795-805.

DePaula-Silva AB, Hanak TJ, Libbey JE, Fujinami RS. Theiler's murine encephalomyelitis virus infection of SJL/J and C57BL/6J mice: Models for multiple sclerosis and epilepsy. Journal of Neuroimmunology 2017; 308: 30-42.

Deshmukh VA, Tardif V, Lyssiotis CA, Green CC, Kerman B, Kim HJ*, et al.* A regenerative approach to the treatment of multiple sclerosis. Nature 2013; 502(7471): 327-32.

Di Cera E. Serine proteases. IUBMB Life 2009; 61(5): 510-5.
Domingues HS, Portugal CC, Socodato R, Relvas JB. Oligodendrocyte, Astrocyte, and Microglia Crosstalk in Myelin Development, Damage, and Repair. Frontiers in Cell and Developmental Biology 2016; 4: 71.

Drucker KL, Gianinni C, Decker PA, Diamandis EP, Scarisbrick IA. Prognostic significance of multiple kallikreins in high-grade astrocytoma. BMC Cancer 2015; 15: 565.

Dukic L, Simundic AM, Martinic-Popovic I, Kackov S, Diamandis A, Begcevic I*, et al.* The role of human kallikrein 6, clusterin and adiponectin as potential blood biomarkers of dementia. Clinical Biochemistry 2016; 49(3): 213-8.

Duncan ID, Marik RL, Broman AT, Heidari M. Thin myelin sheaths as the hallmark of remyelination persist over time and preserve axon function. Proceedings of the National Academy of Sciences of the United States of America 2017; 114(45): E9685-E91.

Dyer CA, Phillbotte T, Wolf MK, Billings-Gagliardi S. Regulation of cytoskeleton by myelin components: studies on shiverer oligodendrocytes carrying an Mbp transgene. Developmental Neuroscience 1997; 19(5): 395-409.

Emery B. Regulation of oligodendrocyte differentiation and myelination. Science 2010; 330(6005): 779-82.

Eschenroeder AC, Vestal-Laborde AA, Sanchez ES, Robinson SE, Sato-Bigbee C. Oligodendrocyte responses to buprenorphine uncover novel and opposing roles of mu-opioid- and nociceptin/orphanin FQ receptors in cell development: implications for drug addiction treatment during pregnancy. Glia 2012; 60(1): 125-36.

Fabri M, Pierpaoli C, Barbaresi P, Polonara G. Functional topography of the corpus callosum investigated by DTI and fMRI. World J Radiology 2014; 6(12): 895-906.

Feltri ML, Poitelon Y, Previtali SC. How Schwann Cells Sort Axons: New Concepts. Neuroscientist 2016; 22(3): 252-65.

Ferris HA, Perry RJ, Moreira GV, Shulman GI, Horton JD, Kahn CR. Loss of astrocyte cholesterol synthesis disrupts neuronal function and alters whole-body metabolism. Proceedings of the National Academy of Sciences of the United States of America 2017; 114(5): 1189-94.

Franklin RJM, Ffrench-Constant C. Regenerating CNS myelin - from mechanisms to experimental medicines. Nature Reviews: Neuroscience 2017; 18(12): 753-69.

Frischer JM, Bramow S, Dal-Bianco A, Lucchinetti CF, Rauschka H, Schmidbauer M*, et al.* The relation between inflammation and neurodegeneration in multiple sclerosis brains. Brain 2009; 132(Pt 5): 1175-89.

Ghadiri M, Rezk A, Li R, Evans A, Luessi F, Zipp F*, et al.* Dimethyl fumarate-induced lymphopenia in MS due to differential T-cell subset apoptosis. Neurology Neuroimmunology and Neuroinflammation 2017; 4(3): e340.

Ghasemlou N, Jeong SY, Lacroix S, David S. T cells contribute to lysophosphatidylcholine-induced macrophage activation and demyelination in the CNS. Glia 2007; 55(3): 294-302.

Gonzalez-Gronow M, Cuchacovich M, Francos R, Cuchacovich S, Blanco A, Sandoval R*, et al.* Catalytic autoantibodies against myelin basic protein (MBP) isolated from serum of autistic children impair in vitro models of synaptic plasticity in rat hippocampus. Journal of Neuroimmunology 2015; 287: 1-8.

Green AJ, Gelfand JM, Cree BA, Bevan C, Boscardin WJ, Mei F*, et al.* Clemastine fumarate as a remyelinating therapy for multiple sclerosis (ReBUILD): a randomised, controlled, double-blind, crossover trial. Lancet 2017; 390(10111): 2481-9.

Gudi V, Gingele S, Skripuletz T, Stangel M. Glial response during cuprizone-induced de- and remyelination in the CNS: lessons learned. Frontiers in Cellular Neuroscience 2014; 8: 73.

Guttmann CR, Jolesz FA, Kikinis R, Killiany RJ, Moss MB, Sandor T*, et al.* White matter changes with normal aging. Neurology 1998; 50(4): 972-8.

Hai NT, Kim J, Park ES, Chi SC. Formulation and biopharmaceutical evaluation of transdermal patch containing benztropine. International Journal of Pharmaceutics 2008; 357(1-2): 55-60.

Haider L, Zrzavy T, Hametner S, Hoftberger R, Bagnato F, Grabner G*, et al.* The topograpy of demyelination and neurodegeneration in the multiple sclerosis brain. Brain 2016; 139(Pt 3): 807-15.

Haji Abdolvahab M, Mofrad MR, Schellekens H. Interferon Beta: From Molecular Level to Therapeutic Effects. International Review of Cell and Molecular Biology 2016; 326: 343-72.

Harlow DE, Honce JM, Miravalle AA. Remyelination Therapy in Multiple Sclerosis. Frontiers in Neurology 2015; 6: 257.

Hebb AL, Bhan V, Wishart AD, Moore CS, Robertson GS. Human kallikrein 6 cerebrospinal levels are elevated in multiple sclerosis. Current Drug Discov Technol 2010; 7(2): 137-40.

Herbert AL, Monk KR. Advances in myelinating glial cell development. Current Opinion in Neurobiology 2017; 42: 53-60.

Herder V, Hansmann F, Stangel M, Skripuletz T, Baumgartner W, Beineke A. Lack of cuprizone-induced demyelination in the murine spinal cord despite oligodendroglial alterations substantiates the concept of site-specific susceptibilities of the central nervous system. Neuropathology and Applied Neurobiology 2011; 37(6): 676-84.

Hibbits N, Pannu R, Wu TJ, Armstrong RC. Cuprizone demyelination of the corpus callosum in mice correlates with altered social interaction and impaired bilateral sensorimotor coordination. ASN Neuro 2009; 1(3).

Hirase H, Koizumi S. Astrocytes as therapeutic targets in brain diseases. Neuroscience Research 2018; 126: 1-2.

Housley WJ, Pitt D, Hafler DA. Biomarkers in multiple sclerosis. Clinical Immunology 2015; 161(1): 51-8.

Hu Y, Lee X, Ji B, Guckian K, Apicco D, Pepinsky RB*, et al.* Sphingosine 1-phosphate receptor modulator fingolimod (FTY720) does not promote remyelination in vivo. Molecular and Cellular Neuroscience 2011; 48(1): 72-81.

International Multiple Sclerosis Genetics C, Wellcome Trust Case Control C, Sawcer S, Hellenthal G, Pirinen M, Spencer CC*, et al.* Genetic risk and a primary role for cell-mediated immune mechanisms in multiple sclerosis. Nature 2011; 476(7359): 214-9.

Iwata A, Maruyama M, Akagi T, Hashikawa T, Kanazawa I, Tsuji S*, et al.* Alpha-synuclein degradation by serine protease neurosin: implication for pathogenesis of synucleinopathies. Human Molecular Genetics 2003; 12(20): 2625-35.

Jakimovski D, Weinstock-Guttman B, Ramanathan M, Kolb C, Hojnacki D, Minagar A*, et al.* Ocrelizumab: a B-cell depleting therapy for multiple sclerosis. Expert Opinion on Biological Therapy 2017; 17(9): 1163-72.

Jakovcevski I, Zecevic N. Olig transcription factors are expressed in oligodendrocyte and neuronal cells in human fetal CNS. Journal of Neuroscience 2005a; 25(44): 10064-73.

Jakovcevski I, Zecevic N. Sequence of oligodendrocyte development in the human fetal telencephalon. Glia 2005b; 49(4): 480-91.

Jeffery ND, Blakemore WF. Remyelination of mouse spinal cord axons demyelinated by local injection of lysolecithin. Journal of Neurocytology 1995; 24(10): 775-81.

Kamentsky L, Jones TR, Fraser A, Bray MA, Logan DJ, Madden KL*, et al.* Improved structure, function and compatibility for CellProfiler: modular high-throughput image analysis software. Bioinformatics 2011; 27(8): 1179-80.

Kamphuis W, Middeldorp J, Kooijman L, Sluijs JA, Kooi EJ, Moeton M*, et al.* Glial fibrillary acidic protein isoform expression in plaque related astrogliosis in Alzheimer's disease. Neurobiology of Aging 2014; 35(3): 492-510.

Kappus N, Weinstock-Guttman B, Hagemeier J, Kennedy C, Melia R, Carl E*, et al.* Cardiovascular risk factors are associated with increased lesion burden and brain atrophy in multiple sclerosis. Journal of Neurology, Neurosurgery and Psychiatry 2016; 87(2): 181-7.

Katz Sand I. Classification, diagnosis, and differential diagnosis of multiple sclerosis. Current Opinion in Neurology 2015; 28(3): 193-205.

Kearney H, Miller DH, Ciccarelli O. Spinal cord MRI in multiple sclerosis--diagnostic, prognostic and clinical value. Nature Reviews: Neurology 2015a; 11(6): 327-38.

Kearney H, Schneider T, Yiannakas MC, Altmann DR, Wheeler-Kingshott CA, Ciccarelli O*, et al.* Spinal cord grey matter abnormalities are associated with secondary progression and physical disability in multiple sclerosis. Journal of Neurology, Neurosurgery and Psychiatry 2015b; 86(6): 608-14.

Keough MB, Jensen SK, Yong VW. Experimental demyelination and remyelination of murine spinal cord by focal injection of lysolecithin. J Vis Exp 2015(97).

Kessaris N, Fogarty M, Iannarelli P, Grist M, Wegner M, Richardson WD. Competing waves of oligodendrocytes in the forebrain and postnatal elimination of an embryonic lineage. Nature Neuroscience 2006; 9(2): 173-9.

Kieseier BC. The mechanism of action of interferon-beta in relapsing multiple sclerosis. CNS Drugs 2011; 25(6): 491-502.

Kilsdonk ID, Jonkman LE, Klaver R, van Veluw SJ, Zwanenburg JJ, Kuijer JP*, et al.* Increased cortical grey matter lesion detection in multiple sclerosis with 7 T MRI: a post-mortem verification study. Brain 2016; 139(Pt 5): 1472-81.

Kim S, Bielawski J, Yang H, Kong Y, Zhou B, Li J. Functional antagonism of sphingosine-1-phosphate receptor 1 prevents cuprizone-induced demyelination. Glia 2017.

Kipp M, Clarner T, Dang J, Copray S, Beyer C. The cuprizone animal model: new insights into an old story. Acta Neuropathologica 2009; 118(6): 723-36.

Kiray H, Lindsay SL, Hosseinzadeh S, Barnett SC. The multifaceted role of astrocytes in regulating myelination. Experimental Neurology 2016; 283(Pt B): 541-9.

Kishibe M, Baida G, Bhalla P, Lavker RM, Schlosser B, Iinuma S*, et al.* Important role of kallikrein 6 for the development of keratinocyte proliferative resistance to topical glucocorticoids. Oncotarget 2016; 7(43): 69479-88.

Koob AO, Paulino AD, Masliah E. GFAP reactivity, apolipoprotein E redistribution and cholesterol reduction in human astrocytes treated with alpha-synuclein. Neuroscience Letters 2010; 469(1): 11-4.

Korbakis D, Soosaipillai A, Diamandis EP. Study of kallikrein-related peptidase 6 (KLK6) and its complex with alpha1-antitrypsin in biological fluids. Clinical Chemistry and Laboratory Medicine 2017; 55(9): 1385-96.

Kotter MR, Li WW, Zhao C, Franklin RJ. Myelin impairs CNS remyelination by inhibiting oligodendrocyte precursor cell differentiation. Journal of Neuroscience 2006; 26(1): 328-32.

Kubo N, Shirakawa O, Kuno T, Tanaka C. Antimuscarinic effects of antihistamines: quantitative evaluation by receptor-binding assay. Japanese Journal of Pharmacology 1987; 43(3): 277-82.

Kuchling J, Ramien C, Bozin I, Dorr J, Harms L, Rosche B*, et al.* Identical lesion morphology in primary progressive and relapsing-remitting MS--an ultrahigh field MRI study. Multiple Sclerosis 2014; 20(14): 1866-71.

Kuhlmann T, Ludwin S, Prat A, Antel J, Bruck W, Lassmann H. An updated histological classification system for multiple sclerosis lesions. Acta Neuropathologica 2017; 133(1): 13-24.

Lapato AS, Szu JI, Hasselmann JPC, Khalaj AJ, Binder DK, Tiwari-Woodruff SK. Chronic demyelination-induced seizures. Neuroscience 2017; 346: 409-22.

Lassmann H. Pathology and disease mechanisms in different stages of multiple sclerosis. Journal of the Neurological Sciences 2013; 333(1-2): 1-4.

Lee DW, Banquy X, Kristiansen K, Kaufman Y, Boggs JM, Israelachvili JN. Lipid domains control myelin basic protein adsorption and membrane interactions between model myelin lipid bilayers. Proceedings of the National Academy of Sciences of the United States of America 2014; 111(8): E768-75.

Lee PR, Johnson TP, Gnanapavan S, Giovannoni G, Wang T, Steiner JP*, et al.* Protease-activated receptor-1 activation by granzyme B causes neurotoxicity that is augmented by interleukin-1beta. Journal of Neuroinflammation 2017; 14(1): 131.

Lee S, Leach MK, Redmond SA, Chong SY, Mellon SH, Tuck SJ*, et al.* A culture system to study oligodendrocyte myelination processes using engineered nanofibers. Nature Methods 2012; 9(9): 917-22.

Li J, Zhang L, Chu Y, Namaka M, Deng B, Kong J*, et al.* Astrocytes in Oligodendrocyte Lineage Development and White Matter Pathology. Frontiers in Cellular Neuroscience 2016; 10: 119.

Li Z, He Y, Fan S, Sun B. Clemastine rescues behavioral changes and enhances remyelination in the cuprizone mouse model of demyelination. Neuroscience Bulletin 2015; 31(5): 617-25.

Liang G, Bowen JP. Development of Trypsin-Like Serine Protease Inhibitors as Therapeutic Agents: Opportunities, Challenges, and their Unique Structure-Based Rationales. Current Topics in Medicinal Chemistry 2016; 16(13): 1506-29.

Liang G, Chen X, Aldous S, Pu SF, Mehdi S, Powers E*, et al.* Virtual Screening and X-ray Crystallography for Human Kallikrein 6 Inhibitors with an

Amidinothiophene P1 Group. ACS Medicinal Chemistry Letters 2012a; 3(2): 159-64.

Liang G, Chen X, Aldous S, Pu SF, Mehdi S, Powers E*, et al.* Human kallikrein 6 inhibitors with a para-amidobenzylanmine P1 group identified through virtual screening. Bioorganic and Medicinal Chemistry Letters 2012b; 22(7): 2450-5.

Linker RA, Gold R. Dimethyl fumarate for treatment of multiple sclerosis: mechanism of action, effectiveness, and side effects. Current Neurology and Neuroscience Reports 2013; 13(11): 394.

Liu J, Dietz K, DeLoyht JM, Pedre X, Kelkar D, Kaur J*, et al.* Impaired adult myelination in the prefrontal cortex of socially isolated mice. Nature Neuroscience 2012; 15(12): 1621-3.

Livak KJ, Schmittgen TD. Analysis of relative gene expression data using real-time quantitative PCR and the 2(-Delta Delta C(T)) Method. Methods 2001; 25(4): 402-8.

Lomakin Y, Arapidi GP, Chernov A, Ziganshin R, Tcyganov E, Lyadova I*, et al.* Exposure to the Epstein-Barr Viral Antigen Latent Membrane Protein 1 Induces Myelin-Reactive Antibodies In Vivo. Frontiers in Immunology 2017; 8: 777.

Love MI, Huber W, Anders S. Moderated estimation of fold change and dispersion for RNA-seq data with DESeq2. Genome Biology 2014; 15(12): 550.

Lucchinetti C, Bruck W, Parisi J, Scheithauer B, Rodriguez M, Lassmann H. A quantitative analysis of oligodendrocytes in multiple sclerosis lesions. A study of 113 cases. Brain 1999; 122 (Pt 12): 2279-95.

Magklara A, Mellati AA, Wasney GA, Little SP, Sotiropoulou G, Becker GW*, et al.* Characterization of the enzymatic activity of human kallikrein 6: Autoactivation, substrate specificity, and regulation by inhibitors. Biochemical and Biophysical Research Communications 2003; 307(4): 948-55.

Makinodan M, Rosen KM, Ito S, Corfas G. A critical period for social experience-dependent oligodendrocyte maturation and myelination. Science 2012; 337(6100): 1357-60.

Matsushima GK, Morell P. The neurotoxicant, cuprizone, as a model to study demyelination and remyelination in the central nervous system. Brain Pathology 2001; 11(1): 107-16.

McCarthy DP, Richards MH, Miller SD. Mouse models of multiple sclerosis: experimental autoimmune encephalomyelitis and Theiler's virus-induced demyelinating disease. Methods in Molecular Biology 2012; 900: 381-401.

McMahon EJ, Bailey SL, Castenada CV, Waldner H, Miller SD. Epitope spreading initiates in the CNS in two mouse models of multiple sclerosis. Nature Medicine 2005; 11(3): 335-9.

Meffre D, Shackleford G, Hichor M, Gorgievski V, Tzavara ET, Trousson A*, et al.* Liver X receptors alpha and beta promote myelination and remyelination in the cerebellum. Proceedings of the National Academy of Sciences of the United States of America 2015; 112(24): 7587-92.

Mei F, Fancy SPJ, Shen YA, Niu J, Zhao C, Presley B*, et al.* Micropillar arrays as a high-throughput screening platform for therapeutics in multiple sclerosis. Nature Medicine 2014; 20(8): 954-60.

Mei F, Lehmann-Horn K, Shen YA, Rankin KA, Stebbins KJ, Lorrain DS*, et al.* Accelerated remyelination during inflammatory demyelination prevents axonal loss and improves functional recovery. Elife 2016; 5.

Mi S, Miller RH, Lee X, Scott ML, Shulag-Morskaya S, Shao Z*, et al.* LINGO-1 negatively regulates myelination by oligodendrocytes. Nature Neuroscience 2005; 8(6): 745-51.

Mi S, Miller RH, Tang W, Lee X, Hu B, Wu W*, et al.* Promotion of central nervous system remyelination by induced differentiation of oligodendrocyte precursor cells. Annals of Neurology 2009; 65(3): 304-15.

Mighdoll MI, Tao R, Kleinman JE, Hyde TM. Myelin, myelin-related disorders, and psychosis. Schizophrenia Research 2015; 161(1): 85-93.

Miller DH, Fazekas F, Montalban X, Reingold SC, Trojano M. Pregnancy, sex and hormonal factors in multiple sclerosis. Multiple Sclerosis 2014; 20(5): 527-36.

Miron VE, Kuhlmann T, Antel JP. Cells of the oligodendroglial lineage, myelination, and remyelination. Biochimica et Biophysica Acta (BBA) - Bioenergetics 2011; 1812(2): 184-93.

Mortazavi MM, Adeeb N, Griessenauer CJ, Sheikh H, Shahidi S, Tubbs RI*, et al.* The ventricular system of the brain: a comprehensive review of its history,

anatomy, histology, embryology, and surgical considerations. Child's Nervous System 2014; 30(1): 19-35.

Moutsianas L, Jostins L, Beecham AH, Dilthey AT, Xifara DK, Ban M*, et al.* Class II HLA interactions modulate genetic risk for multiple sclerosis. Nature Genetics 2015; 47(10): 1107-13.

Muccilli A, Seyman E, Oh J. Spinal Cord MRI in Multiple Sclerosis. Neurologic Clinics 2018; 36(1): 35-57.

Munzel EJ, Becker CG, Becker T, Williams A. Zebrafish regenerate full thickness optic nerve myelin after demyelination, but this fails with increasing age. Acta Neuropathologica Communications 2014; 2: 77.

Murakami K, Jiang YP, Tanaka T, Bando Y, Mitrovic B, Yoshida S. In vivo analysis of kallikrein-related peptidase 6 (KLK6) function in oligodendrocyte development and the expression of myelin proteins. Neuroscience 2013; 236: 1-11.

Muraro PA, Martin R, Mancardi GL, Nicholas R, Sormani MP, Saccardi R. Autologous haematopoietic stem cell transplantation for treatment of multiple sclerosis. Nature Reviews: Neurology 2017; 13(7): 391-405.

Nave KA, Werner HB. Myelination of the nervous system: mechanisms and functions. Annual Review of Cell and Developmental Biology 2014; 30: 503-33.

Neumann H, Medana IM, Bauer J, Lassmann H. Cytotoxic T lymphocytes in autoimmune and degenerative CNS diseases. Trends in Neurosciences 2002; 25(6): 313-9.

Nieuwenhuys R, Voogd J, van Huijzen C. The Human Central Nervous System, fourth edition. 2008.

Nishiyama A, Komitova M, Suzuki R, Zhu X. Polydendrocytes (NG2 cells): multifunctional cells with lineage plasticity. Nature Reviews: Neuroscience 2009; 10(1): 9-22.

Nociti V, Cianfoni A, Mirabella M, Caggiula M, Frisullo G, Patanella AK*, et al.* Clinical characteristics, course and prognosis of spinal multiple sclerosis. Spinal Cord 2005; 43(12): 731-4.

Noorbakhsh F, Vergnolle N, Hollenberg MD, Power C. Proteinase-activated receptors in the nervous system. Nature Reviews Neuroscience 2003; 4(12): 981-90.

Oikonomopoulou K, Diamandis EP, Hollenberg MD. Kallikrein-related peptidases: proteolysis and signaling in cancer, the new frontier. Biological Chemistry 2010; 391(4): 299-310.

Oikonomopoulou K, Hansen KK, Saifeddine M, Vergnolle N, Tea I, Blaber M*, et al.* Kallikrein-mediated cell signalling: targeting proteinase-activated receptors (PARs). Biological Chemistry 2006a; 387(6): 817-24.

Oikonomopoulou K, Hansen KK, Saifeddine M, Vergnolle N, Tea I, Diamandis EP*, et al.* Proteinase-mediated cell signalling: targeting proteinase-activated receptors (PARs) by kallikreins and more. Biological Chemistry 2006b; 387(6): 677-85.

Ottoboni L, Keenan BT, Tamayo P, Kuchroo M, Mesirov JP, Buckle GJ*, et al.* An RNA profile identifies two subsets of multiple sclerosis patients differing in disease activity. Science Translational Medicine 2012; 4(153): 153ra31.

Ousman SS, David S. Lysophosphatidylcholine induces rapid recruitment and activation of macrophages in the adult mouse spinal cord. Glia 2000; 30(1): 92-104.

Pampalakis G, Sykioti VS, Ximerakis M, Stefanakou-Kalakou I, Melki R, Vekrellis K*, et al.* KLK6 proteolysis is implicated in the turnover and uptake of extracellular alpha-synuclein species. Oncotarget 2017; 8(9): 14502-15.

Pavelko KD, van Engelen BG, Rodriguez M. Acceleration in the rate of CNS remyelination in lysolecithin-induced demyelination. Journal of Neuroscience 1998; 18(7): 2498-505.

Pedraza CE, Taylor C, Pereira A, Seng M, Tham CS, Izrael M*, et al.* Induction of oligodendrocyte differentiation and in vitro myelination by inhibition of rho-associated kinase. ASN Neuro 2014; 6(4).

Pender MP, Burrows SR. Epstein-Barr virus and multiple sclerosis: potential opportunities for immunotherapy. Clin Transl Immunology 2014; 3(10): e27.

Peters A. The formation and structure of myelin sheaths in the central nervous system. Journal of Biophysical and Biochemical Cytology 1960; 8: 431-46.

Peters A. The effects of normal aging on myelin and nerve fibers: a review. Journal of Neurocytology 2002; 31(8-9): 581-93.

Peters A, Rosene DL, Moss MB, Kemper TL, Abraham CR, Tigges J*, et al.* Neurobiological bases of age-related cognitive decline in the rhesus monkey. Journal of Neuropathology & Experimental Neurology 1996; 55(8): 861-74.

Peters A, Sethares C. Is there remyelination during aging of the primate central nervous system? Journal of Comparative Neurology 2003; 460(2): 238-54.

Petiet A, Aigrot MS, Stankoff B. Gray and White Matter Demyelination and Remyelination Detected with Multimodal Quantitative MRI Analysis at 11.7T in a Chronic Mouse Model of Multiple Sclerosis. Frontiers in Neuroscience 2016; 10: 491.

Petraki C, Dubinski W, Scorilas A, Saleh C, Pasic MD, Komborozos V*, et al.* Evaluation and prognostic significance of human tissue kallikrein-related peptidase 6 (KLK6) in colorectal cancer. Pathology, Research and Practice 2012; 208(2): 104-8.

Petraki CD, Karavana VN, Skoufogiannis PT, Little SP, Howarth DJ, Yousef GM*, et al.* The spectrum of human kallikrein 6 (zyme/protease M/neurosin) expression in human tissues as assessed by immunohistochemistry. Journal of Histochemistry and Cytochemistry 2001; 49(11): 1431-41.

Pierrot-Deseilligny C, Souberbielle JC. Vitamin D and multiple sclerosis: An update. Multiple Sclerosis and Related Disorders 2017; 14: 35-45.

Plemel JR, Manesh SB, Sparling JS, Tetzlaff W. Myelin inhibits oligodendroglial maturation and regulates oligodendrocytic transcription factor expression. Glia 2013; 61(9): 1471-87.

Podbielska M, Banik NL, Kurowska E, Hogan EL. Myelin recovery in multiple sclerosis: the challenge of remyelination. Brain Sciences 2013; 3(3): 1282-324.

Poliak S, Peles E. The local differentiation of myelinated axons at nodes of Ranvier. Nature Reviews: Neuroscience 2003; 4(12): 968-80.

Ponath G, Park C, Pitt D. The Role of Astrocytes in Multiple Sclerosis. Frontiers in Immunology 2018; 9.

Ponath G, Ramanan S, Mubarak M, Housley W, Lee S, Sahinkaya FR*, et al.* Myelin phagocytosis by astrocytes after myelin damage promotes lesion pathology. Brain 2017; 140(2): 399-413.

Poutiainen P, Jaronen M, Quintana FJ, Brownell AL. Precision Medicine in Multiple Sclerosis: Future of PET Imaging of Inflammation and Reactive Astrocytes. Frontiers in Molecular Neuroscience 2016; 9: 85.

Powers BE, Sellers DL, Lovelett EA, Cheung W, Aalami SP, Zapertov N*, et al.* Remyelination reporter reveals prolonged refinement of spontaneously regenerated myelin. Proceedings of the National Academy of Sciences of the United States of America 2013; 110(10): 4075-80.

Prassas I, Eissa A, Poda G, Diamandis EP. Unleashing the therapeutic potential of human kallikrein-related serine proteases. Nature Reviews: Drug Discovery 2015; 14(3): 183-202.

Preisner A, Albrecht S, Cui QL, Hucke S, Ghelman J, Hartmann C*, et al.* Non-steroidal anti-inflammatory drug indometacin enhances endogenous remyelination. Acta Neuropathologica 2015; 130(2): 247-61.

Prineas JW, Connell F. Remyelination in multiple sclerosis. Annals of Neurology 1979; 5(1): 22-31.

Promjunyakul NO, Lahna DL, Kaye JA, Dodge HH, Erten-Lyons D, Rooney WD*, et al.* Comparison of cerebral blood flow and structural penumbras in relation to white matter hyperintensities: A multi-modal magnetic resonance imaging study. Journal of Cerebral Blood Flow and Metabolism 2016; 36(9): 1528-36.

Purger D, Gibson EM, Monje M. Myelin plasticity in the central nervous system. Neuropharmacology 2016; 110(Pt B): 563-73.

Radulovic M, Yoon H, Larson N, Wu J, Linbo R, Burda JE*, et al.* Kallikrein cascades in traumatic spinal cord injury: in vitro evidence for roles in axonopathy and neuron degeneration. Journal of Neuropathology & Experimental Neurology 2013; 72(11): 1072-89.

Radulovic M, Yoon H, Wu J, Mustafa K, Scarisbrick IA. Targeting the thrombin receptor modulates inflammation and astrogliosis to improve recovery after spinal cord injury. Neurobiology of Disease 2016; 93: 226-42.

Ramsay AJ, Hooper JD, Folgueras AR, Velasco G, Lopez-Otin C. Matriptase-2 (TMPRSS6): a proteolytic regulator of iron homeostasis. Haematologica 2009; 94(6): 840-9.

Rangachari M, Kuchroo VK. Using EAE to better understand principles of immune function and autoimmune pathology. Journal of Autoimmunity 2013; 45: 31-9.

Ranger A, Ray S, Szak S, Dearth A, Allaire N, Murray R*, et al.* Anti-LINGO-1 has no detectable immunomodulatory effects in preclinical and phase 1 studies. Neurology Neuroimmunology and Neuroinflammation 2018; 5(1): e417.

Ransohoff RM. Animal models of multiple sclerosis: the good, the bad and the bottom line. Nature Neuroscience 2012; 15(8): 1074-7.

Ransohoff RM, Hafler DA, Lucchinetti CF. Multiple sclerosis-a quiet revolution. Nature Reviews: Neurology 2015; 11(3): 134-42.

Richards MH, Getts MT, Podojil JR, Jin YH, Kim BS, Miller SD. Virus expanded regulatory T cells control disease severity in the Theiler's virus mouse model of MS. Journal of Autoimmunity 2011; 36(2): 142-54.

Rivera A, Vanzuli I, Arellano JJ, Butt A. Decreased Regenerative Capacity of Oligodendrocyte Progenitor Cells (NG2-Glia) in the Ageing Brain: A Vicious Cycle of Synaptic Dysfunction, Myelin Loss and Neuronal Disruption? Current Alzheimer Research 2016; 13(4): 413-8.

Ronaghan NJ, Shang J, Iablokov V, Zaheer R, Colarusso P, Dion S*, et al.* The serine protease-mediated increase in intestinal epithelial barrier function is dependent on occludin and requires an intact tight junction. American Journal of Physiology: Gastrointestinal and Liver Physiology 2016; 311(3): G466-79.

Rostami J, Holmqvist S, Lindstrom V, Sigvardson J, Westermark GT, Ingelsson M*, et al.* Human Astrocytes Transfer Aggregated Alpha-Synuclein via Tunneling Nanotubes. Journal of Neuroscience 2017; 37(49): 11835-53.

Ruckert F, Hennig M, Petraki CD, Wehrum D, Distler M, Denz A*, et al.* Co-expression of KLK6 and KLK10 as prognostic factors for survival in pancreatic ductal adenocarcinoma. British Journal of Cancer 2008; 99(9): 1484-92.

Ruggieri S, Tortorella C, Gasperini C. Anti lingo 1 (opicinumab) a new monoclonal antibody tested in relapsing remitting multiple sclerosis. Expert Review of Neurotherapeutics 2017; 17(11): 1081-9.

Sachs HH, Bercury KK, Popescu DC, Narayanan SP, Macklin WB. A new model of cuprizone-mediated demyelination/remyelination. ASN Neuro 2014; 6(5).

Sam K, Crawley AP, Conklin J, Poublanc J, Sobczyk O, Mandell DM*, et al.* Development of White Matter Hyperintensity Is Preceded by Reduced Cerebrovascular Reactivity. Annals of Neurology 2016; 80(2): 277-85.

Sampaio-Baptista C, Khrapitchev AA, Foxley S, Schlagheck T, Scholz J, Jbabdi S*, et al.* Motor skill learning induces changes in white matter microstructure and myelination. Journal of Neuroscience 2013; 33(50): 19499-503.

Santoro A, Spinelli CC, Martucciello S, Nori SL, Capunzo M, Puca AA*, et al.* Innate immunity and cellular senescence: The good and the bad in the developmental and aged brain. Journal of Leukocyte Biology 2018.

Scarisbrick IA, Blaber SI, Lucchinetti CF, Genain CP, Blaber M, Rodriguez M. Activity of a newly identified serine protease in CNS demyelination. Brain 2002; 125(Pt 6): 1283-96.

Scarisbrick IA, Epstein B, Cloud BA, Yoon H, Wu J, Renner DN*, et al.* Functional role of kallikrein 6 in regulating immune cell survival. PLoS One 2011; 6(3): e18376.

Scarisbrick IA, Linbo R, Vandell AG, Keegan M, Blaber SI, Blaber M*, et al.* Kallikreins are associated with secondary progressive multiple sclerosis and promote neurodegeneration. Biological Chemistry 2008; 389(6): 739-45.

Scarisbrick IA, Radulovic M, Burda JE, Larson N, Blaber SI, Giannini C*, et al.* Kallikrein 6 is a novel molecular trigger of reactive astrogliosis. Biological Chemistry 2012a; 393(5): 355-67.

Scarisbrick IA, Yoon H, Panos M, Larson N, Blaber SI, Blaber M*, et al.* Kallikrein 6 regulates early CNS demyelination in a viral model of multiple sclerosis. Brain Pathology 2012b; 22(5): 709-22.

Scholz J, Klein MC, Behrens TE, Johansen-Berg H. Training induces changes in white-matter architecture. Nature Neuroscience 2009; 12(11): 1370-1.

Schultz V, van der Meer F, Wrzos C, Scheidt U, Bahn E, Stadelmann C*, et al.* Acutely damaged axons are remyelinated in multiple sclerosis and experimental models of demyelination. Glia 2017; 65(8): 1350-60.

Seiz L, Dorn J, Kotzsch M, Walch A, Grebenchtchikov NI, Gkazepis A*, et al.* Stromal cell-associated expression of kallikrein-related peptidase 6 (KLK6) indicates poor prognosis of ovarian cancer patients. Biological Chemistry 2012; 393(5): 391-401.

Sharma N, Oikonomopoulou K, Ito K, Renaux B, Diamandis EP, Hollenberg MD*, et al.* Substrate specificity determination of mouse implantation serine proteinase and human kallikrein-related peptidase 6 by phage display. Biological Chemistry 2008; 389(8): 1097-105.

Shavit E, Beilin O, Korczyn AD, Sylantiev C, Aronovich R, Drory VE*, et al.* Thrombin receptor PAR-1 on myelin at the node of Ranvier: a new anatomy and physiology of conduction block. Brain 2008; 131(Pt 4): 1113-22.

Silva RN, Oliveira LC, Parise CB, Oliveira JR, Severino B, Corvino A*, et al.* Activity of human kallikrein-related peptidase 6 (KLK6) on substrates containing sequences of basic amino acids. Is it a processing protease? Biochimica et Biophysica Acta (BBA) - Bioenergetics 2017; 1865(5): 558-64.

Silver J, Miller JH. Regeneration beyond the glial scar. Nature Reviews: Neuroscience 2004; 5(2): 146-56.

Simon MJ, Iliff JJ. Regulation of cerebrospinal fluid (CSF) flow in neurodegenerative, neurovascular and neuroinflammatory disease. Biochimica et Biophysica Acta (BBA) - Bioenergetics 2016; 1862(3): 442-51.

Simons M, Nave KA. Oligodendrocytes: Myelination and Axonal Support. Cold Spring Harbor Perspectives in Biology 2015; 8(1): a020479.

Siva A. Common Clinical and Imaging Conditions Misdiagnosed as Multiple Sclerosis: A Current Approach to the Differential Diagnosis of Multiple Sclerosis. Neurologic Clinics 2018; 36(1): 69-117.

Skripuletz T, Gudi V, Hackstette D, Stangel M. De- and remyelination in the CNS white and grey matter induced by cuprizone: the old, the new, and the unexpected. Histology and Histopathology 2011; 26(12): 1585-97.

Skripuletz T, Hackstette D, Bauer K, Gudi V, Pul R, Voss E*, et al.* Astrocytes regulate myelin clearance through recruitment of microglia during cuprizone-induced demyelination. Brain 2013; 136(Pt 1): 147-67.

Sloka S, Silva C, Pryse-Phillips W, Patten S, Metz L, Yong VW. A quantitative analysis of suspected environmental causes of MS. Canadian Journal of Neurological Sciences 2011; 38(1): 98-105.

Snyder JM, Hagan CE, Bolon B, Keene CD. Nervous System. Comparative Anatomy and Histology, second edition 2018: 403-44.

Spencer B, Michael S, Shen J, Kosberg K, Rockenstein E, Patrick C*, et al.* Lentivirus mediated delivery of neurosin promotes clearance of wild-type alpha-synuclein and reduces the pathology in an alpha-synuclein model of LBD. Molecular Therapy 2013; 21(1): 31-41.

Spencer B, Valera E, Rockenstein E, Trejo-Morales M, Adame A, Masliah E. A brain-targeted, modified neurosin (kallikrein-6) reduces alpha-synuclein accumulation in a mouse model of multiple system atrophy. Molecular Neurodegeneration 2015; 10: 48.

Stadelmann C, Bruck W. Interplay between mechanisms of damage and repair in multiple sclerosis. Journal of Neurology 2008; 255 Suppl 1: 12-8.

Stahnke AM, Holt KM. Ocrelizumab: A New B-cell Therapy for Relapsing Remitting and Primary Progressive Multiple Sclerosis. Annals of Pharmacotherapy 2017: 1060028017747635.

Stangel M, Kuhlmann T, Matthews PM, Kilpatrick TJ. Achievements and obstacles of remyelinating therapies in multiple sclerosis. Nature Reviews: Neurology 2017; 13(12): 742-54.

Steelman AJ, Thompson JP, Li J. Demyelination and remyelination in anatomically distinct regions of the corpus callosum following cuprizone intoxication. Neuroscience Research 2012; 72(1): 32-42.

Stratchko L, Filatova I, Agarwal A, Kanekar S. The Ventricular System of the Brain: Anatomy and Normal Variations. Seminars in Ultrasound, CT and MR 2016; 37(2): 72-83.

Sun J, Zhou H, Bai F, Zhang Z, Ren Q. Remyelination: A Potential Therapeutic Strategy for Alzheimer's Disease? Journal of Alzheimers Disease 2017.

Tagge I, O'Connor A, Chaudhary P, Pollaro J, Berlow Y, Chalupsky M*, et al.* Spatio-Temporal Patterns of Demyelination and Remyelination in the Cuprizone Mouse Model. PLoS One 2016; 11(4): e0152480.

Tatebe H, Watanabe Y, Kasai T, Mizuno T, Nakagawa M, Tanaka M*, et al.* Extracellular neurosin degrades alpha-synuclein in cultured cells. Neuroscience Research 2010; 67(4): 341-6.

Taveggia C, Thaker P, Petrylak A, Caporaso GL, Toews A, Falls DL*, et al.* Type III neuregulin-1 promotes oligodendrocyte myelination. Glia 2008; 56(3): 284-93.

Taylor LC, Gilmore W, Matsushima GK. SJL mice exposed to cuprizone intoxication reveal strain and gender pattern differences in demyelination. Brain Pathology 2009; 19(3): 467-79.

Tejedor LS, Wostradowski T, Gingele S, Skripuletz T, Gudi V, Stangel M. The Effect of Stereotactic Injections on Demyelination and Remyelination: a Study in the Cuprizone Model. Journal of Molecular Neuroscience 2017; 61(4): 479-88.

Terayama R, Bando Y, Jiang YP, Mitrovic B, Yoshida S. Differential expression of protease M/neurosin in oligodendrocytes and their progenitors in an animal model of multiple sclerosis. Neuroscience Letters 2005; 382(1-2): 82-7.

Thompson AJ, Banwell BL, Barkhof F, Carroll WM, Coetzee T, Comi G*, et al.* Diagnosis of multiple sclerosis: 2017 revisions of the McDonald criteria. Lancet Neurology 2017.

Thorburne SK, Juurlink BH. Low glutathione and high iron govern the susceptibility of oligodendroglial precursors to oxidative stress. Journal of Neurochemistry 1996; 67(3): 1014-22.

Trapani JA. Granzymes: a family of lymphocyte granule serine proteases. Genome Biology 2001; 2(12): REVIEWS3014.

Trejo J. Protease-activated receptors: new concepts in regulation of G protein-coupled receptor signaling and trafficking. Journal of Pharmacology and Experimental Therapeutics 2003; 307(2): 437-42.

Vandermarliere E, Mueller M, Martens L. Getting intimate with trypsin, the leading protease in proteomics. Mass Spectrometry Reviews 2013; 32(6): 453-65.

Watkins TA, Emery B, Mulinyawe S, Barres BA. Distinct stages of myelination regulated by gamma-secretase and astrocytes in a rapidly myelinating CNS coculture system. Neuron 2008; 60(4): 555-69.

Webb M, Tham CS, Lin FF, Lariosa-Willingham K, Yu N, Hale J*, et al.* Sphingosine 1-phosphate receptor agonists attenuate relapsing-remitting experimental autoimmune encephalitis in SJL mice. Journal of Neuroimmunology 2004; 153(1-2): 108-21.

Weisel JW, Litvinov RI. Fibrin Formation, Structure and Properties. Sub-Cellular Biochemistry 2017; 82: 405-56.

Whitcomb DC, Lowe ME. Human pancreatic digestive enzymes. Digestive Diseases and Sciences 2007; 52(1): 1-17.

Williamson EML, Berger JR. Diagnosis and Treatment of Progressive Multifocal Leukoencephalopathy Associated with Multiple Sclerosis Therapies. Neurotherapeutics 2017; 14(4): 961-73.

Winger RC, Zamvil SS. Antibodies in multiple sclerosis oligoclonal bands target debris. Proceedings of the National Academy of Sciences of the United States of America 2016; 113(28): 7696-8.

Yeung MS, Zdunek S, Bergmann O, Bernard S, Salehpour M, Alkass K*, et al.* Dynamics of oligodendrocyte generation and myelination in the human brain. Cell 2014; 159(4): 766-74.

Yoon H, Radulovic M, Drucker KL, Wu J, Scarisbrick IA. The thrombin receptor is a critical extracellular switch controlling myelination. Glia 2015; 63(5): 846-59.

Yoon H, Scarisbrick IA. Kallikrein-related peptidase 6 exacerbates disease in an autoimmune model of multiple sclerosis. Biological Chemistry 2016; 397(12): 1277-86.

Yousef GM, Diamandis EP. The new human tissue kallikrein gene family: structure, function, and association to disease. Endocrine Reviews 2001; 22(2): 184-204.

Yousef GM, Luo LY, Scherer SW, Sotiropoulou G, Diamandis EP. Molecular characterization of zyme/protease M/neurosin (PRSS9), a hormonally regulated kallikrein-like serine protease. Genomics 1999; 62(2): 251-9.

Zeisel A, Munoz-Manchado AB, Codeluppi S, Lonnerberg P, La Manno G, Jureus A*, et al.* Brain structure. Cell types in the mouse cortex and hippocampus revealed by single-cell RNA-seq. Science 2015; 347(6226): 1138-42.

Zhang Y, Barres BA. Astrocyte heterogeneity: an underappreciated topic in neurobiology. Current Opinion in Neurobiology 2010; 20(5): 588-94.

Zhang Y, Chen K, Sloan SA, Bennett ML, Scholze AR, O'Keeffe S*, et al.* An RNA-sequencing transcriptome and splicing database of glia, neurons, and vascular cells of the cerebral cortex. Journal of Neuroscience 2014; 34(36): 11929-47.

Zhang Y, Sloan SA, Clarke LE, Caneda C, Plaza CA, Blumenthal PD*, et al.* Purification and Characterization of Progenitor and Mature Human Astrocytes Reveals Transcriptional and Functional Differences with Mouse. Neuron 2016; 89(1): 37-53.

Zuchero JB, Fu MM, Sloan SA, Ibrahim A, Olson A, Zaremba A*, et al.* CNS myelin wrapping is driven by actin disassembly. Developmental Cell 2015; 34(2): 152-67.

CURRICULUM VITAE